

Université de Montréal

Investigation of pH-sensitive mechanism and anticancer application of switchable lipid  
nanoparticles

*Par*

Victor Passos Gibson

Faculté de Pharmacie

Mémoire présenté en vue de l'obtention du grade de M. Sc. en sciences pharmaceutiques,  
option technologie pharmaceutique

Décembre 2019

© Victor Passos Gibson, 2019



Université de Montréal

Faculté de Pharmacie

---

*Ce mémoire intitulé*

**Investigation of pH-sensitive mechanism and anticancer application of switchable lipid nanoparticles**

*Présenté par*

**Victor Passos Gibson**

*A été évalué par un jury composé des personnes suivantes*

**Grégoire Leclair**

Président-rapporteur

**Jeanne Leblond Chain**

Directeur de recherche

**Pierre Hardy**

Codirecteur

**Gaétan Mayer**

Membre du jury



## Résumé

Les lipides « switch » - bascules - appartiennent à la famille des matériaux sensibles à un stimulus. Quand ces lipides bascules sont incorporés aux nanoparticules lipidiques (LNP), ils permettent la délivrance contrôlée grâce à un changement de conformation activé par une baisse de pH. Des expériences précédentes avaient démontré que les LNP bascules ont transfecté les petits ARN interférents (siRNA) *in vitro* et *in vivo*, silençant la protéine fluorescente verte (GFP) et la protéine hépatique Facteur VII, respectivement. La double administration de micro ARN (miRNA) et d'agent anticancéreux melphalan a également été réalisée par les LNP bascule sur un modèle de rétinoblastome murin. Ces résultats prometteurs nous ont encouragé à élargir les applications de LNP bascules en tant que vecteur de siRNA. De plus, le mécanisme par lequel les LNP bascules induisent la déstabilisation de la membrane et la libération de matériaux encapsulé au milieu acide reste obscur. La compréhension de ce mécanisme est cruciale pour cerner les avantages et les limites des LNP bascules, pour proposer des futures applications et pour prévenir leur toxicité.

Dans ce mémoire, nous avons comme objectif d'évaluer le potentiel des LNP bascules pour le traitement du cancer. Nous avons évalué les LNP bascules comme vecteur de livraison du siRNA ciblant l'une des protéines cancéreuses les plus spécifiques découvertes à ce jour, la survivine. En parallèle, nous avons étudié le comportement biophysique des membranes contenant des lipides bascules dans des vésicules de taille micrométrique.

Dans la première étude, nous avons démontré que les LNP bascules ont permis le silençage de la survivine dans une gamme de lignées cellulaires cancéreuses (poumon, cervical, ovaire, sein, côlon, rétinoblastome). Dans les cellules du rétinoblastome humain (Y79), nous avons examiné plusieurs agents cytotoxiques utilisés en clinique quant à leur synergie avec le silençage de la survivine: melphalan, topotécan, téniposide et carboplatine. Le prétraitement avec les LNP chargées de siRNA-survivine a amélioré de manière synergique la cytotoxicité du carboplatine et du melphalan mais dans une moindre mesure celle du topotécan et du téniposide. Cet effet était spécifique aux cellules cancéreuses car les cellules saines (ARPE.19) n'exprimaient pas de survivine. L'inhibition de la survivine par silençage de siRNA s'est révélée plus spécifique et moins

dommageable pour les cellules saines (ARPE.19) que le YM155, un inhibiteur moléculaire de la survivine.

Dans la deuxième étude, nous avons observé par microscopie confocale que les lipides bascules induisaient rapidement le stress, la fission et une courbure positive dans les membranes des vésicules unilamellaires géantes lorsqu'elles étaient exposées à des conditions acides. La dynamique de la membrane a été confirmée par des expériences de diffusion dynamique de la lumière (DLS) et de fuite de calcéine. Ces phénomènes ont également été observés lorsque des lipides bascules ont été incorporés dans une membrane hybride polymère/lipide, fournissant des propriétés sensibles au pH aux vésicules hybrides. À notre connaissance, c'est la première fois qu'une vésicule hybride sensible au pH est reportée.

Nos résultats corroborent l'applicabilité des LNP bascules en tant qu'agents de vectorisation des siRNA pour le traitement du cancer grâce au silençage de la survivine, en particulier comme adjuvant à la chimiothérapie. L'investigation biophysique a révélé que les lipides bascules agissent sur la fluidité de la membrane, en particulier à pH acide. Cette sélectivité en pH garantit leur biocompatibilité à pH neutre ainsi que la libération efficace et rapide de leur cargo à pH acide. La compatibilité avec les vésicules hybrides polymère/lipide ouvre de nouvelles applications au niveau de vésicules biomimétiques et l'administration de médicaments.

**Mots-clés :** lipides bascules cationiques, nanoparticules lipidiques bascules, siRNA ciblant la survivine, rétinoblastome, vésicules géantes unilamellaires, vésicules géantes hybrides polymère/lipide unilamellaires, vésicules pH-sensibles

## Abstract

Cationic switchable lipids belong to the class of stimuli-responsive materials. When incorporated in lipid nanoparticles (LNP), switchable LNP promote pH-triggered delivery of payload based on a molecular switch mechanism. Previous studies have demonstrated that switchable LNP successfully delivered small interfering RNA (siRNA) *in vitro* and *in vivo*, promoting the silencing of a reporter Green Fluorescence Protein (GFP) protein and liver-produced factor VII, respectively. Dual delivery of micro RNA (miRNA) and anticancer agent melphalan was also achieved through switchable LNP in a retinoblastoma rat model. These promising results encouraged us to enlarge the applications of switchable LNP as siRNA carrier. Moreover, the mechanism whereby switchable LNP mediate acid-triggered membrane destabilization and, thus, payload release remains elusive. Understanding this mechanism is crucial to draw the advantages and limitations of switchable LNP, and to tailor their future applications and prevent their potential toxicity.

In this dissertation, we aimed to further understand the potential of switchable LNP for cancer treatment. We assessed switchable LNP as a siRNA delivery carrier by targeting one of the most specific cancer protein discovered to date, survivin. Meanwhile, we investigated the biophysical behavior of switchable-lipid containing membranes in micron-sized vesicles.

In the first study, we demonstrated that switchable LNP efficiently silenced survivin in a range of cancer cell line models (lung, cervical, ovary, breast, colon, retinoblastoma). In retinoblastoma (RB) cells (Y79), several clinically used cytotoxic agents were screened for their synergy with survivin silencing: melphalan, topotecan, Teniposide, and carboplatin. Pretreatment with LNP loaded with siRNA targeted against survivin synergistically enhanced the cytotoxicity of carboplatin and melphalan but in lesser extent topotecan and teniposide. This effect was specific to cancer cells since healthy cells (ARPE.19) did not express survivin. Survivin inhibition through siRNA silencing revealed more specific and less damageable for healthy cells (ARPE.19) than a molecular approach, such as YM155.

In the second study, we observed by confocal microscopy that switchable lipids rapidly induced stress, fission, and positive curvature in giant unilamellar vesicles' membranes when submitted to acidic conditions. The membrane dynamics was confirmed by dynamic light scattering and calcein leakage experiments. Remarkably, these phenomena were also observed when switchable lipids were embedded into a hybrid polymer/lipid membrane, providing pH-sensitive properties to hybrid vesicles. To the best of our knowledge, this is the first time a pH-sensitive hybrid vesicle is reported.

Our findings corroborate with the applicability of switchable LNP as siRNA delivery agents for cancer treatment through survivin silencing, especially as an adjuvant to chemotherapy. The biophysical investigation revealed that the switchable lipids act on the membrane fluidity, specifically at acidic pH. This pH selectivity guarantees their biocompatibility at neutral pH as well as its efficient and quick release of their cargo at acidic pH. Their compatibility with hybrid polymer/lipid vesicles opens new applications in biomimetic vesicles and drug delivery.

**Keywords** : cationic switchable lipid, switchable lipid nanoparticle, survivin-targeted siRNA, retinoblastoma, giant unilamellar vesicles, giant hybrid polymer/lipid unilamellar vesicles, pH-sensitive vesicles.



# Table of Contents

Résumé .....	5
Abstract.....	7
Table of Contents.....	9
List of Tables .....	15
List of Figures .....	17
List of symbols and abbreviations.....	21
Remerciements.....	24
Chapter 1 – Introduction .....	27
1.1. Cancer .....	27
1.1.1 History and definition .....	27
1.1.2. Chemotherapeutic strategies.....	28
1.1.3. Retinoblastoma .....	29
1.2. Survivin.....	34
1.2.1. Definition .....	34
1.2.2. Survivin and cancer .....	36
1.2.2.1. Immunotherapies.....	37
1.2.2.2. Small molecules inhibitors .....	37
1.2.2.3. mRNA targeting strategies .....	38
1.3. siRNA delivery .....	40
1.3.1. Challenges and vector rational design .....	40
1.3.1.1. siRNA Complexation and serum stability .....	42
1.3.1.2. Cell internalization .....	43

1.3.1.3.	Endosomal escape.....	44
1.3.2.	Methods of preparation for lipid nanoparticles (LNP) .....	47
1.3.2.1.	Lipid nanoparticles (LNP) .....	47
1.3.2.2.	pH-sensitive liposomes .....	50
1.4.	Hybrid polymer/lipid vesicles.....	54
1.4.1.	Polymersomes: definitions and structure .....	54
1.4.2.	Hybrid polymer/lipid vesicles: definition, preparation and recent developments	56
1.4.3.	Methods of preparation for hybrid polymer/lipid vesicles .....	60
1.4.4.	pH-sensitive hybrid vesicles: an opportunity for pH-sensitive lipids .....	62
1.5.	Project presentation .....	64
1.5.1.	Research hypothesis .....	64
1.5.2.	Specific objectives .....	65
1.5.2.1.	1 <sup>st</sup> publication:.....	66
1.5.2.2.	2 <sup>nd</sup> publication.....	66
Chapter 2 – Paper submitted to the Journal Molecular Therapy – Nucleic Acids .....		68
2.1.	Title page .....	68
2.2.	Abstract.....	68
2.3.	Introduction .....	69
2.4.	Materials and method .....	71
2.4.1.	Preparation of cationic switchable lipid nanoparticles.....	71
2.4.2.	Physicochemical characterization of switchable LNP .....	72
2.4.3.	siRNA complexation, characterization and encapsulation efficiency .....	73
2.4.5.	Cell culture .....	73
2.4.6.	Cell transfection .....	74

2.4.7. Relative quantification of target genes by RT-qPCR .....	75
2.4.8. Western blot assay.....	76
2.4.9. Viability assay.....	77
2.4.10. Synergistic effect.....	78
2.4.11. Statistical analysis .....	78
2.5. Results.....	78
2.5.1. Preparation of switchable lipid nanoparticles .....	78
2.5.2. <i>In vitro</i> survivin silencing by switchable LNP.....	79
2.5.3. Drugs used in the RB protocol induce survivin expression differently .....	82
2.5.4. Survivin downregulation followed by drug treatment on Y79 cells.....	84
2.5.5. Specificity of survivin downregulation .....	87
2.6. Discussion .....	91
2.7. Conclusion.....	93
2.8. Supporting information .....	94
Chapter 3 – Paper published in the journal Polymers .....	99
3.1. Title page .....	99
3.2. Abstract.....	99
3.3. Introduction .....	100
3.4. Materials and methods.....	102
3.4.1. GUV and GHUV preparation .....	102
3.4.2. LUV and LHUV preparation .....	103
3.4.3. <sup>1</sup> H NMR measurement .....	103
3.4.4. Dynamic and static light scattering.....	103
3.4.5. Confocal imaging.....	104

3.5. Results.....	104
3.5.1. CSL was successfully inserted into LUV or LHUV.....	104
3.5.2. Acid-related morphological modifications.....	106
3.5.2.1. DLS and $\zeta$ -measurements.....	106
3.5.2.2. Confocal observations.....	107
3.5.3. Study of the pH-Triggered Membrane Permeability to GUV and GHUV.....	110
3.5.3.1. pH-triggered calcein release from GUV.....	110
3.5.3.2. pH-triggered calcein release from GHUV.....	112
3.6. Discussion.....	114
3.7. Conclusion.....	115
3.8. Supporting information.....	116
Chapter 4 – Discussion and perspectives.....	129
4.1. Switchable lipids : a robust delivery platform.....	129
4.1.1. Targeting survivin : advantages and limitations.....	132
Advantages of survivin targeting.....	132
Limitations of survivin targeting.....	133
Other considerations into survivin targeting strategies.....	135
4.3. pH-triggered switch : a selective fluidity modulation.....	137
4.4. Perspectives.....	142
4.4.1. Optimizing survivin targeting strategy in RB.....	142
4.4.2. Optimizing pH-responsive hybrid polymer/lipid vesicles.....	143
4.4.3. Further investigation on the mechanism whereby switchable lipid mediates membrane destabilization.....	144
Chapter 5 – Conclusion.....	145

References ..... 147



## List of Tables

Table 1. – OnPattro (Patisiran) composition and role of each lipid component. ....	46
Table 2. – siRNA sequences used in the study.....	71
Table 3. – The sequence of oligos used in PCR analysis. ....	76
Table 4. – Physicochemical characteristics of switchable LNPs, through two preparation methods.....	79
Table 5. – Relative (%) survivin mRNA expression in different cancer cell lines after switchable LNP transfection.. ....	95
Table 6. – Physico-chemical properties of LUVs and LHUVs.....	105
Table 7. – Morphological changes in GUV and GHUV upon HCl or NaCl treatment.....	109
Table 8. – Physico-chemical properties of LUVs and LHUVs before and after treatment with HCl or NaCl.....	120
Table 9. – Applications of switchable LNP as a drug/gene carrier.....	130
Table 10. – Morphological changes in GUV-Di12diMe 50% treated with HCl. ....	141





## List of Figures

Figure 1. – The Hallmarks of Cancer and tailored strategies proposed.....	28
Figure 2. – Genetic causes of RB1-associated retinoblastoma.....	31
Figure 3. – Retinoblastoma classification according to the IIRC and recommended therapeutic interventions.....	33
Figure 4. – Connectivity links between the survivin cell division and cell death networks.....	35
Figure 5. – Survivin and cancer research.....	36
Figure 6. – Mechanism of siRNA-mediated mRNA silencing.....	39
Figure 7. – General structure of unmodified siRNA.....	41
Figure 8. – Physiological barriers faced by siRNA strategies..	42
Figure 9. – Possible pathways of nanoparticles internalization. ....	44
Figure 10. – Schematic diagram of the ion-pair membrane disruption mechanism mediated by cationic lipids... ..	45
Figure 11. – Stepwise representation of LNP preparation by combining preformed liposomes with siRNA.....	48
Figure 12. – Schematic representation of siRNA encapsulated LNP formulated by microfluidics technique.....	49
Figure 13. – Cryogenic transmission electron microscopy (Cryo-TEM) micrographs of extrusion- and microfluidics-formulated liposomes.. ..	50
Figure 14. – pH-sensitive lipid undergoes conformation change upon acidification leading to switchable LNP destabilization and siRNA delivery. ....	51
Figure 15. – Cationic switchable LNP efficiently delivered siRNA <i>in vitro</i> and <i>in vivo</i> .. ..	52
Figure 16. – Switchable LNP as a transfection vector for retinoblastoma cells (Y79).. ..	53
Figure 17. – Graphic representation of a liposome and a polymersome.. ..	55
Figure 18. – Fluorescence microscopy observation of pure giant liposomes (POPC, red), polymersomes (PB-PEO, green) and hybrid polymer/lipid vesicles (Hybrids, merged color, composed of 70:30 % mol PB-PEO:POPC) (142). ....	56
Figure 19. – Graphical representation of possible hybrid membrane phase arrangements.....	57

Figure 20. – Different membrane arrangements of a hybrid vesicle with regard to molar proportion between the polymer and lipid content and the thermodynamic phase of the phospholipid..... 58

Figure 21. – *In vitro* toxicity (A) and *in vivo* targeting (B) of HER2/neu-targeted hybrid vesicles. Arrow indicates tumor site. .... 59

Figure 22. – Illustrative representation of the preparation of asymmetric giant hybrid vesicles containing an outer lipid layer and an inner amphiphilic diblock copolymer shell surrounding an aqueous nucleus core.. .... 60

Figure 23. – Liposomes and polymersomes can be formulated at giant scale (higher than 1  $\mu\text{m}$ ). SUV: small unilamellar vesicles (< 100nm); LUV: large unilamellar vesicles (100 nm < LUV < 1000 nm); GUV: giant unilamellar vesicles (GUV > 1000 nm)..... 61

Figure 24. – Schematic representation of Giant Unilamellar Vesicles (GUV) formed by the electroformation method. .... 62

Figure 25. – Confocal observation of extruded hybrid polymer/lipid vesicles composed of cholesteryl Methacrylate (pCMA)-block-poly(2-(dimethylamino)-ethyl Methacrylate) blended with POPC and the cationic lipid POEPC (7:2:1 % wt)..... 63

Figure 26. – Heat map of survivin downregulation on a range of cancer cells using siSurvivin switchable LNP..... 80

Figure 27. – *In vitro* survivin downregulation in Y79 cells with switchable LNP..... 81

Figure 28. – RT-qPCR and western blot of Y79 cells after 48 h incubation with different chemotherapeutics..... 83

Figure 29. – Viability of Y79 cells after survivin downregulation by siRNA/LF for 48 h followed by treatment with either (A) carboplatin, (B) topotecan, (D) melphalan or (E) teniposide for 48 h. (C) Y79 survivin protein expression of cells treated with siRNA/LF (48 h) followed by 50  $\mu\text{M}$  CBDA (48 h)..... 84

Figure 30. – Viability of (A) Y79 and (B) Y79-luc cells 96 hours after siSurvivin delivery by switchable LNP (48 h, siLNP) followed by carboplatin incubation (48 h). (C) Western blot of Y79-Luc cells treated or not with siSurvivin (LF, 20 nM siRNA) and/or Carboplatin (25  $\mu\text{M}$ ) ..... 86

Figure 31. – Carboplatin cytotoxicity in (A) Y79 cells transfected with scramble (scrLNP, 20nM siRNA) or survivin-targeted siRNA switchable LNP (siLNP, 20 nM siRNA) and in (B) ARPE.19 cells transfected with siSurvivin (LF, 20 nM siRNA). (C) Survivin immunoblotting of non-treated Y79 and ARPE.19 prior and after survivin silencing (LF, 20 nM siRNA).....	87
Figure 32. – Viability of Y79 (A and B) and primary RB cells (C) after siLNP or scrLNP transfection followed by chemotherapeutics. ....	90
Figure 33. – Lipofectamine RNAiMAX carrying siRNA survivin (20nM) downregulates survivin protein in both Y79 and Y79-luc cells. ....	95
Figure 34. – Y79 cells viability 48 hours upon (A) carboplatin, (B) topotecan, (C) melphalan or (D) teniposide treatment. (E) IC <sub>50</sub> before and after survivin silencing treatment with siRNA/LF (20nM).....	96
Figure 35. – Effect of survivin silencing on carboplatin and topotecan combined therapy in Y79 cells.....	97
Figure 36. – Viability of Y79 (A) and ARPE.19 (B) cells 48 hours after treatment with LF carrying siSurvivin (20 nM) or chemical inhibitor YM155 (2 nM). . ....	98
Figure 37. – DLS and zeta potential measurements of LUV and LHUV at pH 6.8 and 2.8.. ....	106
Figure 38. – Overall calcein fluorescence intensity in GUVs before and after acidification (pH 6.8 and 4.8).....	111
Figure 39. – Overall calcein fluorescence intensity distribution in GHUVs before and after acidification.....	113
Figure 40. – <sup>1</sup> H NMR spectrum of GUV-CSL 20% in CDCl <sub>3</sub> .....	117
Figure 41. – <sup>1</sup> H NMR spectrum of GUV-CSL 50% in CDCl <sub>3</sub> .....	117
Figure 42. – <sup>1</sup> H NMR spectrum of GHUV-CSL 20% in CDCl <sub>3</sub> .....	118
Figure 43. – <sup>1</sup> H NMR spectrum of GHUV-CSL 50% in CDCl <sub>3</sub> .....	118
Figure 44. – Size distribution and correlogram fit of LUV and LHUV at pH 6.8 and 2.8. (a) LUV-POPC, (b) LHUV-POPC 20%, (c) LHUV-POPC 50%, (d) LHUV-CSL 20%. ....	119
Figure 45. – Morphological changes of GUVs upon HCl or NaCl treatment. ....	121
Figure 46. – Snapshots of morphological changes in GUV-CSL 50% treated with HCl. White boxes in the upper left corner indicate frame order. Scale bar: 10 μm.....	123

Figure 47. – Morphological changes of GHUVs upon HCl treatment. Open arrows: vesicles with outward projections. ....	123
Figure 48. – Snapshots of morphological changes in GHUV-CSL 20% treated with HCl .....	124
Figure 49. – Permeability of calcein-loaded GUV-POPC 50% treated with HCl. ....	125
Figure 50. – Snapshots of morphological changes in GUV-CSL 50% treated with HCl. ....	126
Figure 51. – Snapshots of calcein-loaded GHUV-CSL 50% treated with HCl.....	127
Figure 52. – Comparison of <i>in vivo</i> dose-dependent silencing of FVII by switchable LNP (CSL3, filled circles, left) or ionizable lipid-containing LNP (1 <sup>st</sup> and 2 <sup>nd</sup> generations, right).....	132
Figure 53. – Effects of transfection of siRNA survivin (20 nM) on cell cycle and proliferation in Y79 cells.....	135
Figure 54. – Endosomal escape pathways mediated by pH-sensitive liposomes.....	138
Figure 55. – GUV-C12diMe 50% and calcein-loaded GUV-C12diMe 50% submitted to HCl treatment.....	142
Figure 56. – Lymphocyte-derived microparticles (LMPs) mediate SYK silencing (A) and induce p53 and p21 expression (B). ....	143
Figure 57. – Polymers are labelled in green (filter I), lipids are labelled in red (filter II). Filter III, merged filters.....	144

## List of symbols and abbreviations

$^1\text{H}$ RMN	Proton nuclear magnetic resonance
$^{31}\text{P}$ RMN	Phosphorus-31 nuclear magnetic resonance
AC	Electrical field
ACTB	Beta actin
AFM	Atomic force microscopy
AOS	Antisense oligonucleotides
CBDA	Carboplatin
$\text{CDCl}_3$	Deuterated chloroform
Cryo-TEM	Cryogenic transmission electron microscopy
CSL	Cationic switchable lipid
DLin-MC3-DMA	dilinoleylmethyl-4-dimethylaminobutyrate
DLS	Dynamic Light Scattering
DMPG-PEG	1,2-dimyristoyl-rac-glycero-3-methoxypolyethylene glycol-2000
DNA	Deoxyribonucleic acid
DOPE	1,2-dioleoyl-sn-glycerol-3-phosphoethanolamine
DOTAP	1,2-dioleoyl-3-trimethylammonium-propane
DSPC	1,2-distearoyl-sn-glycerol-3-phosphocholine
FDA	Food and drug administration
GHUV	Giant unilamellar hybrid polymer/lipid vesicles

GUV	Giant unilamellar vesicles
HCl	Hydrochloride acid
HSPC	Hydrogenated soy phosphatidylcholine
IAC	Intra-arterial -chemotherapy
IAP	Inhibitors of apoptosis protein
IIRC	International Classification of Intraocular Retinoblastoma
ITO	Indium tin oxide
IVC	Intravenous chemotherapy
LF	Lipofectamine
LHUV	Large hybrid polymer/lipid unilamellar vesicles
LNP	Lipid nanoparticle
LUV	Large unilamellar vesicles
MELPH	Melphalan
miRNA	micro RNA
mRNA	Messenger RNA
OS	Overall survival
PB-PEO	poly(butadiene)-b-poly(ethylene oxide)
PCC	Pearson correlation coefficient
PCL	Polycaprolactone
PDMS-g-PEO	Poly(dimethylsiloxane)- <i>graft</i> -poly(ethylene oxide)
PEG	Polyethylene glycol

PEI	Polyethylenimine
PEO-PBD	Poly(ethylene oxide)-block-polybutadiene
POEPC	1-palmitoyl-2-oleoyl-sn-glycero-3-ethylphosphocholine
qPCR	quantitative real-time Polymerase Chain Reaction
RB	Retinoblastoma
RISC	RNA-induced silencing complex
RNA	Ribonucleic acid
scrLNP	Scrambled siRNA complexed switchable LNP
siLNP	Survivin-targeted siRNA complexed switchable LNP
siRNA	Small interfering RNA
SUV	Small unilamellar vesicles
TENI	Teniposide
TOPO	Topotecan
WB	Western Blot
WHO	World Health Organization
Y79-Luc	Luciferase-expressing Y79 cells
YM155	Sepantronium Bromide

## Remerciements

The first acknowledgment I'd like to express will never fit in this line. It would never fit in more than the 100 pages of this dissertation. It would never fit in any thesis I may write. Mom, I will be always grateful for all the support, motivation and faith you put on me. Pursuing an education abroad is hard. Being apart from the family, culture, friends is a challenge, especially if a language barrier is involved. But being apart from a son must be even harder (even though it is the third time I'm away, I guess you will never be used to it). Thank you for always being there for me. By extent, I express my gratitude to my family for allowing me to fully dedicate to my education in a fostering environment. Like you all have always said to me: you wanna see the world? "Vá estudar"! Guess what? you were right.

Secondly, I must thank you, Jeanne. You have welcomed me three times in your lab: first as an intern in 2016, then as a Master student and again in Bordeaux (there not necessarily in your lab, but thanks for the networking). Merci for these opportunities. It was of an immeasurable growth, both scientifically and personally. Thank you for your mentoring, formation, scientific discussion, and biking around Bordeaux! Proud of being part of the Laboratoire de Vectorisation Génétique. I hope I've met your expectations. I'm confident you will achieve great things scientifically and I wish you luck in your future endeavors. Looking forward to future collaborations.

My co-supervisor also played an important role during this M. Sc degree. Thank you, Dr. Hardy, for trusting me with this project. I extend my gratitude to all the lab for the support and formation.

Part of this study would not have been done without the support and opportunity given by Prof. Jean-François Le Meins at the Laboratoire de Chimie des Polymères Organiques (LCPO) in Bordeaux. Thank you, Jeff, for the valuable contribution to this research. It was a unique experience. Thank you, Martin and Emmanuel, for the valuable training.

In the same perspective, I must express my gratitude to Mouna and Warren, two excellent researchers who trained me at Université de Montréal. Mouna, you are more than a colleague now, so I'm also thankful for your friendship. I express my acknowledgment to all the team from



the 4<sup>th</sup> floor and the personnel the Faculté de Pharmacie. Outside the university, some people helped me through this journey; thank you, Marcela, Hudson, and Lucas.

I thank the jury for your valuable time to read this dissertation and precious consideration. Finally, thank you Mitacs for the Globalink and Fellowship studentships.



# Chapter 1 – Introduction

## 1.1. Cancer

### 1.1.1 History and definition

A swelling mass accompanied by a grieving prognosis, for which no treatment was available. That might have been the first-ever recorded description of the group of diseases currently named cancer (1). It belongs to the Edwin Smith Papyrus dating back to 3000 BC, and the Egyptians might have encountered cancer many times throughout their history, making their medical records a valuable source of understanding that cancer is a long-lived unwanted brother in human history (2). It was not before Hippocrates (460-370 BC), however, that the word cancer started being fashioned, but it belongs to the Roman physician Galen (130-200 AD) the first register of the term *onkos*, that later coined the scientific field dedicated to the study of cancer: oncology.

The World Health Organization (WHO) classifies cancer as the second leading cause of death worldwide (3). In 2018, 18.1 million people were estimated to be diagnosed with cancer, while 9.6 million were expected to have died from the same disease (4). Interestingly, for the same year, the global incidence is higher than mortality in all WHO world regions', but in Africa and Asia, where incidence shares were estimated to be 5.8% and 48.4%, while mortality reached 7.3% and 57.3%, respectively (5). Multiple factors can contribute to high mortality statistics, but the economy plays an important role in cancers' fate. Late diagnosis, difficult access to health care, non-compliance with drug therapy and high rates of relapse are a few examples shared among low- and middle-income countries that deeply impact cancer's prognosis and cure (6, 7). Such problematic becomes more evident when analyzing the statistics for pediatric cancers, which reaches 80% of cure in high-income countries, but drops to 20% in low- and middle- income ones (7). One specific type of pediatric cancer has its prognosis deeply affected by the country it is diagnosed: retinoblastoma. The implication of a late diagnosis on Retinoblastoma's progression and treatment will be further discussed in this chapter (in section 1.1.1).

A normal cell evolves progressively towards a malignant state through the acquisition of mutations on specific pathways that provides adaptative traits to the cancer cell. In 2011, Hanahan and Weinberg (8) proposed the Hallmarks of Cancer, categorizing the acquired mutations by tumors during the neoplastic development. Dividing the complex tumorigenesis process into key altered pathways enabled researchers to exploit tumor's characteristics by looking for vulnerabilities and specificities within the hallmarks that could differentiate malignant cells from healthy ones and, thus, allowing us to propose more efficient and tailored therapies (Figure 1).

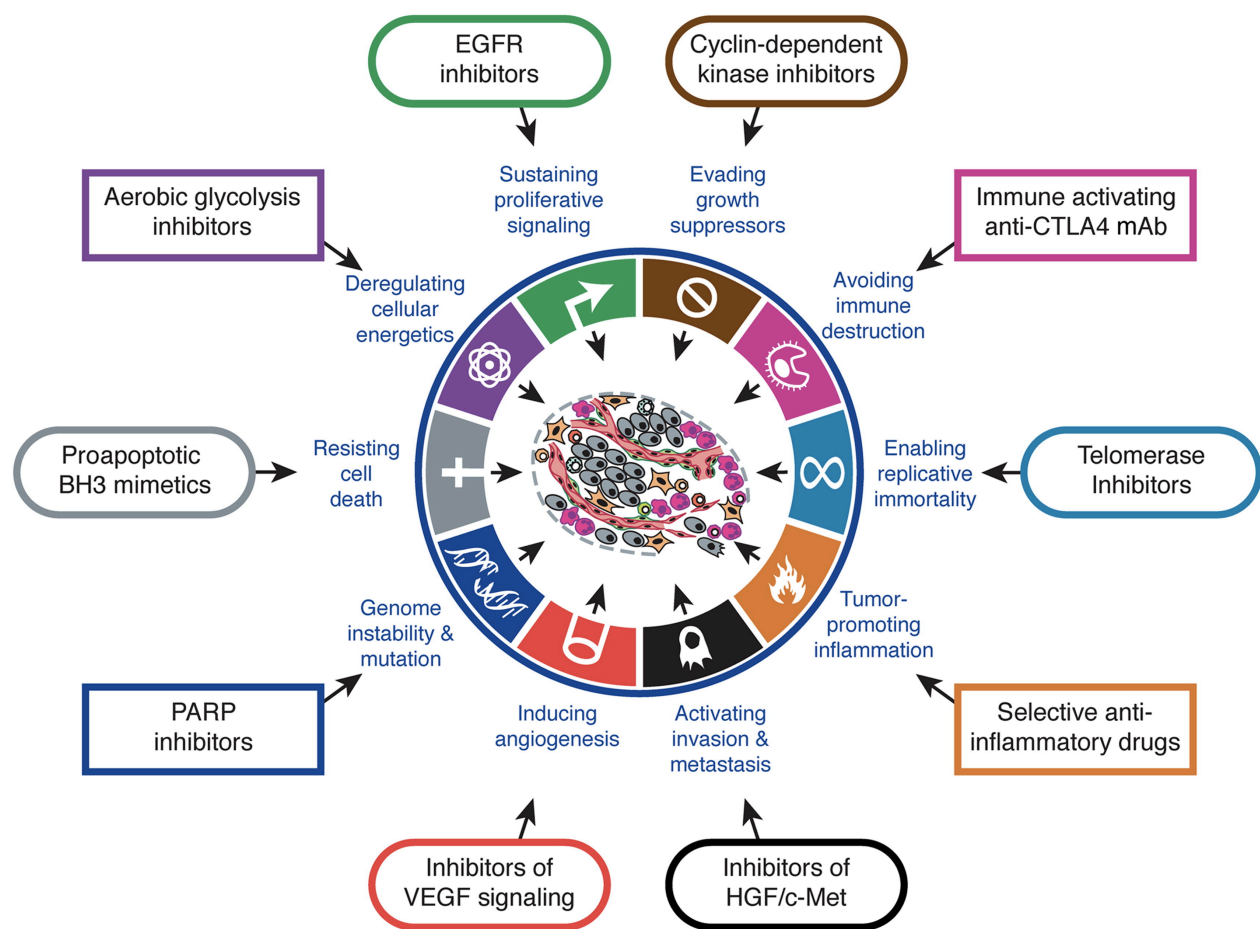


Figure 1. – The Hallmarks of Cancer and tailored strategies proposed (8).

### 1.1.2. Chemotherapeutic strategies

The debut of chemotherapy is attributed to the weaponry development during wartime when researchers linked the cytotoxicity of analogs of sulfur mustards to the proliferative state of the

targeted tissue (9). The leading study fostered the introduction of a series of alkylating agents into medical practice, some of which are still in use today, as melphalan (10, 11). Around the same time, Farber & Diamond (12) published the clinical success of aminopterin in treating acute leukemia in children, giving birth to another class of chemotherapeutics: the antimetabolites (13). By then, neither Farber nor Gillman were aware they have taken advantage of one of the hallmarks of cancer (sustained proliferative signaling, Figure 1), but the wave of compounds followed by their discovery have significantly killed cancer halting the vital activated tumor intracellular machinery that enables replicative immortality. Researchers have long envisaged a universal therapy that specifically targeted cancer cells and cancer cells only. The utopic idea of the magic bullet proposed by Paul Ehrlich (14) nearly thrived with the advent of first targeted therapy in cancer research. Herceptin was the first FDA-approved monoclonal antibody against solid cancer that selectively targeted the HER2/neu surface receptor enriched in cancer cells, but not in healthy ones, a biomarker-driven drug discovery that halted the sustained proliferative signaling (Figure 1).

In 2003, the genomic era flourished with the terminus of the Human Genome Project and alongside it came the improvement of sequencing and genomic techniques, which enabled researchers to understand molecular events that define cancer at a personalized level, as well finding targets that are specifically activated and expressed by malignant cells. A valuable resource that emerged in the genomic era was the small interfering RNA (siRNA) technology. The Nobel prize-winning discovery (15) allowed scientists to interrogate virtually any target within the cell to understand or block key components of the hallmarks that might not be spatially available for antibody targeting or harbor a catalytic site for small molecule inhibition.

### **1.1.3. Retinoblastoma**

In 1872, Hilário de Gouvêia, a Brazilian ophthalmologist practicing in Rio de Janeiro, identified retinoblastoma (RB) in a young boy and removed the eye surgically. Years later, the now-grown-man married a healthy woman and two of their offspring were diagnosed by Dr. Gouvêia with bilateral RB (16). Although largely obliterated by the scientific community, Dr. Gouvêia pioneer identification of a familiar case of RB laid ground to the “Two-hit-hypothesis” proposed by

Knudson in 1971, who explained that two consecutive mutations, either one inherited or both acquired somatically, are necessary to trigger retinal tumorigenesis (17). Knudson theory was validated after the identification of the tumor suppressor *Rb1* gene in the chromosome 13, a sequence that was inactivated in all patient-derived RB samples (18). Now, a multi-hit hypothesis is commonly accepted for the tumorigenesis process (19). In RB, the *Rb1* gene inactivation is a tumor-driven trigger during the maturation of cone-precursor cells that culminates in a malignant state after further genetic and epigenetic alterations (20) (Figure 2).

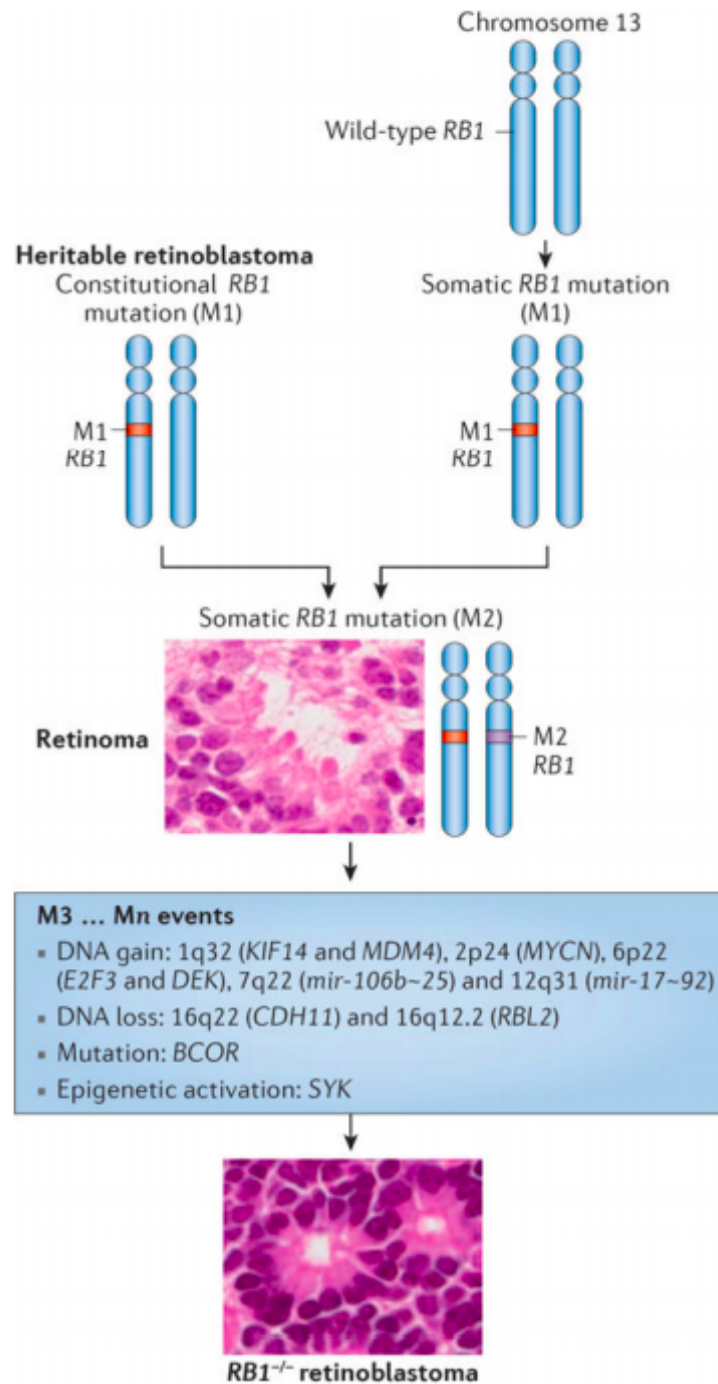


Figure 2. – Genetic causes of RB1-associated retinoblastoma. Adapted from (20)

Heritable cases of RB are characterized by a constitutive RB1 mutation (Mutation 1, M1). A second hit (M2) is somatically acquired in a susceptible retinal cell. In non-heritable cases, the two mutations occur somatically in the same retinal cell. A benign retinoma evolves towards a malign state (retinoblastoma, RB) through a third (M3) or more (Mn) genetic or epigenetic alterations.

Although not presented in Figure 2, a third rare genetic subtype of RB is known. It is characterized by the presence of wild-type RB1 and amplification of the MYCN oncogene (RB1+/+ MYCNA).

RB remains a rare type of cancer with an overall 8000 new cases per year worldwide (20). It is the most common intraocular cancer in children, being responsible for 3% of all cases of childhood malignancies. The overall survival (OS) of RB varies considerably according to the economic development of the region it is diagnosed in. Whereas the OS is higher than 95% in high-income countries (21, 22), the OS is lower than 40% in low-income ones (23, 24). Difficult access to healthcare, unavailability of clinical resources and, thus, late diagnosis and treatment, enucleation denial by the family and incomppliance to chemotherapy are a few examples underlying such discrepancy (20). To tackle the difference, international engagement to promote awareness and collaboration between countries are playing an important role to fight RB in economically undeveloped regions of the globe (25, 26).

The International Classification of Intraocular Retinoblastoma (IIRC) categorizes RB in 6 stages, from a 0 phase, where no disease is detected, to stage A through E, corresponding to a minor tumor with less than 3 mm to a more severe case with diffuse vitreous seeds and potential extraocular invasion, respectively. As later the diagnosis, the worse the prognosis is, once the tumor tends to migrate back through the optic nerve to colonize the brain, when it becomes incurable. Therefore, RB staging is crucial to determine the clinical protocol. Clinical management of RB takes into consideration the probability of survival of the patient, salvage of the eye, vision preservation and reducing secondary tumors (Figure 3).



Eye Group	General Feature	Specific Feature (Presence of $\geq 1$ )	Therapy
A	Small tumor away from fovea and optic disc	Tumor $\leq 3$ mm	Laser photocoagulation Thermotherapy Cryotherapy Plaque brachytherapy
B	Larger tumor Macular Juxtapapillary Subretinal fluid	Tumor $> 3$ mm Tumor located $< 3$ mm from fovea Tumor located $\leq 1.5$ mm from optic disc Presence of subretinal fluid $\leq 3$ mm from tumor margin	Laser photocoagulation Thermotherapy Cryotherapy Plaque brachytherapy Intravenous/intra-arterial chemoreduction
C	Focal seeds	Presence of subretinal, vitreous seeds, or both located $\leq 3$ mm from main tumor	Intra-arterial chemotherapy Intravitreal chemotherapy
D	Diffuse seeds	Presence of subretinal, vitreous seeds, or both located $> 3$ mm from main tumor	Intra-arterial chemotherapy Intravitreal chemotherapy Enucleation
E	Extensive tumor	Tumor occupying $> 50\%$ of the globe Neovascular glaucoma Opaque media from hemorrhage in anterior chamber, vitreous, or subretinal space Invasion of postlaminar optic nerve, choroid ( $> 2$ mm), sclera, orbit, anterior chamber	Intra-arterial chemotherapy Enucleation Adjuvant intravenous chemotherapy if high-risk histopathological features present

Figure 3. – Retinoblastoma classification according to the IIRC and recommended therapeutic interventions (27).

RB treatment could be classified in chemotherapy (either systemic or locally delivered), focal therapy and enucleation (27-29).

- **Systemic**, or intravenous, chemotherapy (IVC) is usually a combination of 2 to 3 drugs with different mechanisms of action. Standard drugs include alkylating agents (carboplatin, cisplatin), topoisomerase II inhibitors (etoposide, topotecan, and teniposide) and vinka alkaloids (vincristine). A major drawback in IVC is the reduced drug bioavailability in the vitreous due to the blood-retina barrier. As a result, IVC by itself rarely eradicates the tumor, being commonly combined with focal therapies.
- **Local administration** includes intra-arterial (IAC), intravitreal or periocular chemotherapy. IAC has been successfully applied for the initial stages of RB. For stages D and E, IAC can be combined with IVC. IAC requires highly skilled physicians at dedicated cancer centers, which are not usually available in developing countries. Intervention is made through a micro-catheter through the femoral artery up to the ophthalmic artery of the affected eye where melphalan, a mustard alkylating agent, is delivered. A drug combination is also preferred if extensive vitreous seeds are present. Intravitreal chemotherapy is the chosen

intervention for advanced stages with extensive vitreous seeds unresponsive to IVC or IAC, as it bypasses the drug delivery challenge of nonvascularized vitreous. Melphalan can be solely injected or in combination with topotecan. Special concern is given during needle withdrawal. It's important to seal the site of injection with cryotherapy as the tumor could migrate through needle track after the intervention. Finally, the periocular injection of either carboplatin or topotecan allows rapid and high vitreous concentration. It can be used to control retinoblastoma or as an adjuvant of IVC for advanced stages of RB with the presence of vitreous seeds.

- **Focal therapy** is the primary treatment for initial stages of retinoblastoma and englobes laser therapy, cryotherapy, and plaque radiotherapy. Laser therapy is designed to either cytotoxicity heat the tumor directly using an 810-nm diode laser (thermotherapy) or a 510-nm argon laser to coagulate blood vessels that supply the tumor (laser photocoagulation). Cryotherapy uses a metal probe cooled to very low temperatures to freeze and kill small tumors. Plaque radiotherapy consists of implementing a radiative robe, usually Iodine-125 and ruthenium-106, to deliver ionizing radiation to small tumors over 4-7 days.
- **Enucleation** remains the ultimate and most effective intervention for advanced stages of RB (group E). It is the first-line treatment in non-familial cases of RB, as the disease is usually identified at later stages.

## 1.2. Survivin

### 1.2.1. Definition

Baculoviral IAP repeat-containing protein 5, commonly known as survivin, is the smallest member of the inhibitors of apoptosis protein family (IAP). Survivin is a multitask protein implicated in proliferation and cell cycle progression (30), angiogenesis (31), DNA repair (32), cancer invasiveness and stemness properties (33) and mediates resistance to chemotherapeutics by inhibiting both extrinsic and intrinsic apoptosis signaling (34) through a complex mechanism yet to be fully elucidated. Possessing such a vast network of interaction, survivin's nodal function can be viewed as two-fold: (i) a key role in cell division (mediating microtubule dynamics and their

attachment to the centrosomes – kinetochore survivin) and (ii) cell death and genomic fidelity regulator (Figure 4).

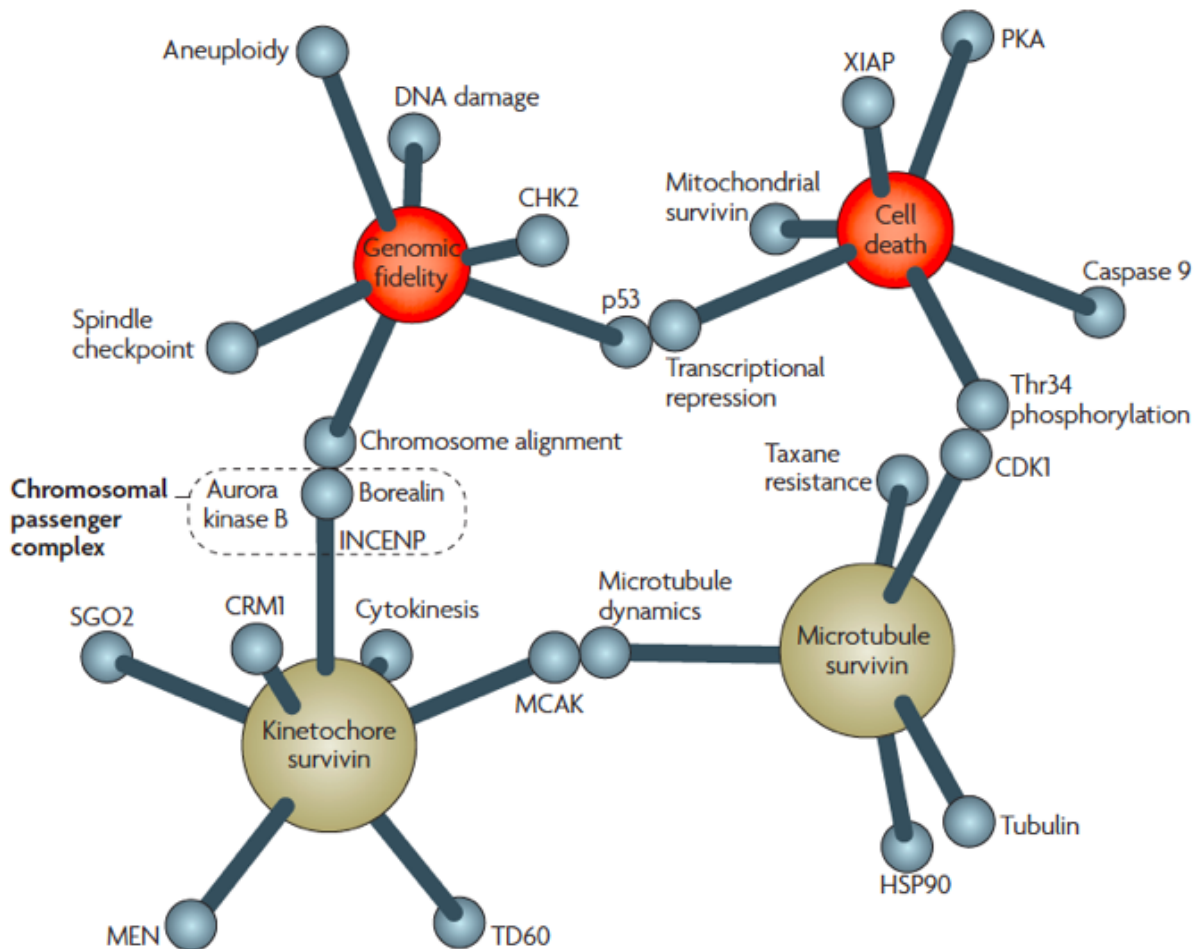


Figure 4. – Connectivity links between the survivin cell division and cell death networks. The functions of survivin intersect with mechanisms of cell division control, genomic fidelity, mitotic spindle assembly, subcellular trafficking, checkpoint regulation and apoptosis (35). CHK2 ; XIAP, X-linked inhibitor of apoptosis protein; PKA, protein kinase A; CDK1, cyclindependent kinase 1; HSP90, heat shock protein 90; MCAK, mitotic centromere-associated kinesin; TD60, telophase disk protein of 60 kD; MEN, mitotic exit network; SGO2, shugoshin 2; CRM1, chromosome region maintenance protein 1; INCENP, inner centromere protein antigens.

There is a large room for debate about survivin’s importance in cellular homeostasis. Although one may categorize its function at two levels as described above (Figure 4), we should not rule out that many of the survivin’s pathways could be connected, demanding a holistic or systems

biology interpretation of its cellular role. Such a nodal protein implicated in key cellular pathways became an obvious target for scientific investigation, especially in cancer, where it is abnormally overexpressed (36).

### 1.2.2. Survivin and cancer

Since its discovery (37), survivin has puzzled cancer biologists: it is extensively expressed in embryonic development, silenced in most healthy adult differentiated cells, but it rises again at the malignancy stage. Survivin is deeply implicated in cancer resistance to chemotherapeutics, radiation, and usually associated with poor patient prognosis in colorectal (38), breast (39) and bladder cancer (40), as human gliomas (41), melanoma (42) and retinoblastoma (43). Besides, survivin has been linked to other hallmarks of cancer beyond its firstly reported ability to confer resistance to cell death (Figure 5A). This is why reports involving survivin considerably increased in the last 15 years (Figure 5B).

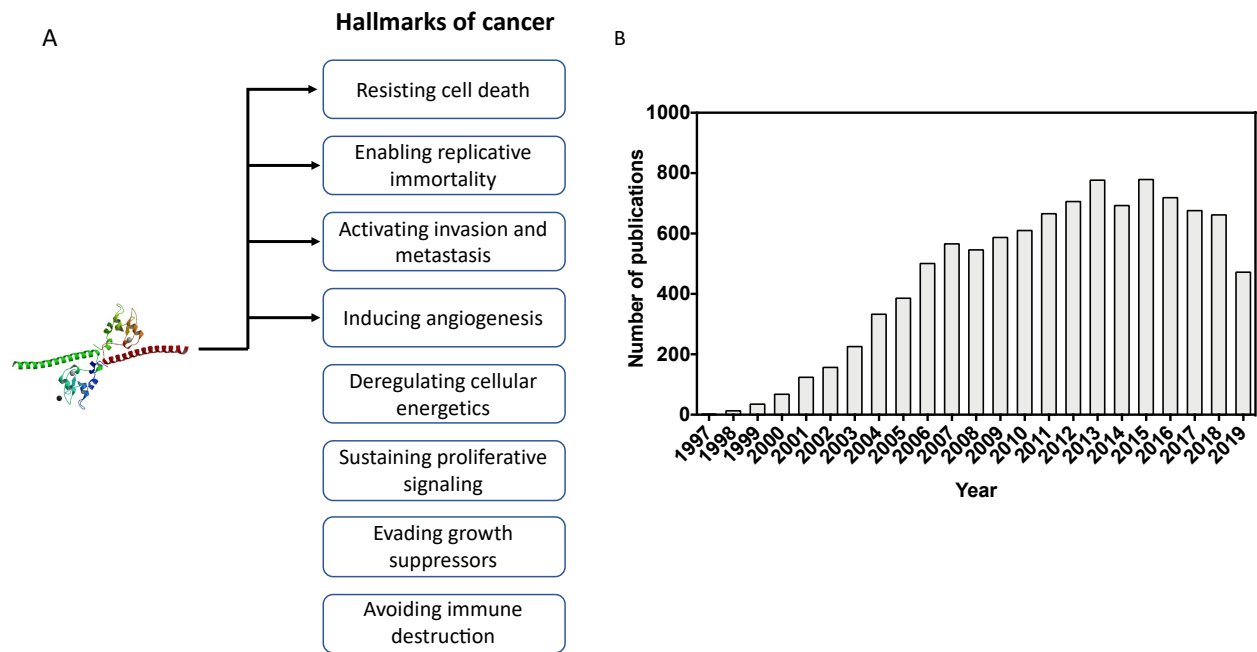


Figure 5. – Survivin and cancer research. (A) Arrows indicate scientific evidence of survivin and the hallmarks of cancer. (B) Number of publications from 1997 to 2019 retrieved from Web of Science (Thomson Scientific) using the entry “Survivin” on Title, Abstract or Keyword. Total

number of publications: 10.304, as of October 22 of 2019. Left side, a 3D crystallography representation of survivin protein (PDB entry: 1E31).

There is scientific evidence of survivin's implication on the following hallmarks of cancer: resistance to cell death (44); Enabling replicative immortality (here, survivin as key player in cell division (45), which is highly exploited by cancer cells, as well as its possible contribution to stemness properties in cancer (46, 47)), were considered as a link to this hallmark); activation of metastasis and invasion (48, 49); and inducer of angiogenesis (50).

Furthermore, survivin was unveiled to be the 4<sup>th</sup> most expressed transcript in colon, brain, breast and lung cancer, and melanoma in comparison to their corresponding normal tissues (36). Not surprisingly, many anti-survivin strategies have been pursued *in vitro* and *in vivo* with a few fruitful approaches reaching clinical trials. It must be noted, however, that targeting survivin isn't an easy strategy. As an intracellular protein, localized in different subcompartments (nucleus, mitochondria, and cytosol), one of each possibly contributing to circumvent cell death, and lacking a catalytic site for small molecules inhibitors, survivin can easily be considered an "undruggable" target (51, 52). Therefore, scientists used to target survivin with: (i) immunotherapies that recognize survivin as a tumor-associated antigen (TAA), (ii) agents capable of regulating survivin at DNA level repressing its promoter region or (iii) at mRNA precursors.

#### 1.2.2.1. Immunotherapies

Survivin emerged as a good candidate for immune-based strategies (53) due to its poor expression in healthy adult cells and high expression in cancer cells (37). As a result, multiple clinical trials are being carried with Survivin-targeting cytotoxic T lymphocytes (54) and survivin-directed immunization (55, 56), the later also combined with immune checkpoint blockers (NCT03349450). However, caveats to immune-based therapies remain the high cost associated to adoptive T cell therapy (57), tumor heterogeneity with regards to TAAs (58) and absence of long-lasting efficiency in survivin-directed immunization (59).

#### 1.2.2.2. Small molecules inhibitors

The most studied survivin-targeting small molecule is the imidazolium-based compound, YM155. The molecule's mechanism of action was first assumed to be due to inhibition of survivin's

promoter region at the DNA level (60). Later on, it was speculated that YM155 actually induced DNA damage and resulted in survivin inhibition in an unspecific fashion (61, 62). Regardless of its true pharmacodynamics, YM155 inhibited tumor growth in several cancer models either alone or in combination with other anti-cancer strategies both *in vitro* (63, 64) and *in vivo* (65-67). YM155 sensitized human RB cells (Y79) to carboplatin, *in vitro* and in an orthotopic RB model (68). Finally, the molecule gathered enough evidence to move forward towards clinical trials. Although encouraging results were reported combining YM155 with CD20-targeting monoclonal antibody to treat relapsed aggressive B-cell Non-Hodgkin lymphoma (69), only modest efficacy or failure to achieve primary endpoints were reported in other trials (70-73). No clinical trial is currently active to investigate YM155 as an interventional drug to treat cancer (clinicaltrials.gov as of October 23 of 2019).

#### 1.2.2.3. mRNA targeting strategies

Another strategy to circumvent the undruggable survivin protein is to repress its expression by cleaving the mRNA precursor. Ribozymes are enzymatic RNAs capable of recognizing an mRNA target and cleaving it, impairing protein translation (74). Survivin-targeted ribozymes sensitized prostate cancer (75), lung adenocarcinoma (A549) (76) and breast cancer cells (MCF7) (77) to etoposide, and head and neck squamous cell carcinomas to etoposide and carboplatin (78). Although interesting results were achieved *in vitro*, no survivin-targeting ribozyme-based strategy was further developed *in vivo*.

A second survivin mRNA-targeted strategy is antisense oligonucleotides (ASO). ASO are a single RNA or DNA strand complementary to a target mRNA sequence. ASO may exert their repressive effect by recruiting enzymes to cleave the ASO-mRNA complex, modulating mRNA splicing or steric blocking of ribosome-mediated translation (79). LY2181308 is an ASO against survivin that demonstrated good human tolerability (80), tumor bioaccumulation, evident survivin silencing and restored tumor apoptosis signaling (81) in a phase I human trial, but failed to achieve its primary endpoint at a subsequent trial in combination with docetaxel (82, 83). No clinical trial is currently active using LY2181308 as an anti-survivin strategy (clinicaltrials.gov).

Finally, small interfering RNA (siRNA) has been used as anti-survivin strategies. siRNA is a double-stranded RNA that, when incorporated into the cells, activates the well-conserved naturally occurring RNAi mechanism to mediate mRNA cleavage and protein silencing (84). Mechanistically, once inside the cell, the double-stranded siRNA is incorporated into the RNA-induced silencing complex (RISC) which unwinds and cleaves the sense strand through the argonaute 2 (AGO2) enzyme-containing within the RISC. The antisense strand remains in the RISC and the now active RISC-antisense strand complex seeks the complementary RNA sequence to mediate mRNA suppression (Figure 6). Long double-stranded siRNA follows the same pathway once it is cleaved in the cytoplasm into siRNA by the enzyme DICER. The silencing complex is regenerated after each mRNA cleavage, being capable of promoting gene silencing for less than a week in rapidly dividing cells, but up to 3 weeks in slow dividing ones (85).

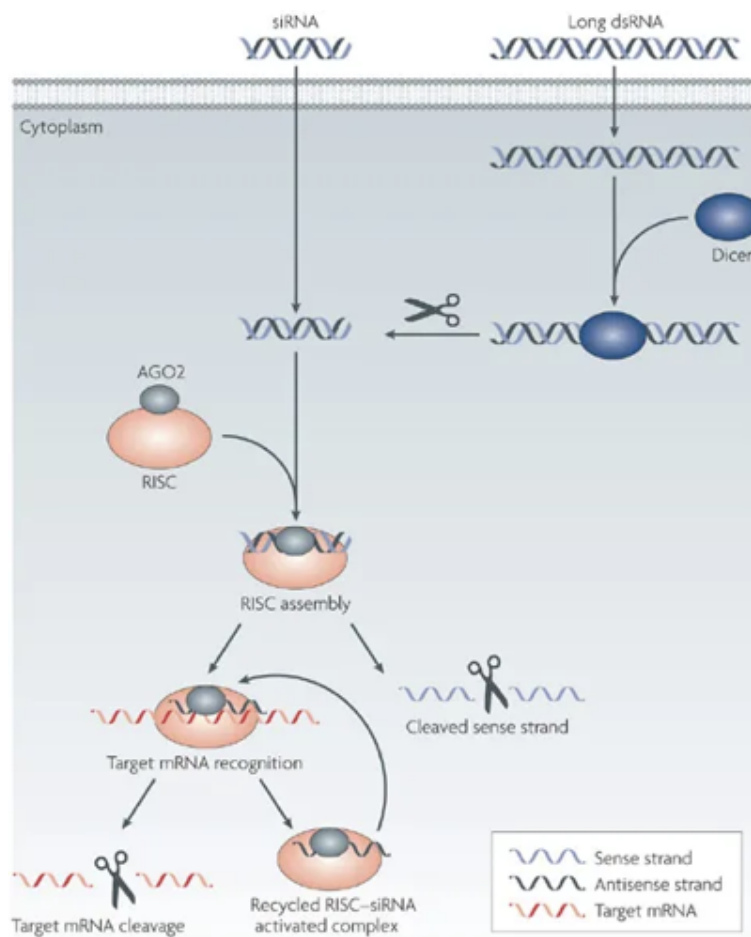


Figure 6. – Mechanism of siRNA-mediated mRNA silencing (86).

Survivin-targeting siRNA has demonstrated tumor growth inhibition in patient-derived colorectal cancer (87) and glioblastoma (88) xenografts. In retinoblastoma, survivin-targeted siRNA inhibited human RB cells (Y79) proliferation, growth and invasiveness, *in vitro* (89, 90). As an adjuvant therapy, siRNA against survivin sensitized SKOV-3 cells to cisplatin (91), synergistically improved paclitaxel tumor growth inhibition in breast-cancer bearing mice (92) and reversed Apo2L/TRAIL resistance in melanoma cells (93).

Despite the remarkable success *in vitro*, siRNA-based therapies face considerable challenges to be translated *in vivo*. Biological barriers naturally evolved to prevent eukaryotic cell infection by exogenic nucleic materials. Of many naturally occurring biological barriers that need to be surmounted before clinical translation, 3 are primarily addressed during *in vitro* optimization: poor serum stability, low cell penetration due to electrostatic impairment and lysosomal degradation of the fraction uptaken by the cell (94). Fortunately, it is possible to circumvent the pitfalls that restrain siRNA delivery using viral or non-viral vectors (95). In fact, the latter approach has recently been responsible for OnPattro, the first RNAi-based drug to be approved by the FDA in 2018 (96), a milestone for gene therapies that shed a hopeful light into the future of gene medicines. **Lipid nanoparticles (LNP)**, a non-viral vector approach for gene medicines delivery, as taken the siRNA strategy from the bench to the bedside.

### **1.3. siRNA delivery**

#### **1.3.1. Challenges and vector rational design**

Gene silencing through siRNA technology has significantly pushed the medical frontier forward. Numerous siRNA-based therapeutics are now on clinical trials (97) following the steps of the first FDA-approved RNAi-based drug, OnPattro (Patisiran). Considering non-viral vector approaches, siRNA could be delivered as lipoplexes or polyplexes, if carried through a lipid or polymer formulation, respectively. A first essential step before proposing an optimal carrier to enable siRNA delivery is to understand the chemical nature of siRNAs to identify their weakness and biologically imposed barriers.



Structurally, siRNA is a double-stranded RNA, containing ~21-23 base pairs anchored in a ribose backbone linked by anionic phosphodiester bonds (Figure 7). The hydroxyl group in the 2' position of ribose moiety renders chemical susceptibility to siRNA, especially to serum nucleases. The 2' position is often used for chemical modification to improve siRNA stability (98).

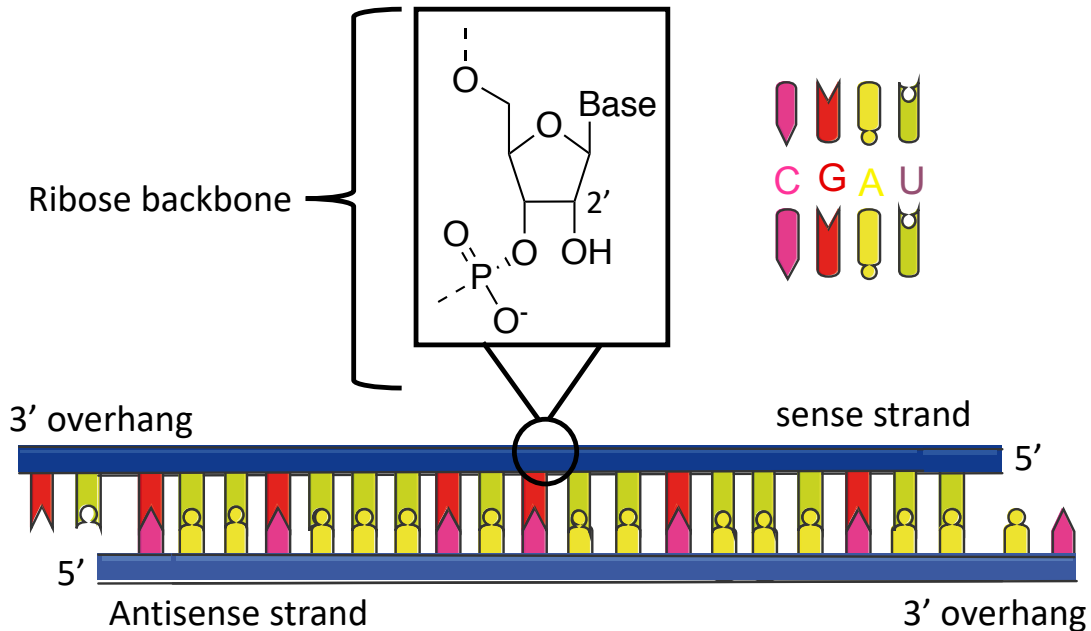


Figure 7. – General structure of unmodified siRNA.

By its structure, it is possible to identify the siRNA as a highly hydrophilic and negatively charged macromolecule with susceptible instability against nucleases. The first chemical characteristic implies two additional challenges: big macromolecules as siRNAs (i) cannot cross the cell membranes due to electrostatic impairment and low lipophilicity (94), and (ii) are rapidly eliminated through renal clearance (99). Considering that an intact siRNA reaches the desired cell and is internalized, nature imposes yet another challenge; upon endocytosis, the siRNA must escape the endosomal compartment before vesicle maturation and eventual lysosomal degradation of siRNA (100). Based on these assumptions, a good vector candidate must minimally act at 3 levels: (i) complex the siRNA, protect it from nuclease degradation and avoid fast renal clearance, (ii) promote cell internalization and (iii) allow endosomal escape and cytosolic delivery of intact siRNA. The aforementioned barriers and other physiological challenges to be circumvented by siRNA strategies are summarized below (Figure 8).

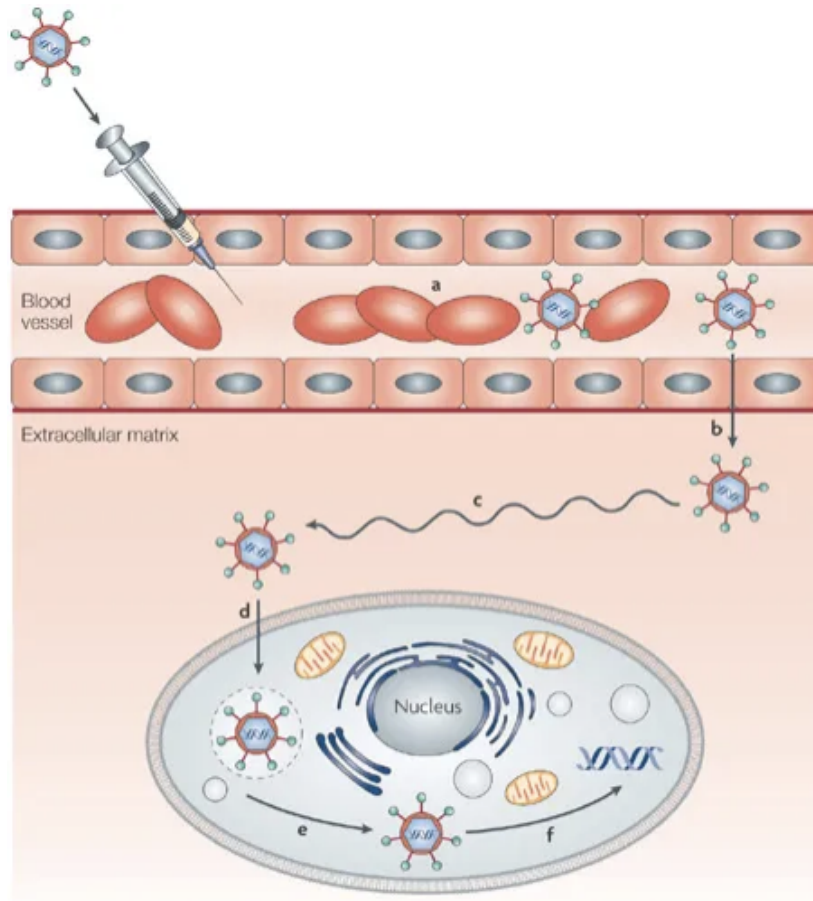


Figure 8. – Physiological barriers faced by siRNA strategies. (86). The vector carrying the siRNA should (a) avoid renal clearance, phagocytosis and protect siRNA from blood stream degradation; (b) be transported across endothelial barrier; (c) reach the target site; (d) be taken up into the cell; (e) mediate endosomal escape; (f) promote cytosolic delivery of siRNA.

Being aware of the limitations involved in siRNA delivery, we can now propose a bottom-up approach to design an optimal non-viral vector harboring the essential moieties required to overcome each challenge.

#### 1.3.1.1. siRNA Complexation and serum stability

An ideal candidate for siRNA delivery would be able to closely pack the siRNA, protecting it from nuclease degradation. Obvious candidates would take advantage of the negatively charged phosphate groups within siRNA backbones. That's the case of cationic lipids, as 1,2-dioleoyl-3-trimethylammonium-propane (DOTAP), 3 $\beta$  - [N-(N0,N0-dimethylaminoethane) - carbamoyl]

cholesterol hydrochloride (DC-Chol) and N-[1-(2,3-dioleoyloxy)propyl] - N,N,N-trimethylammonium chloride (DOTMA), which in combination with other neutral lipids, as cholesterol and 1,2-dioleoyl-sn-glycerol-3-phosphoethanolamine (DOPE), self-assemble with siRNA into lipoplexes for efficient gene delivery *in vitro* (101-103). The branched cationic polymer polyethylenimine (PEI), as its lipids counterpart, also self-assembles with nucleic acids into polyplexes (104). However, the resulting positively charged lipo- and polyplexes (nanocomplexes) are rapidly coated by negatively charged serum proteins *in vivo*, halting transfection ability and promoting its recognition and clearance by macrophages (105). An elegant approach to hinder the nanocomplexes from reticuloendothelial system-mediated clearance and serum proteins adsorption was incorporating polyethylene glycol (PEG)-grafted lipids or polymers can provide to nanocomplexes stealth properties due to new hydrophilic surface coating (106). Caution must be considered when incorporating PEG-grafted elements into nanovectors since the steric hindrance provided by PEG might also prevent endocytosis and endosomal escape of genetic cargo, impairing siRNA transfection (107).

Another strategy to avoid opsonization and fast serum clearance is to eliminate the net positive charge of nanocomplexes. Ionizable cationic lipids are able to electrostatically complex siRNA at an acidic pH, where amino groups are protonated, but reach neutrality as the pH is gradually elevated at physiological values (108). After synthesizing a library of ionizable lipids, Jayaraman and coworkers (109) found DLin-MC3-DMA as the leading component with the highest silencing efficiency *in vitro*. The authors unveiled the pKa for ionizable lipids between 6.2 and 6.5 is a critical parameter effective hepatocyte gene silencing. Lipid chain length from 10 to 13 carbons was another parameter unveiled by combinatorial synthesis reported to influence siRNA efficient silencing *in vivo* (110, 111).

#### 1.3.1.2. Cell internalization

The self-assembly of the cationic vector with siRNA at the right proportion (measured as the ratio between nitrogen groups per cationic lipid/polymer and phosphate moieties in the siRNA, proportion known as the N/P ratio) results in a complex able to electrostatically bind to the negatively charged cell membrane if the overall charge of the vector is positive (112, 113). After binding, different endocytic pathways could be activated to mediate nanocomplex internalization

(Figure 9) (114-116). The mechanisms whereby nanocomplexes enter the cells are still the focus of many studies, since it relies on various parameters such as nanoparticles structure, shape, size, surface charge, but also the cell type and culture conditions. Nevertheless, a deeper understanding of these mechanisms would truly contribute to the rational design of nanovectors to gene therapy.

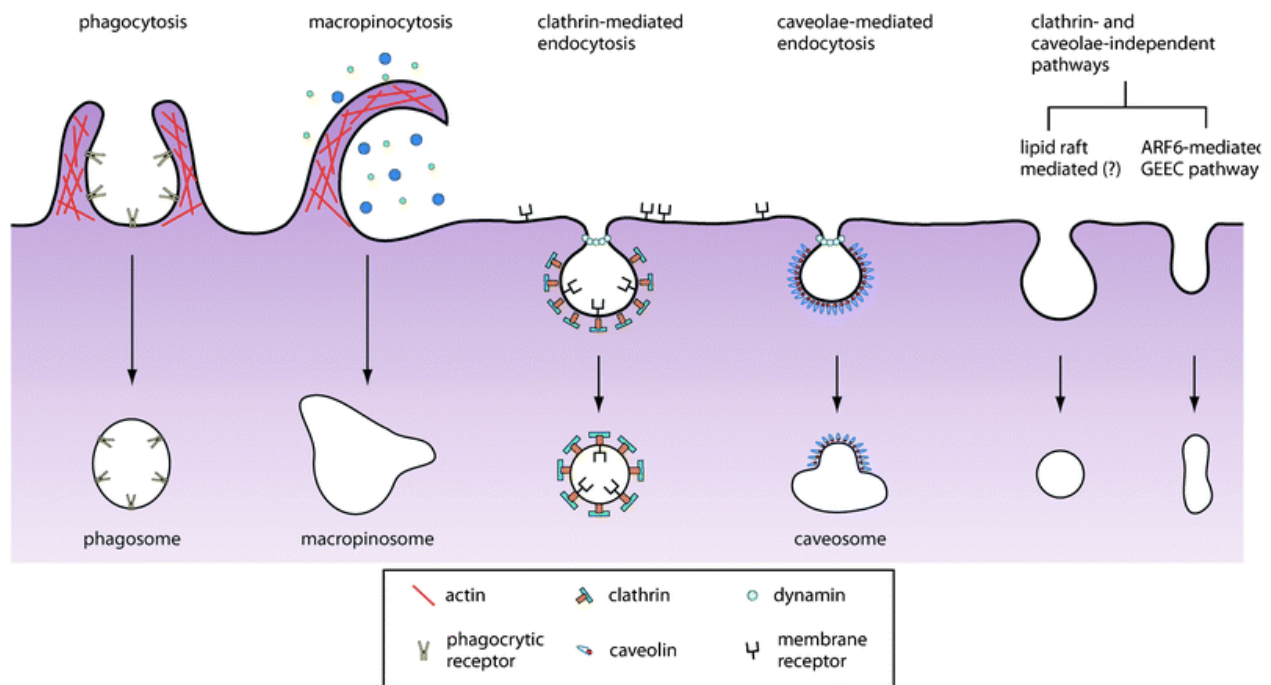


Figure 9. – Possible pathways of nanoparticles internalization (117).

### 1.3.1.3. Endosomal escape

Once internalized, nanocomplexes must avoid lysosomal degradation. Intriguingly, the majority of the cargo and vector is degraded upon endosomal maturation or recycled back to the extracellular space (115, 116, 118). Therefore, the nanocomplexes require fusogenic or endosomolytic properties to allow endosomal escape and, thus, the release of siRNA within the cytosol.

Cationic lipids are not only able to self-assemble with siRNA into lipoplexes, but also mediate endosomal escape through a mechanism known as “ion-pair” theory (119). Once inside the endosome, cationic lipids interact with the negatively charged lipids in the inner leaflet of the endosomal lumen forming an ion-pair complex, a non-lamellar (HII) structure that mediates

endosomal disruption (120). Non-lamellar lipids, like cholesterol and DOPE, known as “helper lipids”, facilitate HII transition, thus improving transfection efficiency (119) (Figure 10).

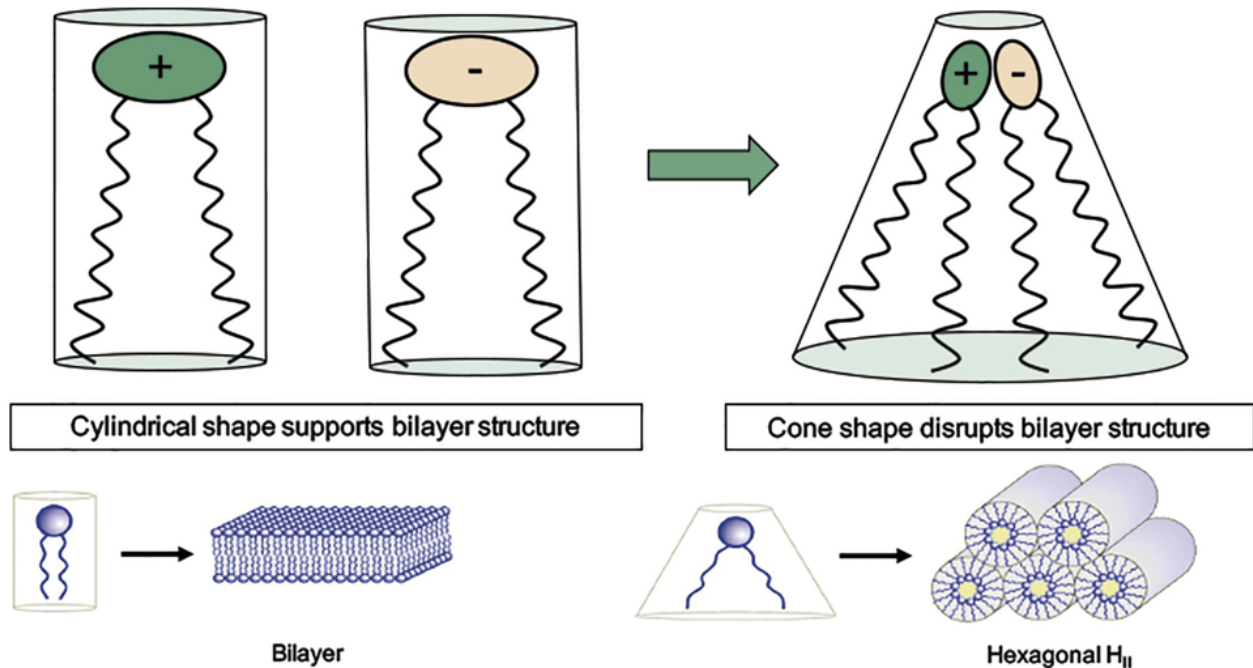


Figure 10. – Schematic diagram of the ion-pair membrane disruption mechanism mediated by cationic lipids (120). Lamellar lipids support bilayer structures whereas cone shape lipids adopt a non-bilayer conformation. The structure formed by the electrostatic interaction between cationic and anionic lipids (ion-pair) behave as a cone shape lipid, hence adopting an inverted hexagonal phase (H<sub>II</sub>) and disrupting the bilayer structure.

However, the endosomal destabilization mediated by cationic lipids is far beyond its full efficacy, as already demonstrated that only 1-2% of siRNA was released from the endosomal when encapsulated in lipid nanoparticles (LNP) containing the gold standard ionizable lipid DLin-MC3-DMA, cholesterol as helper lipid, DMG-PEG for stealth properties and distearylphosphatidyl choline (DSPC) as membrane structural lipid (116). Therefore, endosomal entrapment is still a major barrier that prevents full translation of siRNA therapies mediated by non-viral vectors. Researchers have addressed this issue by developing responsive materials to improve endosomal escape, thus enhancing cytosolic delivery of siRNA. Adding a pH-responsive material into lipoplex composition has shown to promote cytosolic delivery of siRNA and efficient silencing *in vivo* (121, 122).

Based on these premises, an ideal classical non-viral vector for siRNA delivery would contain at least, but not limited to, the following components:

General:

- A cationic moiety for siRNA complexation and initial cell-binding;
- A PEG-grafted component for stealth properties;

For lipoplexes:

- A “helper” lipid to ameliorate non-bilayer transition and boost endosomal escape and;
- A structural lamellar-forming lipid.

Such a design was employed in the development of OnPattro (Patisiran) formulation, the first RNAi-based drug to be approved by the FDA (table 1).

Lipid component	Function
DLin-MC3-DMA	<ul style="list-style-type: none"> <li>• Complexes siRNA at values below pKa</li> <li>• Mediates endosome disruption (ion-pair complex with negatively charged lipids inside the endosome lumen)</li> </ul>
Cholesterol	<ul style="list-style-type: none"> <li>• helper lipid</li> </ul>
DSPC <sup>1</sup>	<ul style="list-style-type: none"> <li>• Structural lipid</li> </ul>
DMPG-PEG <sup>2</sup>	<ul style="list-style-type: none"> <li>• Provides stealth property</li> </ul>

<sup>1</sup>DSPC: 1,2-distearoyl-sn-glycero-3-phosphocholine; <sup>2</sup>DMPG-PEG: 1,2-dimyristoyl-rac-glycero-3-methoxypolyethylene glycol-2000

Table 1. – OnPattro (Patisiran) composition and role of each lipid component (120).

Lipid nanoparticles (LNP) are the most advanced non-viral vectors for gene medicines. Therefore, we will focus on methods of preparation for LNP, exemplifying *in vitro* or *in vivo* approaches of siRNA delivery. Next-generation of responsive LNP capable to boosting cytosolic delivery of siRNA upon endosomal acidification, pH-sensitive LNP, will also be presented.

### 1.3.2. Methods of preparation for lipid nanoparticles (LNP)

#### 1.3.2.1. Lipid nanoparticles (LNP)

Liposomes are defined as spherical structures composed of an aqueous core enclosed by one or more lipid bilayers. Initially proposed by Bangham as simplified cell membrane models in the early 60s (123, 124), the potential of liposomes as drug and gene carriers has significantly advanced (94, 120, 125).

The classic method for designing liposomes to enable siRNA delivery consist of (A) formulating cationic liposomes, (B) submitting resulting lipid vesicles to size reduction and homogenization and (C) incubation with siRNA to afford LNP (Figure 11).

- A. Pre-formulated liposomes are prepared by hydrating a lipid film. Briefly, the lipids are selected based on the rational design of a gene delivery vector as aforementioned discussed, and solubilized in an organic solvent, preferentially ethanol to decrease in vivo toxicity of traces of organic solvent. In a round bottom flask, the organic solvent is evaporated under reduced pressure, forming a thin lipid film, which is then hydrated with an aqueous solution of low concentrated buffer or 5 % dextrose solution to maintain human osmolarity compatibility (Figure 7A). Hydration of the lipid film will afford multilamellar vesicles (MLV).
- B. MLV are subsequently submitted to size reduction by extrusion through polycarbonate membranes of defined porosity (Figure 7B). The resulting homogeneous vesicles could be classified as small unilamellar liposomes (SUV) if smaller than 100 nm or large unilamellar liposomes (LUV) if bigger than 100 nm but smaller than 1000 nm.
- C. SUV or LUV are diluted in dextrose 5% to achieve the desired N/P ratio before combining with genetic cargo to afford a complex structure containing a centered aqueous core with the genetic cargo complexed between the multilayers of the lipoplex (120, 126) (Figure 7C).

The hydration of the lipid film, extrusion and self-assemble of SUV with genetic material into lipoplexes are carried at a temperature above the gel-to-liquid transition ( $T_m$ ) point for the lipid composition.

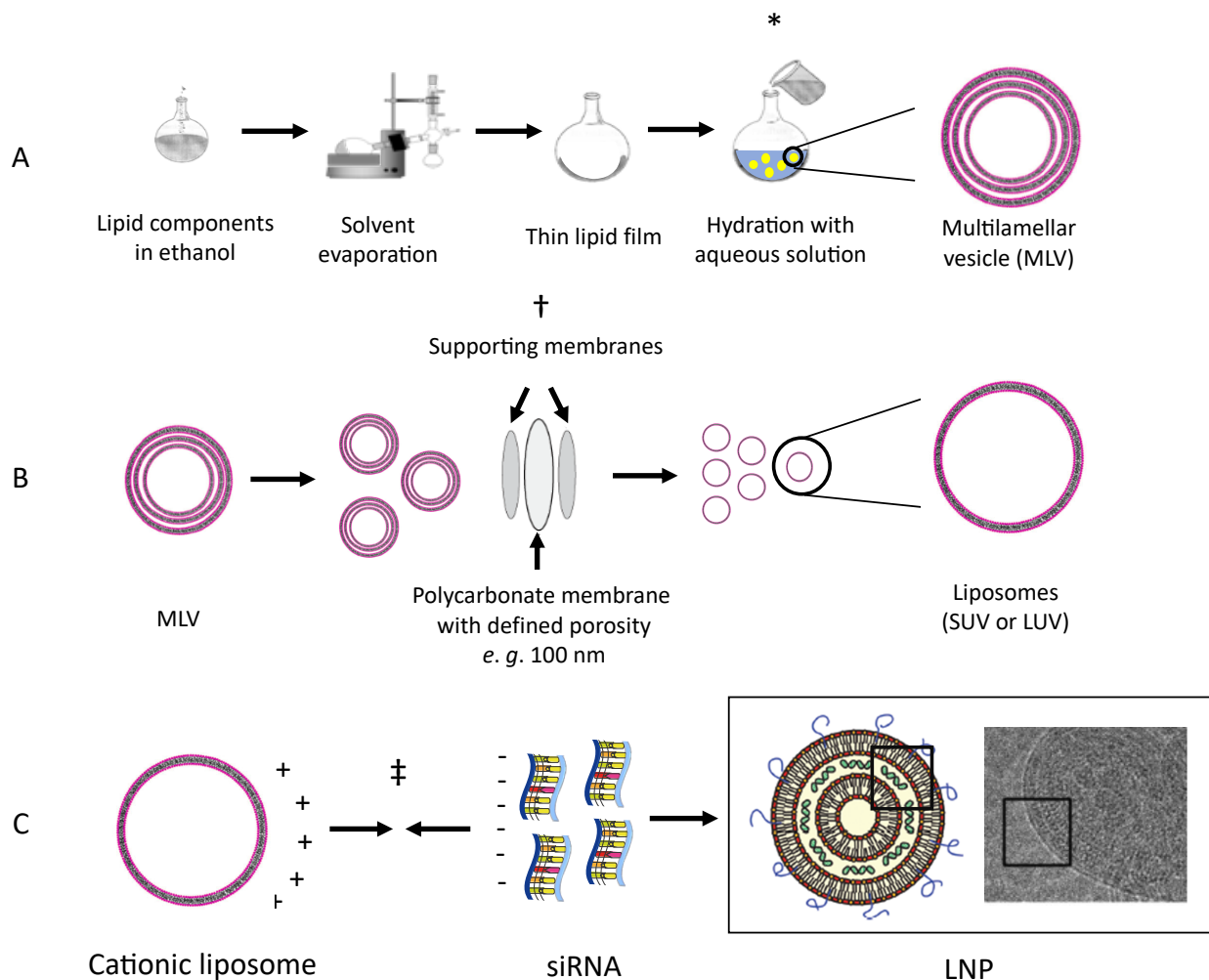


Figure 11. – Stepwise representation of LNP preparation by combining preformed liposomes with siRNA. See the text for details. Big square: left: schematic representation of PEGylated lipoplex with siRNA complexed within lipid bilayers; right: cryo-TEM micrograph of cationic lipid/siRNA complexes (bis (guanidinium)-tren-cholesterol (BGTC):siRNA) (127). Small boxes highlight the siRNA complexed within the bilayers of the lipoplex. \*, † and ‡ indicate steps performed under heating.

A second approach consists of an all-in-one fast mixing step of an organic (ethanol) lipid solution with an aqueous solution containing the genetic cargo to spontaneously afford lipid nanoparticles. The strategy was further optimized with the advent of microfluidic devices for the controlled and reproducible mixing process.



Briefly, two syringe pumps are oppositely placed, one loaded with an aqueous miscible organic solvent containing a mixture of desired lipids, whilst the second contains the genetic cargo solubilized in an aqueous solution. Pumps are connected into a mixing Tee, or a microfluidic chamber, with an exit tubing towards a sterile container to receive the resulting LNP (Figure 12). The lipid and nucleic acid solutions are mixed at a controlled ratio and speed and, as the polarity of the system is increased, the lipids spontaneously self-assemble onto the genetic cargo brought together by electrostatic interaction (Figure 12A). The inverted micelles containing the genetic cargo enclosed at internalized aqueous cores are finally surrounded by PEGylated lipids, which maintain the hydrophilic head group orientated towards the exterior aqueous medium (figure 12B). LNP is dialyzed against low concentration buffer or 5% dextrose to remove the ethanol (Figure 12C).

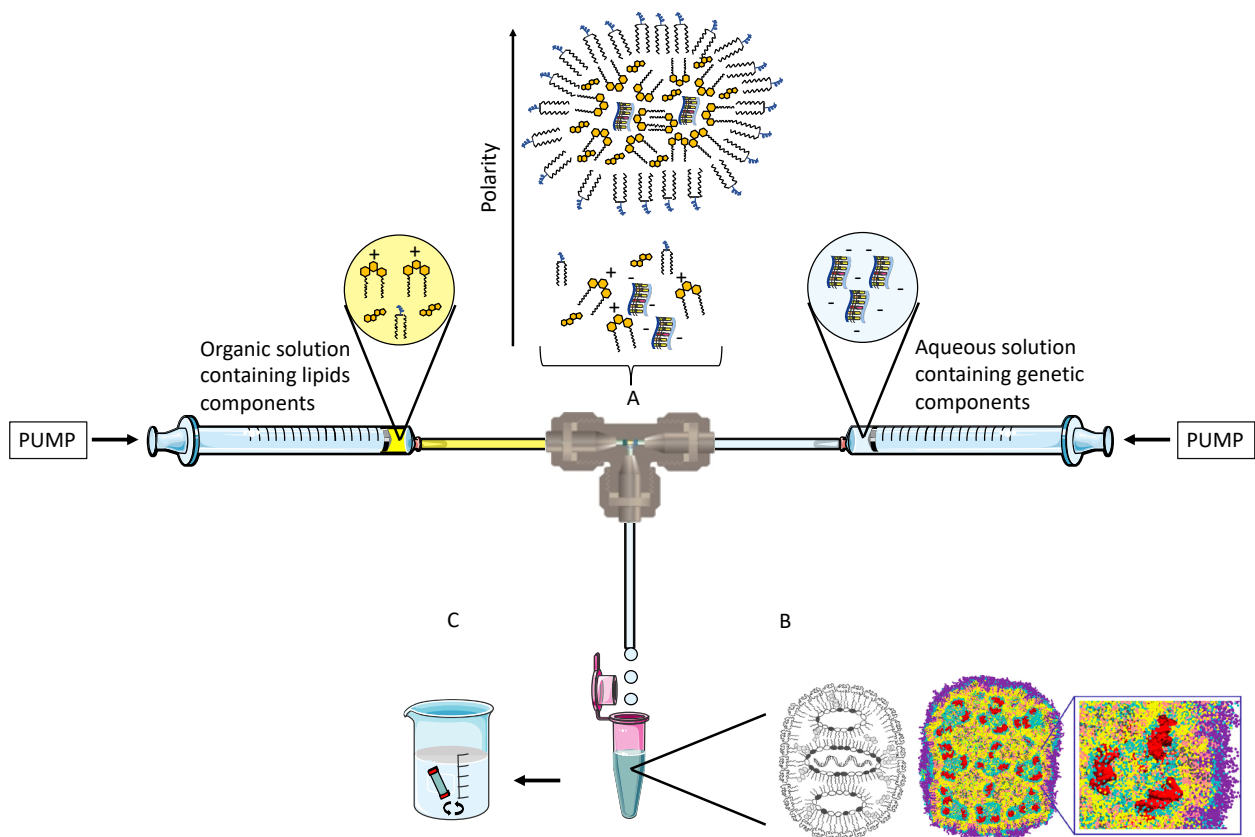


Figure 12. – Schematic representation of siRNA encapsulated LNP formulated by microfluidics technique. (A) represents the interior of the mixing tee chamber. As the polarity is increased, the siRNA precipitates at the interior of the newly formed LNP. (B) Left in black and white: schematic

representation of LNP. Middle, colored: Molecular representation of LNP. Yellow, cyan and pink represent lipids; red is the complexed siRNA, while blue is the PEGylated shell. Right, colored: zoom view of the LNP interior. (C) Dialysis against an aqueous solution as the final step to remove the solvent. Adapted from (120, 128).

T tube/microfluidics mixing affords smaller LNP than when prepared by pre-formulate liposomes due to all-in-one precipitation of materials at the interior of LNP rather post-complexation of siRNA within the multilayers of lipoplexes (Figure 13).

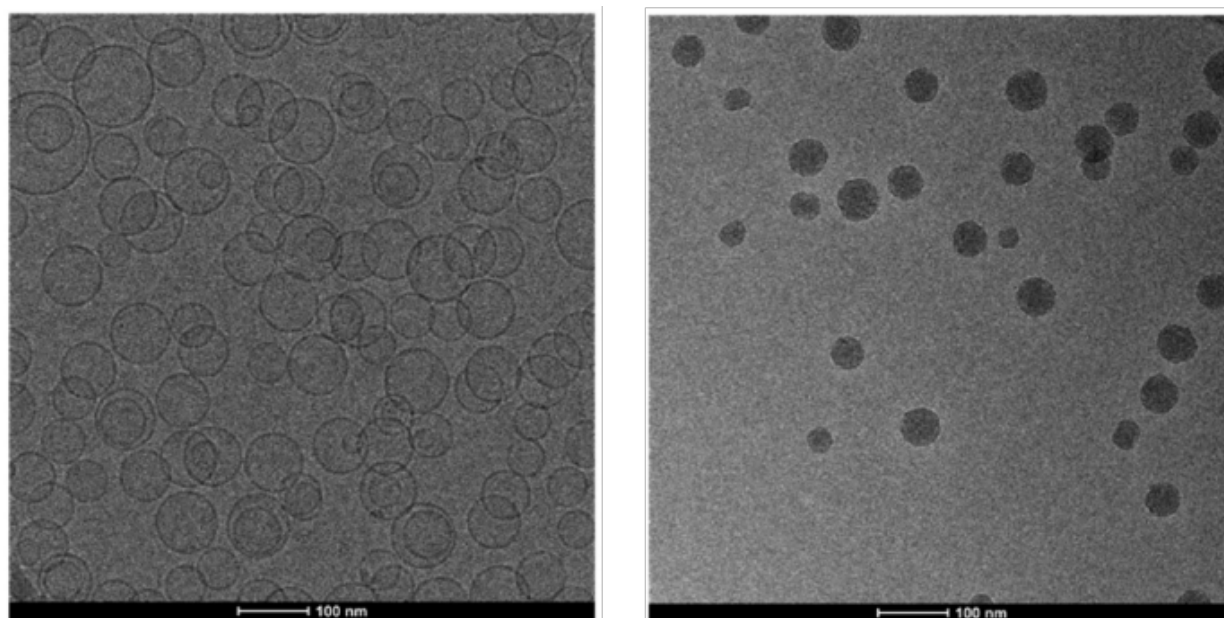


Figure 13. – Cryogenic transmission electron microscopy (Cryo-TEM) micrographs of extrusion- and microfluidics-formulated liposomes. Left: POPC:Cholesterol (1:1 mol/mol) liposomes formulated by the extrusion method. Unilamellar liposomes formulated by this method present an aqueous core surrounded by a lipid bilayer. Right: Cationic liposomes formulated by microfluidics technique (DLinKC2-DMA/DSPC/Chol/PEG-lipid (40/11.5/47.5/1 mol/mol). Adapted from (128).

#### 1.3.2.2. pH-sensitive liposomes

Stimuli-responsive delivery systems take advantage of early endosomal acidification to promote membrane destabilization and fast cytosolic cargo delivery. It is now recognized that optimal lipid formulation requires a pH-sensitive component. To this end, numerous pH-sensitive materials,

based on polymers, peptides, or hydrolyzable chemical bonds, have been developed. Our laboratory previously demonstrated the efficiency of a **pH-sensitive liposome** based on a principle of a molecular switch (129). In this lipid structure, the di(methoxyphenyl)-pyridine is in a trans conformation with the pyridine nitrogen (Figure 14A). The protonation of pyridine (predicted  $pK_a \approx 5.28$ ) at a value within the early endosomal pH ( $\sim 5-6$ ), triggers the conformation change to enable H bonding between di(methoxyphenyl) group and the protonated pyridine (Figure 14B). By consequence, the alkyl chains change from a lipid stacking bilayer-favoring position to an open bilayer-disfavoring conformation that might destabilize the endosomal membrane, promoting siRNA cytosolic delivery (Figure 14C).

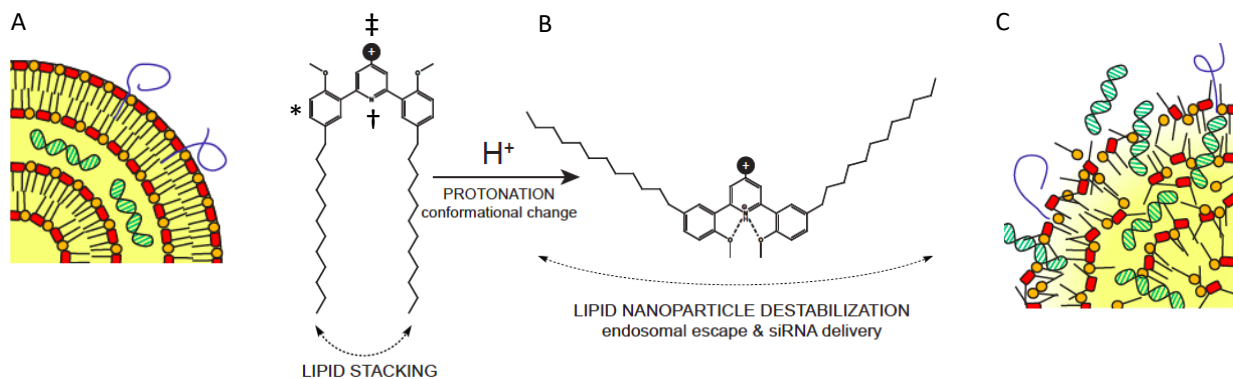


Figure 14. – pH-sensitive lipid undergoes conformation change upon acidification leading to switchable LNP destabilization and siRNA delivery. (A) Left: Schematic representation of switchable LNP Right: Structural representation of cationic switchable lipid. \* is the di(methoxyphenyl)-pyridine pH-switchable unit; † site of protonation under acid environment; ‡ cationic polar group responsible for complexing the genetic material. (B) protonation-induced conformational change of switchable lipid. (C) Schematic representation of the destabilized switchable LNP and siRNA delivery upon tweezer-like proton-induced conformational change. Adapted from (121).

The switchable LNP successfully delivered hydrophilic cargo *in vitro* (130) and it was further optimized into a cationic switchable LNP, able to deliver a GFP-targeted siRNA *in vitro* (Figure 15A). Three different switchable lipids, CSL1, CSL3 and CSL3 were synthesized on that study. CSL3 possessed a predicted  $pK_a$  within the early endosomal pH and constituted the most efficient

cationic switchable LNP in the *in vitro* assay. The transfection ability of CSL3 (from this point on in this investigation, one will refer to CSL3 only as CSL) was further evaluated in a proof-of-concept *in vivo* study using the cationic switchable LNP carrying the factor VII-targeted siRNA for hepatic targeting (Figure 15B) (121). The specific pH-triggered siRNA delivery through cationic switchable LNP was confirmed by the inability of the non-switchable LNP (formulated with compound CSL4) in silencing the targeted protein both *in vitro* and *in vivo*. CSL4 does not possess the two methoxy moieties necessary to initiate pH-triggered intramolecular hydrogen bonding with the protonated pyridine, thus preventing conformational switch and LNP destabilization.

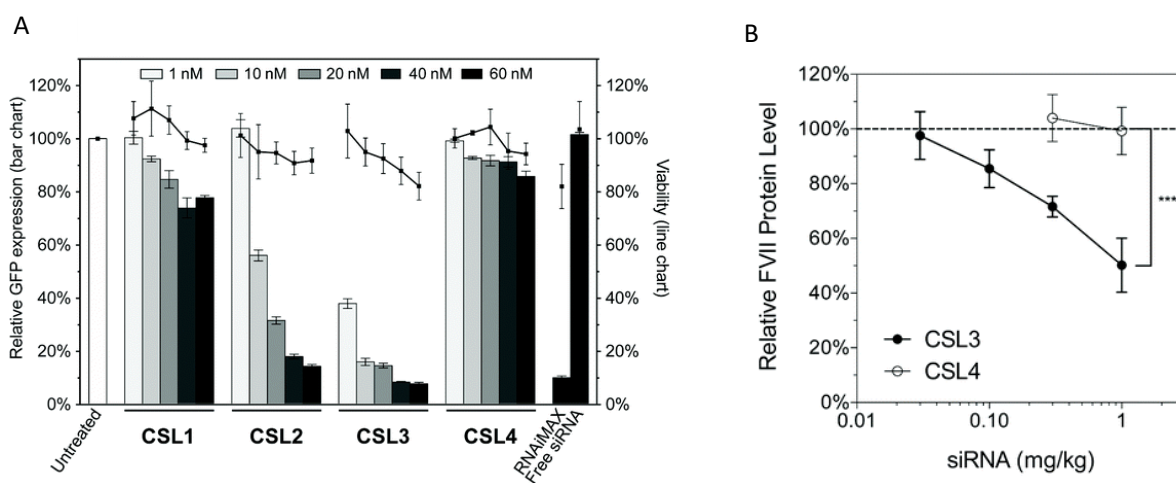


Figure 15. – Cationic switchable LNP efficiently delivered siRNA *in vitro* and *in vivo*. (A) GFP *In vitro* knockdown and viability of GFP-HELA cells after GFP-targeted siRNA transfection by cationic switchable LNP. (B) *In vivo* hepatic targeting of cationic switchable LNP carrying factor VII-targeted siRNA (121).

Importantly, the efficient cytosolic delivery of genetic cargo was not impaired by PEGylated liposomes formulated by either microfluidics for *in vivo* siRNA hepatic targeting or, as demonstrated recently, by extrusion method for intravitreal delivery of micro RNA (mir-181a) (122). In that study, Tabatabaei and coworkers demonstrated that cationic switchable lipid prepared with indocarbocyanine dye accumulated within retinoblastoma cell lines as soon as 2 hours after transfection, with strong internalization visualized 24 hours initial incubation (Figure 16A). Previously, the same group had attested that the switchable LNP preferentially accumulated within RB tumor cells, sparing retinal and adjacent tissues after intravitreal injection in an

orthotopic rabbit RB model (Figure 16B) (131). The ability of cationic switchable LNP to accumulate within human RB cells (Y79) was reflected by the decreased viability of Y79 cells after treatment with mir-181a *in vitro* (Figure 16C) (122). Mir-181a was previously demonstrated to be downregulated in tumors and play a regulatory role during cancer development and progression (132). Finally, Tabatabaei and coworkers (122) co-encapsulated the anticancer drug melphalan and miR-181a in switchable LNP for a proof-of-concept *in vivo* study. Intravitreal injection of switchable LNP containing both melphalan and miR-181 in an orthotopic RB rat model significantly decreased the number of viable cells, as compared with animals treated with either melphalan or miR-181a-encapsulated switchable LNP (Figure 15D).

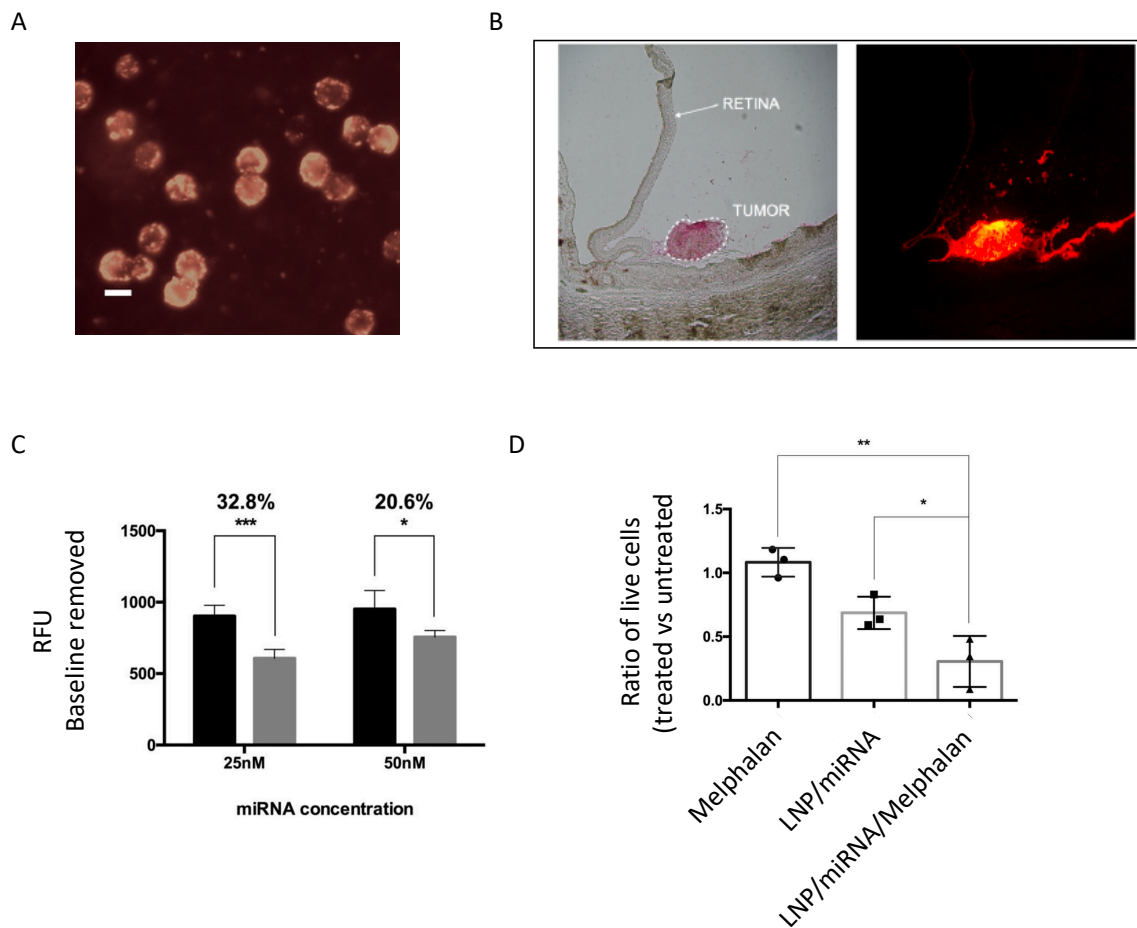


Figure 16. – Switchable LNP as a transfection vector for retinoblastoma cells (Y79). (A) switchable LNP doped with the fluorescent molecule DiIC<sub>18</sub> accumulates within Y79 cells 24 hours of transfection (exposure time 300ms, objective 40X – scale bar is 15 μm). (B) switchable LNP

doped with DiIc18 preferentially accumulates in tumor cells after intravitreal injection in an orthotopic RB rabbit model xenografted with Y79 cells. (C) 25 and 50 nM of mir-181a transfected by cationic switchable LNP impairs Y79 cells viability 48 hours after initial incubation. (D) intravitreal injection of melphalan and mir-181a coencapsulated in cationic switchable LNP significantly affected retinoblastoma cells *in vivo* as expressed by the ratio of live cells between treated and untreated cells (122, 131).

## **1.4. Hybrid polymer/lipid vesicles**

### **1.4.1. Polymersomes: definitions and structure**

Liposomes are the simplest analog model of a cell membrane, consisting of a controllable cell-like synthetic approach to investigate the complexity of living cells. Although liposomes benefit from the resemblance with the naturally occurring bilayers, especially their biocompatibility when formulated with phospholipids, the lipid vesicles lack stability, possess limited chemical functionality and are relatively permeable (133).

To overcome liposomes' limitations, a new class of cell membrane's analog has been proposed: polymersomes. Polymersomes are composed of amphiphilic block copolymers capable of self-assemble into a vesicle when in an aqueous solution (133). Unlike the hard-polymeric core nanoparticles covered so far, polymersomes consist of an aqueous hollow core surrounded by an amphiphilic polymeric shell (Figure 17).

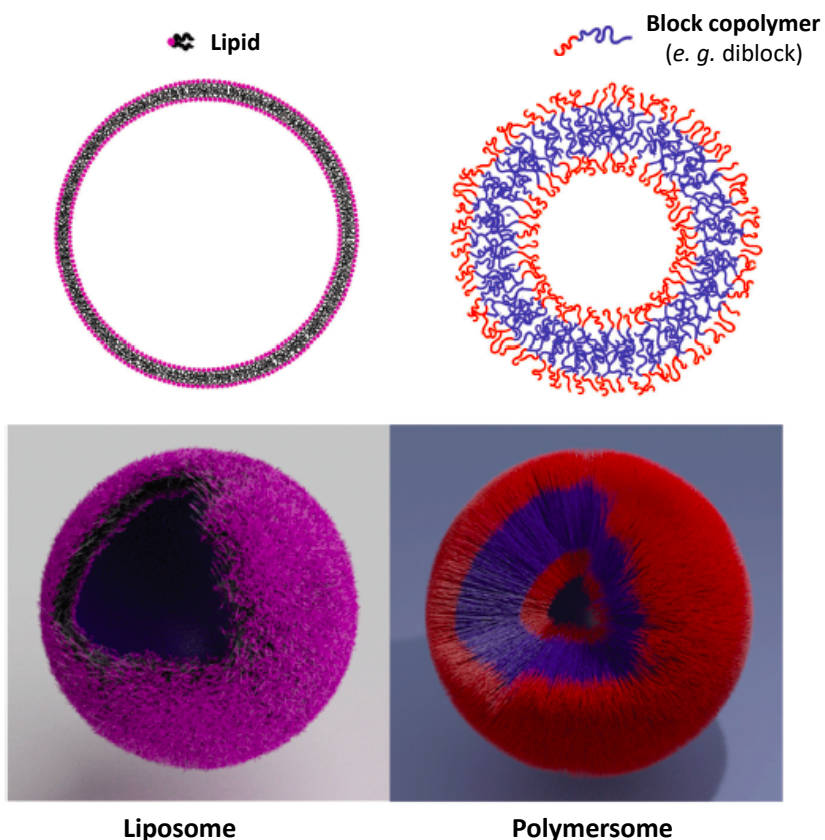


Figure 17. – Graphic representation of a liposome and a polymersome. Adapted from (133).

The advantages of polymersomes over their lipidic counterparts are their increased stability and high versatility of chemical functionalities. Furthermore, polymersomes are generally less leaky than liposomes due to a lower lateral molecule diffusion and higher molecular weight of their building block copolymers. In such structures, the release of encapsulated content occurs only through passive diffusion across the vesicle membrane (134). Nevertheless, given the feasibility and versatility of polymer chemistry, it is possible to tune polymersomes' membrane parameters and permeability (135). For example, polymersomes based on poly(dimethylsiloxane)-*graft*-poly(ethylene oxide) (PDMS-*g*-PEO) possess high fluidity and self-assemble into a vesicular structure with a membrane thickness of 5 nm, close to a typical lipid bilayer (136). Moreover, chemical modifications on amphiphilic block copolymers allow the design of “smart” polymersomes that are envisaged as nanocarriers to deliver payloads at specific locations and/or under certain microenvironments (137) or as nanoreactors (138).

Despite the physicochemical advantages of polymersomes over liposomes, the former is based on synthetic made amphiphilic copolymers, whilst the latter is made of phospholipids structurally related to biocomponents of cell membranes. In order to overcome the limited biocompatibility of polymersomes, efforts are being made to use biodegradable (139) and/or biosourced (140) copolymers. In addition, doping lipids into the polymeric membrane has been envisaged as an interesting strategy to provide biomimetic functions for those vesicles. Such a design affords structures known as hybrid polymer/lipid vesicles.

#### 1.4.2. Hybrid polymer/lipid vesicles: definition, preparation and recent developments

Hybrid polymer/lipid system consists of amphiphilic block copolymers and lipids combined in a new single hybrid membrane vesicle (134) (Figure 18). The hybrid design merges the stability and chemical versatility of polymersomes with the biocompatibility of naturally occurring phospholipids. The modulation of nature and proportion between amphiphilic block co-polymers and lipids allows fine-tuning modification of membrane properties, a useful resource to study membrane-like cells (141) or envision novel drug delivery systems.

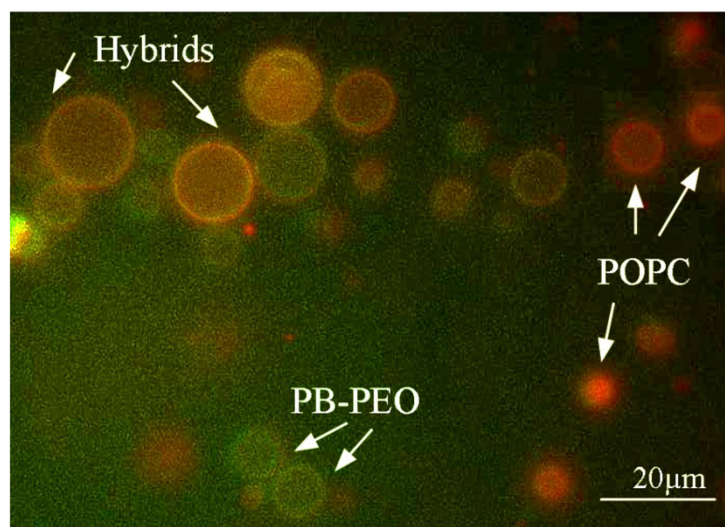


Figure 18. – Fluorescence microscopy observation of pure giant liposomes (POPC, red), polymersomes (PB-PEO, green) and hybrid polymer/lipid vesicles (Hybrids, merged color, composed of 70:30 % mol PB-PEO:POPC) (142).



It is important to note that critical parameters govern the structure of hybrid polymer/lipid vesicles. The balance between the hydrophobic length of the amphiphilic block copolymer and the hydrophobic tail of the lipid (hydrophobic mismatch), the temperature of the gel-to-liquid phase transition of lipidic components and the ratio between polymers and lipids are parameters that deeply influence hybrid membrane organization (133, 134, 143). Modulation of those parameters might lead to a homogeneous hybrid membrane (Figure 19A), the presence of lipid nanodomains (Figure 19B) or budding and eventual segregation of the hybrid vesicle into pure liposomes and polymersomes (Figure 19C).

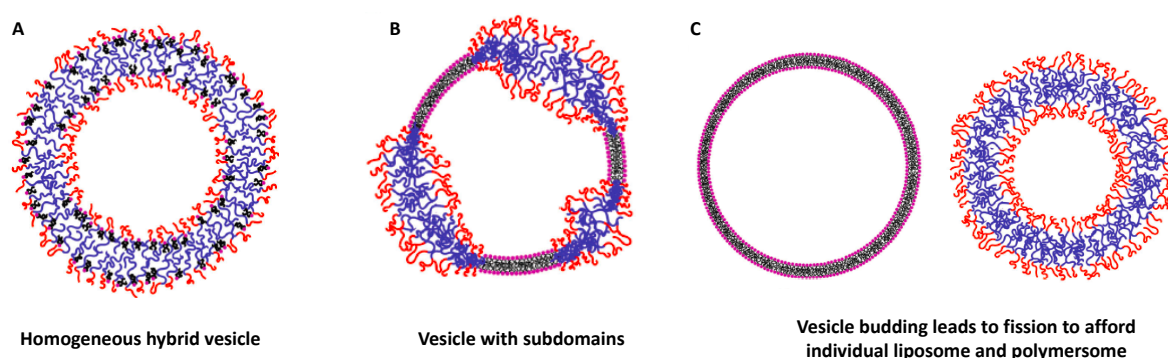


Figure 19. – Graphical representation of possible hybrid membrane phase arrangements (133).

Research carried by Chemin and coworkers (144) and the implications thereof, further reviewed by Le Meins and coworkers (134), provided a well-accepted understanding of the parameters governing the spatial disposition of lipids and polymers within a hybrid vesicle. Considering a above micron hybrid system composed of PDMS-g-PEO, which naturally self-assembles into polymersomes with approximately 5 nm membrane thickness, close to liposomes' thickness (133), the hybrid membrane arrangement relies on the molar proportion between the polymer and lipids and the thermodynamic phase of the phospholipids (Figure 20). For instance, a hypothetical hybrid polymer/lipid composed of amphiphilic diblock PDMS-g-PEO and the phospholipid POPC, which is the liquid state at room temperature, will present a homogeneous membrane at lipid content up to 60% (Figure 20). Molar amounts higher than this threshold will lead to lipid/polymer demixing, budding and eventual fission originating pure liposomes and polymersomes.

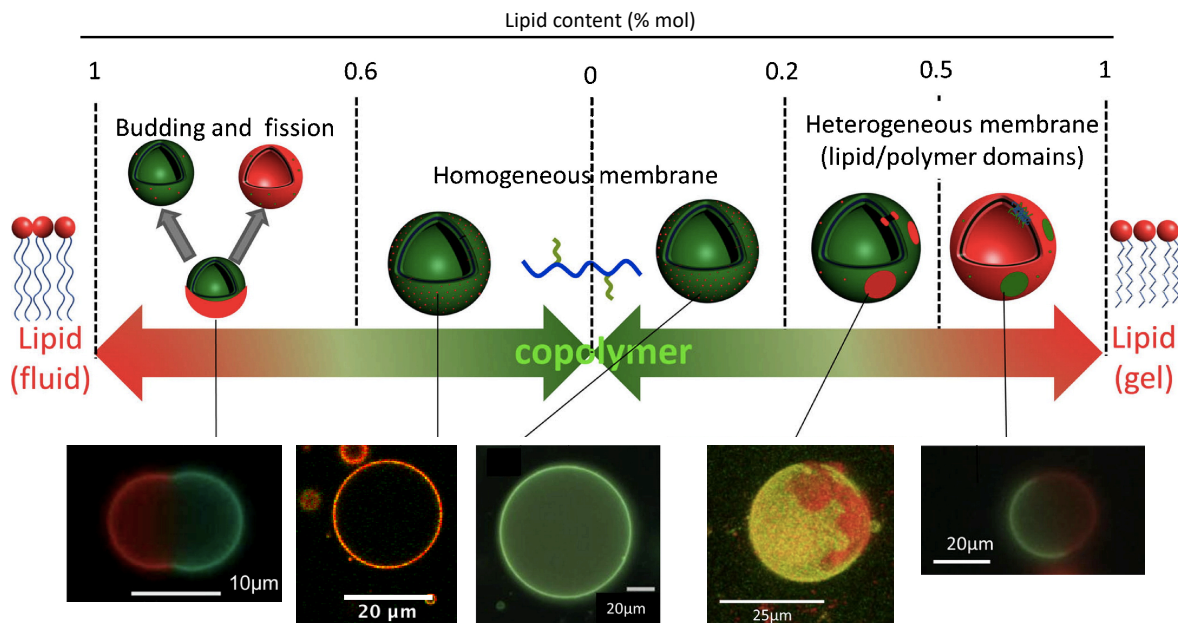


Figure 20. – Different membrane arrangements of a hybrid vesicle with regard to molar proportion between the polymer and lipid content and the thermodynamic phase of the phospholipid. Adapted from (134).

The applications of hybrid vesicles are still in their infancy. But it is fairly accepted that blending amphiphilic block copolymers and lipids into a single membrane gives rise to a new structure with advantages of both isolated polymeric and lipidic vesicles. It is, hence, of utmost importance to understand the parameters that rule the self-assembly of a hybrid vesicle in order to precisely modulate its membrane properties to reach the desired application. The fine control of the hybrid membrane would allow researchers to interrogate complex biological processes using a simple analog vesicle. For example, the formulation of lipid rafts-bioinspired hybrid vesicle containing a lipid reservoirs would help clarify processes governed by those lipid microdomains that naturally occur in living cells, such as virus uptake (145), signaling (146) trafficking (147) and other biological events (148). At the pharmaceutical level, the polymeric feature adds stiffness to the pure lipidic membranes to circumvent liposomes' low stability in circulation. Such a robust vehicle would be desired for the development of drug carriers resistant to the strong osmotic pressure and high flow shear present in the *in vivo* environment.

Cautious consideration of preliminary data sheds the first light on the application of hybrid polymer/lipid vesicles. Hybrid vesicles composed of poly(ethylene oxide)-block-polybutadiene copolymer (PEO-PBD) and hydrogenated soy phosphatidylcholine (HSPC) at 75:25 molar ratio were not significantly toxic to human fibroblast NIH 3T3 *in vitro* up to 200  $\mu\text{M}$  of polymeric content (Figure 21A). Furthermore, HER2/neu-targeted hybrid vesicles, at the same molar ratio, significantly accumulated at the tumor site in T6–17 tumor-bearing mice 24 h post injection when compared to pure HER2/neu-targeted polymeric vesicles (Figure 21B) (149). The authors did not precise the spatial disposition of the components within the hybrid membrane.

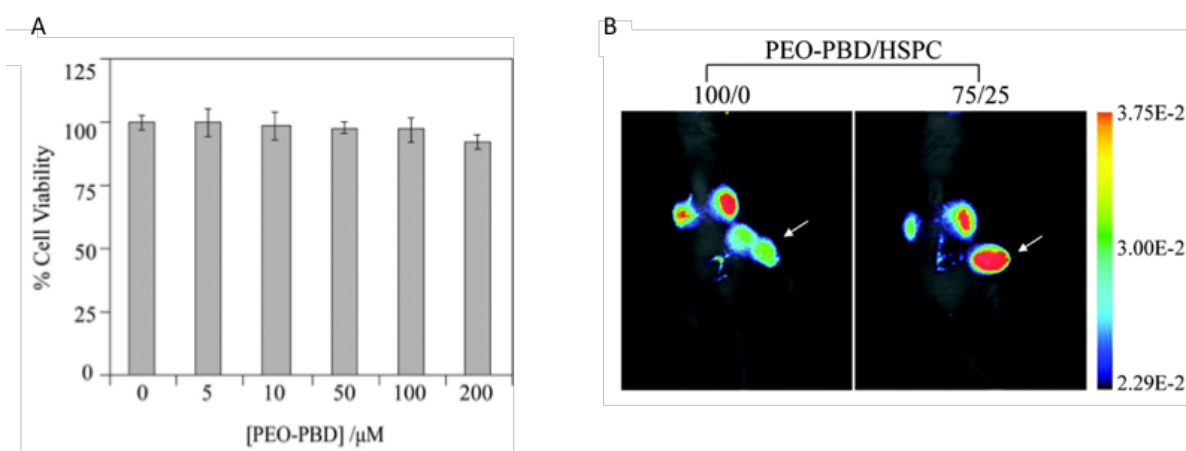


Figure 21. – *In vitro* toxicity (A) and *in vivo* targeting (B) of HER2/neu-targeted hybrid vesicles. Arrow indicates tumor site. Adapted from (149).

Similarly, Khan and coworkers (150) introduced a hybrid polymer/lipid nanovesicle composed of an amphiphilic diblock copolymer containing the FDA-approved PEG and biodegradable polycaprolactone (PCL) (PEG-PCL) and the biocompatible POPC as a promising drug carrier. The tunable hybrid vesicle had better incorporation of a small hydrophilic molecule when compared to the pure polymersome and decreased the burst release observed in pure liposomes.

In the context of cell biomimicry, the ability to modulate the composition and self-assembly of the polymer/lipid membrane turns the hybrid vesicles into a prospect attractive tool to interrogate biological processes. For example, phospholipids are unevenly distributed between the cell membrane's outer and inner leaflets (151). This biological event is not fully understood but conversely important, as lipids asymmetry mediates important biological events, as cell death

marker activation when phosphatidylserine asymmetrically accumulates at the outer leaflet (152).

Hybrid polymer/lipid vesicles might help cell biologists to better understand this phenomenon. Recently, Peyret and coworkers (153) proposed a versatile and easy approach to formulate asymmetric hybrid polymer/lipid vesicles containing POPC at the outer leaflet, whilst poly(butadiene)-b-poly(ethylene oxide) (PBut-b-PEO) formed the inner polymeric shell (Figure 22). Interestingly, the asymmetric hybrid vesicle presented phospholipid's lateral diffusion at values in agreement to ones found for lipids in biological cells, giving further support to hybrid vesicles as analog models for cell-like studies.

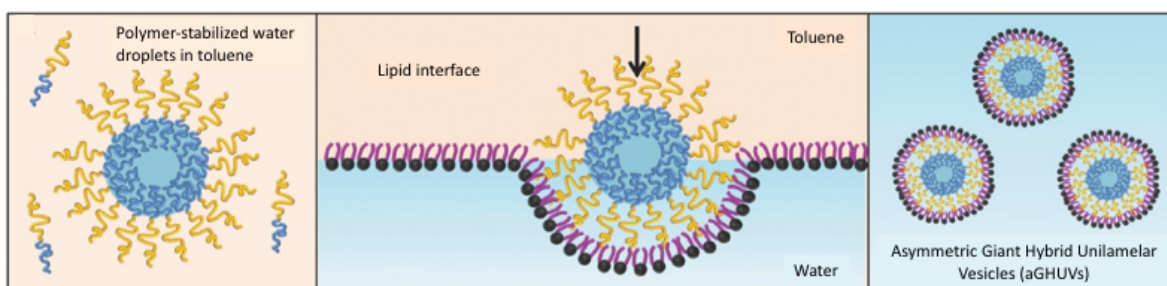


Figure 22. – Illustrative representation of the preparation of asymmetric giant hybrid vesicles containing an outer lipid layer and an inner amphiphilic diblock copolymer shell surrounding an aqueous nucleus core. Adapted from (153).

### 1.4.3. Methods of preparation for hybrid polymer/lipid vesicles

Liposomes, polymersomes or hybrid polymer/lipid vesicles can be formulated above the micron scale ( $> 1 \mu\text{m}$ ) to generate giant vesicles (Figure 23). The supramolecular structures might help to visually interrogate the behavior of stimuli-responsive components in bio-inspired environments, such as the acidified endosome. Such measurement can be highly interesting to understand the mechanism whereby lipids or polymers act inside cell compartments when formulated at nanoscale size for pharmaceutical applications, as gene vectors.

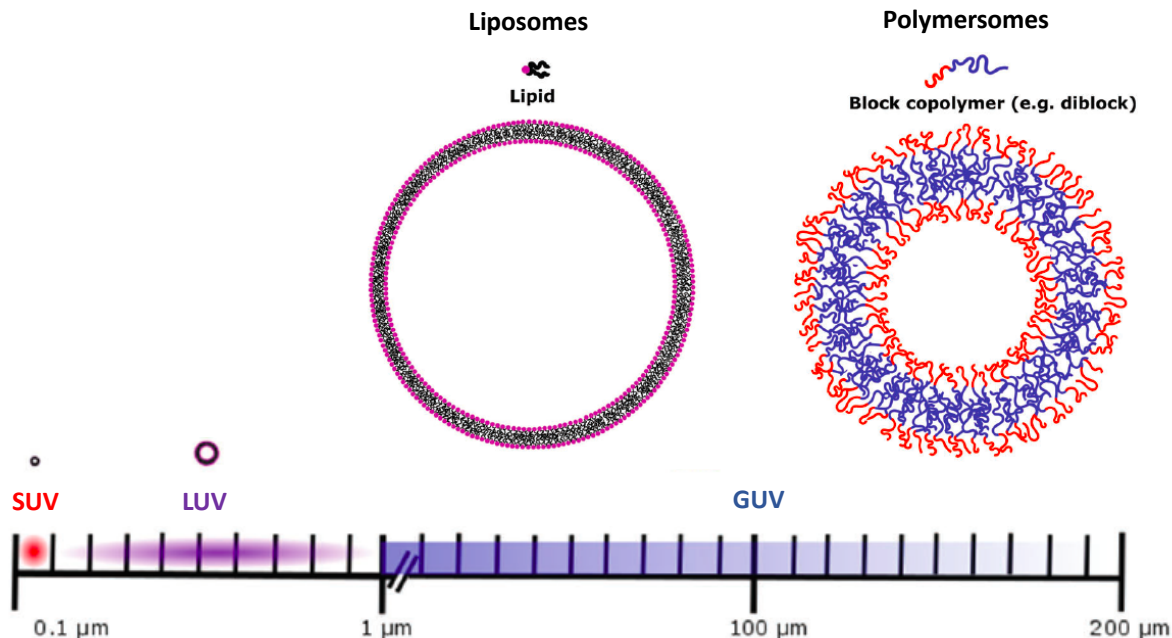


Figure 23. – Liposomes and polymersomes can be formulated at giant scale (higher than 1  $\mu\text{m}$ ). SUV: small unilamellar vesicles (< 100nm); LUV: large unilamellar vesicles (100 nm < LUV < 1000 nm); GUV: giant unilamellar vesicles (GUV > 1000 nm). Adapted from (133).

The preparation of giant hybrid polymer/lipid unilamellar vesicles is usually performed using two different techniques: the natural swelling or the electroformation methods. Either one could equally be used to prepare giant liposomes or polymersomes (154).

The natural swelling method is the simplest and practical technique for both multilamellar and unilamellar giant vesicles (154). It can be carried out for the preparation of giant vesicles with charged lipids (155). The method is similar to the one presented earlier for the preparation of liposomes, except that the hydration of the hybrid film is mandatorily executed overnight without any agitation.

The electroformation method is the most widely used method to prepare giant vesicles, and was proposed in 1986 (156). The principle of the method relies on the hydration of the lipid film by an external electric field (AC) (Figure 24). The method is successfully applied to the formation of giant vesicles with uncharged lipids or cationic charged lipids with slight modifications (157).

Briefly, a stock organic solution of polymer, lipid or a mixture of both is deposited over two indium tin oxide (ITO) coated glasses oppositely attached by an O-ring, the electroformation chamber. The electroformation chamber is further dried under reduced pressure for at least two hours. Afterward, both ITO glasses are connected to an AC generator (2 V, 10 Hz) and filled with a sucrose 100 mM solution. After 45 minutes, lipid or polymer GUV, or GHUV are harvested with aid of a 21-gauge needle and dispensed into a clean tube. GUV prepared using the electroformation method are normally unilamellar and are ready for visualization and/or further testing under confocal microscopy. The internalized sucrose solution is important when vesicles are deposited into a glucose solution-containing chamber. The density difference allows vesicles to sediment at the bottom of the observation chamber and provides a higher contrast between the inner and outer media, facilitating visualization (154).

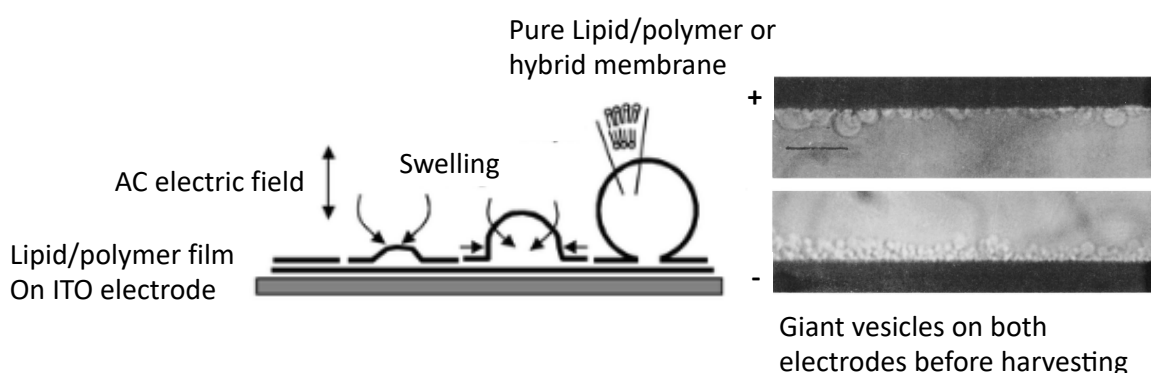


Figure 24. – Schematic representation of Giant Unilamellar Vesicles (GUV) formed by the electroformation method. Adapted from (156, 158).

#### 1.4.4. pH-sensitive hybrid vesicles: an opportunity for pH-sensitive lipids

Tuning the characteristics of the hybrid polymer/lipid membrane is achievable by balancing the nature and proportion between the amphiphilic components (134). To further boost the applicability of hybrid vesicles, it is of all interest to design responsive vesicles by adding stimuli-triggered components to the membrane composition, such as pH-sensitive lipids (130).

Several pathologies develop an acidic microenvironment as a natural physiological response. In cancer, the extracellular matrix is acidified (159). Moreover, specific cellular subcompartments,

as the ones involved in the endocytic pathway, are also marked by lower pH values (160). Exploiting this distinguishing feature by envisaging “smart” vesicles capable of a specific response to pH stimuli can have a wide range of applications, such as drug delivery systems (161, 162).

Polymersomes hold promises as drug carriers, since they are more stable, robust and retain encapsulated cargo to a better extent than liposomes. Due to the versatility of polymer chemistry, pH-responsive polymers are easily designed. A few examples of pH-responsive polymersomes were developed (163, 164). Both investigations encapsulated doxorubicin hydrochloride within polymersomes core. However, a system that allowed the fast pH-triggered release of the payload was not achieved since half of the drug amount was released at pH 5 after 24 hours of incubation in the two investigations.

Zong *et al.* (165) developed a responsive hybrid vesicle based on tertiary amine methacrylate-based block copolymers blended with phospholipids in a 70:30 weight proportion. Phospholipids consisted of a mix of neutral lipid POPC and the cationic 1-palmitoyl-2-oleoyl-sn-glycero-3-ethylphosphocholine (POEPC). The authors observed that 200 nm-extruded hybrid vesicles were readily taken up by cells and, by tracking lysosomes inside the cells, they observed that the vesicles did not fully colocalize with lysosomal compartments, suggesting that hybrid vesicles promoted lysosomal escape (Figure 25). However, more data is needed in order to confirm a pH-mediated lysosomal escape mechanism and investigate the lipid spatial distribution in the blended membrane.

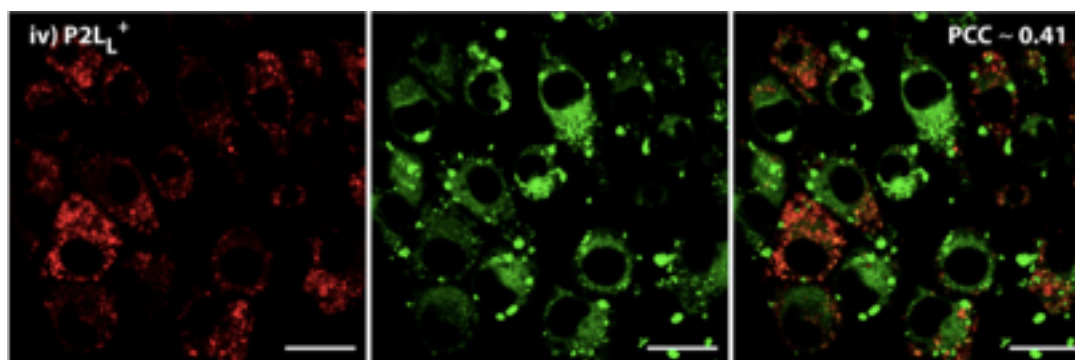


Figure 25. – Confocal observation of extruded hybrid polymer/lipid vesicles composed of cholesteryl Methacrylate (pCMA)-block-poly(2-(dimethylamino)-ethyl Methacrylate) blended with POPC and the cationic lipid POEPC (7:2:1 % wt). Hybrid vesicles were incubated for 1.5 h with

RAW 264.7 macrophages cells before visual distribution of particles within the cell. Red: lysoTracker Red DND-99-stained lysosomes. Green: NBD-tagged polymer. PCC: Pearson correlation coefficient; 1 for perfect correlation and 0 for perfect no correlation. Adapted from (165).

Therefore, tuning polymersome membrane's properties by doping pH-sensitive lipids to generate smart hybrid polymer/lipid vesicles becomes an opportunity to maintain the stiffness and robustness related to polymersomes at physiological pH, but responsive membrane properties at acidic environments. So far, no pH-sensitive hybrid vesicle based on a stimuli-responsive lipid was reported in the literature.

## 1.5. Project presentation

### 1.5.1. Research hypothesis

This project aims at developing further the applications of switchable lipids for drug and gene delivery, while investigating further its biophysical pH-responsive mechanism at both nano and micro scale. We believe that a deeper understanding of the behavior of the system will help defining its advantages and limitations, thereby guiding the potential applications. More precisely, at the nanoscale, we aim to apply switchable LNP to deliver survivin-targeted siRNA *in vitro* in a range of cancer cells and evaluate its synergy with chemotherapeutics using a retinoblastoma model *in vitro*. At the microscale, we aim to visually interrogate the influence of the pH-triggered conformational change of switchable lipid when formulated in a lipid or a blended polymer/lipid membrane.

Our general objective is supported by the following points gathered after the literature review:

- (I) Scientific evidence has shown that cationic switchable lipid (Figure 13) is a promising building block to design pH-sensitive lipid nanoparticles (LNP). The pH-induced conformational change of switchable lipid enabled endosomal escape and cytosolic delivery of encapsulated siRNA *in vitro* and *in vivo* (121);



- (II) Switchable LNP preferentially targeted retinoblastoma tumor cells (Y79) after intravitreal injection (Figure 15), mediating miRNA delivery in an orthotopic human RB rat model (122);
- (III) Survivin stands as a cancer-specific target deeply implicated in tumors progression and resistance to cell death (Figure 5), but survivin-tailored strategies failed to reach the clinics when engaged as monotherapy (51).

Furthermore, the mechanism whereby the pH-triggered conformational change of switchable lipids mediates membrane destabilization and cargo release remains to be elucidated. To this end, we assume that:

- (IV) Giant Unilamellar Vesicles are a resourceful tool to visually investigate membranes response face to external stimulus (133);
- (V) Hybrid polymer/lipid unilamellar vesicle combines the advantages of its two forerunners, liposomes and polymersomes, into a single new hybrid membrane. But hybrid polymer/lipid vesicles lack responsive properties (134).

Based on the aforementioned premises, our hypothesis is two-fold:

- Switchable LNP might be capable of delivering survivin-targeted siRNA *in vitro*, improving therapeutic response to chemotherapeutics in cancer cells; such a design holds potential as a future intravitreal strategy to ameliorate the benefit to risk ratio in retinoblastoma chemotherapeutic protocol;
- Giant unilamellar vesicles might provide visual insights into the behavior of lipid or hybrid polymer/lipid membrane containing the pH-sensitive switchable lipid when submitted to acidic environment mimicking the endosomal compartments;

### **1.5.2. Specific objectives**

To confirm our hypotheses, we proposed the following specific objectives, divided into 2 studies:

#### 1.5.2.1. 1<sup>st</sup> publication:

In the first publication, we will evaluate the ability of switchable LNP in delivering survivin-targeted siRNA and the chemotherapeutic benefits thereof, *in vitro*. The specific objectives are the following:

1. To screen the mRNA survivin silencing ability of survivin-targeted siRNA delivered by switchable LNP (siLNP) in 14 cell lines representative of 6 different types of cancer;
2. To confirm survivin protein downregulation in Y79 cells-transfected with siLNP by western blot;
3. To screen the impact of carboplatin, topotecan, melphalan, and teniposide after incubation with Y79 cells on the mRNA levels of survivin and caspase 3;
4. To calculate the synergistic effect of a temporal approach consisting of first downregulate survivin by siRNA delivery mediated by lipofectamine RNAiMAX or switchable LNP, followed by incubation with cytotoxic agents;
5. To investigate the siRNA specificity of our strategy by transfecting Y79 cells with switchable LNP carrying scrambled siRNA followed by carboplatin or melphalan incubation;
6. To investigate the cancer specificity of our strategy by transfecting siLNP into non-survivin expressing ARPE.19 cells followed by carboplatin incubation;

#### 1.5.2.2. 2<sup>nd</sup> publication

In the second publication, we will examine the acid-triggered effects on switchable lipid-containing giant unilamellar vesicles (GUV) and giant hybrid polymer/lipid unilamellar vesicles (GHUV) by confocal microscopy. The specific objectives are the following:

1. To confirm the incorporation of switchable lipid into GUV and GHUV by <sup>1</sup>H NMR;
2. To evaluate and categorize the membrane structural changes of switchable GUV and GHUV when submitted to HCl treatment;
3. To correlate the membrane behavior of switchable GUV and GHUV with previous results obtained with switchable LNP and switchable lipid-containing large unilamellar vesicles (LUV) and large hybrid polymer/lipid unilamellar vesicles (LHUV);

4. To assess the pH-induced changes on membrane's permeability of calcein-loaded switchable GUV and GHUV.

# Chapter 2 – Paper submitted to the Journal Molecular Therapy

## – Nucleic Acids

Status: submitted

### 2.1. Title page

Title: Survivin silencing improves chemotherapy in retinoblastoma

Authors: Victor Passos Gibson<sup>a</sup>; Rabeb Mouna Derbali<sup>a</sup>, Houda Tahiri<sup>b</sup>, Christine Allen<sup>c</sup>, Pierre Hardy<sup>b</sup>, Jeanne Leblond Chain<sup>a,d\*</sup>

<sup>a</sup> Gene Delivery Laboratory, Faculty of pharmacy, Université de Montréal, H3C 3J7, Montréal, Québec, Canada;

<sup>b</sup> Departments of Pediatrics, Physiology and Pharmacology, Université de Montréal, H3C 3J7, Montréal, Québec, Canada

<sup>c</sup> Leslie Dan Faculty of Pharmacy, University of Toronto, Toronto, ON, M5S 3M2, Canada.

<sup>d</sup> Université de Bordeaux, ARNA Laboratory, INSERM U1212, CNRS UMR 5320, F-33016 Bordeaux, France

\* Correspondence: [jeanne.leblond-chain@inserm.fr](mailto:jeanne.leblond-chain@inserm.fr)

### 2.2. Abstract

Survivin stands out as one of the most specific cancer targets discovered to date. Although single inhibition, *e.g.* through small interfering RNA (siRNA), has shown modest results in clinical trials, its combination with drugs holds promise to sensitize cancer cells to chemotherapeutics. In this study, we propose a sequential treatment of siRNA survivin followed by chemotherapy. Firstly, we demonstrated that siRNA-loaded switchable lipid nanoparticles (siLNP) silence survivin in a panel of cancer cell lines. Subsequently, we selected retinoblastoma (RB) as our model to screen four chemotherapeutic agents: carboplatin, topotecan, melphalan or teniposide. The effect of drugs on survivin expression and caspase-3 was investigated by RT-qPCR. The best drug

combination was selected measuring the viability, survivin expression and the selectivity of the treatment. Our stepwise method revealed that siRNA delivery by switchable LNP sensitized Y79, but not the healthy APRE-19 cell line, to carboplatin and melphalan cytotoxicity. This ability was validated on primary human RB cells. Finally, the distinct behavior of the drugs demonstrated that a diligent screening of drugs should be envisioned when looking for synergy with survivin. Our sequential approach highlighted carboplatin and melphalan as agents to be investigated in future survivin-associated *in vivo* testing to tackle RB.

**Keywords:** Cationic switchable lipid, Survivin targeting siRNA, Retinoblastoma, Cancer

## 2.3. Introduction

More than 20 years ago, Ambrosini and co-workers reported the discovery of the smallest member of the inhibitors of apoptosis protein (IAP) family, survivin (37). Interestingly, the protein is remarkably expressed in human cancers, but not in healthy differentiated adult tissues (166). Its expression has been associated with poor prognosis for several cancers such as lung, colon, pancreas, prostate, breast (37), cervical (167) retinoblastoma (168), as well as lymphomas and acute myeloid leukemia (37, 169, 170). Therefore, downregulating survivin expression has been actively pursued in the last decades (52, 171). Several inhibitors have reached the clinics (166), such as sepantronium bromide YM155 (72), or antisense oligonucleotides (82). Unfortunately, survivin-targeted therapy has shown limited success in clinical trials as a single treatment (172).

In retrospective studies, the role of survivin in resistance to chemotherapeutics has been established in several cancer models (31, 166, 173-175). Thus, combination treatments with doxorubicin (169, 175-177), etoposide (169), carboplatin (68), topotecan (178), paclitaxel (179), or a cocktail of siRNA targeting multiple cellular pathways (88) have been explored to improve chemotherapeutics efficacy in preclinical studies, *in vitro* and *in vivo* (180). In retinoblastoma, combining YM155 with topotecan, carboplatin or radiation, induced apoptosis and reduced the tumor growth in a mice orthotopic retinoblastoma model (68). Nevertheless, antisense therapy, as many gene-based products, face crucial delivery issues. Nanomedicine has recently shown its ability to deliver RNAi-based therapeutics in humans, as witnessed by the FDA approval of OnPattro, a lipid nanoparticle-based formulation siRNA delivery for the treatment of a hereditary

liver disease (96). Such lipid nanoparticle formulations have also shown promise for cancer targeting, such as mantle cell lymphoma,(181) leukemia,(182) glioblastoma (183) and prostate cancer.(184)

Our team has recently developed switchable Lipid Nanoparticles (switchable LNP), based on a pH-triggered molecular switch. Its unique structure undergoes a conformational change upon acidic pH, that triggers membrane destabilization, promotes endosomal escape and cytosolic release of its cargo (130). Such pH-sensitive particles have demonstrated efficient siRNA transfection both *in vitro* and *in vivo* (121). Recently, fluorescence imaging demonstrated that switchable LNP possessed high affinity for retinoblastoma cells (Y79), *in vitro* and *in vivo* (122). The switchable LNP were used as a dual delivery system for miRNA and melphalan, and empowered the synergy of both drugs in human primary cells as well as in a rat model of retinoblastoma (122).

Retinoblastoma (RB) is the most common cancer affecting the eye in children and accounts for 3% of all childhood malignancies (185). Therapeutic success relies in the early diagnosis as advanced stages of RB are usually refractory to chemotherapy, likely to metastasize to brain and can only be handled by enucleation (20). Current regimens are based on chemotherapeutics such as DNA-crosslinking agents (Carboplatin (CBDA)), DNA topoisomerase 2 inhibitors (Topotecan (TOPO), Teniposide (TENI)), Vinca alkaloids (Vincristine) and alkylating drugs (Melphalan (MELPH)) (27). In the past decades, a paradigm shift has favored local administration such as intravitreal or intraarterial injection, especially in cases of presence of vitreous seeds and refractory tumor to standard methods (27, 28). Advantages of site-directed delivery includes overcoming the blood-retinal barrier, promoting bioaccumulation of chemotherapeutics in the poor-vascular vitreous and limiting systemic exposure and side effects (186).

In this study, we screen the ability of switchable LNP in downregulating survivin in a variety of cancer cell lines using survivin-targeted siRNA. Then, using RB as our cancer model, we stepwise evaluate the benefits of survivin downregulation followed by incubation with four standard chemotherapeutics in the RB protocol: carboplatin, melphalan, topotecan and teniposide, as a rational approach to select the best candidate to benefit from survivin downregulation in future clinical applications.

## 2.4. Materials and method

All solvents (HPLC grade), chemicals and reagents were obtained from Sigma-Aldrich (Oakville, ON, Canada) and Thermo Scientific (Waltham, MA, USA). 1,2-distearoyl-sn-glycero-3-phosphocholine (DSPC) and N-(carbonyl-methoxypolyethyleneglycol 2000)-1,2-distearoyl-sn-glycero-3-phosphoethanolamine, sodium salt (DSPE-PEG<sub>2k</sub>) were purchased from Avanti Polar Lipids (Alabaster, AL, USA). Cholesterol was obtained from Sigma-Aldrich. Cationic switchable lipid was synthesized as previous described (121). Dextrose, sodium chloride, Tween-20, Carboplatin, Melphalan and survivin inhibitor YM155 were purchased from Sigma-Aldrich (Oakville, ON, CA). Topotecan was prepared from concentrated solution (Topotecan Hospira, Pfizer Europe, Brussels, Belgium) and Teniposide used as received (Vumon, Bristol-Myers Squibb Company, New York, NY, USA).

Survivin-targeted siRNA is an Ambion In Vivo Pre-designed siRNA purchased from Thermo Scientific (Waltham, ON, CA). Negative control siRNA (scramble siRNA) does not target any human transcript and was purchased from Alpha DNA (Montreal, QC, CA). Both sequences are listed in Table 2.

siRNA	Sense	Antisense
siRNA survivin	GGACCACCGCAUCUCUACATT	UGUAGAGAUGCGGUGGUCCTT
siRNA Scramble	UAGCGACUAAACACAUCAAUU	UUGAUGUGUUUAGUCGCUAAU

Table 2. – siRNA sequences used in the study

### 2.4.1. Preparation of cationic switchable lipid nanoparticles

Cationic switchable lipid nanoparticles (switchable LNP) for *in vitro* survivin screening were prepared by hydration of a lipid film followed by extrusion. Briefly, ethanolic stock solutions of cationic switchable lipid (CSL), DSPC, Cholesterol (Chol) and DSPE-PEG2000 were mixed at a molar ratio of 50:10:37.5:2.5, respectively. Ethanol was removed under reduced pressure. The obtained dried lipid film was hydrated with 1 mL of sterile 5% dextrose solution. This solution was vortexed, heated to 65 °C and stepwise extruded 11 times through 400, 200 and 100 nm polycarbonate

membranes using a heated LiposoFast manual extruder (Avestin Inc., Ottawa, ON, Canada). The resulting liposomes were stored at 4 °C until further use.

For survivin silencing in retinoblastoma cells *in vitro* and *in vivo*, switchable LNP were prepared by microfluidic mixing. Briefly, an ethanolic solution containing CSL, DSPC, DSPE-PEG<sub>2000</sub> and Chol was mixed with a 5% dextrose solution at a flow rate of 12 mL/min, at a 5%Dex/lipid solution ratio of 3:1 using two syringe pumps (KDS-200, KdScientific, Holliston, MA, USA). The final switchable LNP suspension was dialyzed against 5% dextrose using Pur-ALyzer™ Maxi dialysis tubes MWCO 12-14 kDa (Sigma-Aldrich, Oakville, ON, CA), overnight, at room temperature and under gently stirring followed by sterilization using 0.22 µm polyethersulfone 13 mm syringe filter (Pall Corporation, Mississauga, ON, Canada). Formulation was stored at 4 °C until further use. Switchable LNP prepared either by microfluidic mixing or manual extrusion was characterized similarly with regards to size, surface zeta potential and CSL amount.

#### **2.4.2. Physicochemical characterization of switchable LNP**

The amount of CSL in each batch was quantified by HPLC-UV/MS using an Agilent 1260 Infinity HPLC equipped with a PDA detector, a column (Agilent Poroshell 120 EC -C8 (2.7 m) 3 × 30 mm) and a 6120 single-quad mass spectrometer (Mississauga, ON, Canada) against a calibration curve of switchable lipid (25-400 µg/mL; from ethanol stock solution). Liposomal formulation was diluted 25X in HPLC grade methanol and vigorously vortexed. The quantification method employed consisted of a mobile phase A (acetonitrile 95/5 + 0.1% acetic acid) and mobile phase B (acetonitrile +0.1% acetic acid). The mobile phase gradient was: 0 min – 90% A; 1 min – 100% B; followed by a column re-equilibration time of 3 min with the following properties: Flow 1.5 mL/min; UV detection: 254 nm and; Injection volume: 10 µL.

Liposome hydrodynamic diameter, polydispersity index (PDI) and ζ-potential were measured at 20°C using a Malvern Zetasizer Nano ZS (Malvern, Worcestershire, UK). Samples were diluted 10X in dextrose 5% to a final volume up to 1 mL. Size measurements were performed with a scattered angle of 173° and reported as Z-average (intensity). The voltage for ζ-potential was set at 150V. Measurements were performed at least in triplicate.



### 2.4.3. siRNA complexation, characterization and encapsulation efficiency

Equal volumes of survivin-targeted siRNA (siSurvivin) or the negative control scramble-siRNA (siScramble) and switchable LNP were prepared in sterile dextrose 5% in order to achieve a N/P ratio of 4 (number of amino groups of the cationic switchable lipid / number of phosphate groups of siRNA). Each solution was equilibrated at room temperature for 5 minutes, then siRNA was added into the lipid solution, upon gently mixing. Complexation was completed upon incubation of siRNA-LNP solution during 15 minutes at 50 °C under vigorous mixing (1200 rpm) in a Labnet Vortemp™ 56 (Diamed, Mississauga, ON, CA). siSurvivin or siScramble switchable lipid nanoparticles (siLNP and scrLNP, respectively) were then diluted to achieve final siRNA concentration in either dextrose 5% for further characterization or in Opti-MEM (Wisent, Montreal, QC, CA) for *in vitro* transfection.

The encapsulation efficiency of siRNA was performed using the SYBR® Gold assay (Thermo Scientific, Waltham, MA, USA). Briefly, complexes were prepared in dextrose 5% with a final siRNA concentration of 40 nM in 500 µL with N/P ratio ranging from 2 to 16. After 15 minutes incubation at 50 °C under vigorous mixing, complexes were submitted to centrifugation at 20 000 g for 30 minutes. 100 µL of the supernatant was added in a black 96-well plate (Corning Inc., Corning, NY, USA) followed by 60 µL of SYBR® Gold 4X. Free siRNA was quantified against a calibration curve of SYBR® Gold (5 to 80 nM of siRNA) using Safire microplate reader (Tecan, Seestrasse, Switzerland;  $\lambda_{ex/em} = 495/537$ ). siRNA encapsulation efficiency was calculated as follows:

$$EE (\%) = \frac{40 \text{ (nM)} - \text{siRNA concentration in the supernatant (nM)}}{40 \text{ (nM)}} \times 100$$

For the physicochemical characterization of siRNA switchable LNP, samples were diluted 10X in dextrose 5% and their size, PDI and  $\zeta$ -potential were measured as described previously.

### 2.4.5. Cell culture

Hela cells (CCL-2TM, ATCC, Manassas, VA, USA) were cultured in Dulbecco's Modified Eagle's Medium (DMEM, Wisent, Montreal, QC, Canada) supplemented with 10% FBS (Wisent, Montreal, QC, CA). A549 cells were kindly provided by Dr. Sylvain Meloche (IRIC, Univ. Montréal, QC, Canada) and were cultured in Kaighn's Modification of Ham's F-12 Medium (F-12K, Wisent,

Montreal, QC CA) supplemented with 10% FBS. MCF-7 were kindly provided by Dr. Sylvie Mader (IRIC, Univ. Montréal, QC, Canada) and were cultured in Minimum Essential Medium Alpha Medium (AMEM, Wisent, Montreal, CA) supplemented with 10% FBS and 1% L-Glutamine (Gibco, Burlington, ON, Canada). MDA-MB-231, MDA-MB-436, OV90, HEYA 8, H460, H1299, HT29, SKOV3, BT474 and ME180 cells were kindly provided by Dr. Christine Allen (University of Toronto, ON, Canada). MDA-MB-231 and MDA-MB-436 cells were cultured in DMEM/HAMF 12 (1:1 mix) supplemented with 10% FBS. HEYA 8, H460 and H1299 cells were cultured in RPMI 1640 (Gibco, Burlington, ON, Canada) supplemented with 10% FBS. HT29 and SKOV3 cells were cultured in McCoy's 5A (Gibco, Burlington, ON, Canada) supplemented with 10% FBS. The culture media of BT474 was composed by DMEM H21 (Wisent, Montreal, QC, CA) supplemented with 10% FBS. OV90 cells was cultured in MCDB 105/M199 (1:1 mix) (Gibco, Burlington, ON, CA) supplemented with 10% FBS. ME-180 cells were cultured in alpha-minimal essential medium ( $\alpha$ -MEM, Gibco, Burlington, ON, CA) supplemented with 10% FBS. ARPE-19 cells (CRL-2302, ATCC, Manassas, VA, USA) were cultured in DMEM supplemented with 10% FBS. Y79 cells (ATCC HTB-18; Manassas, VA, USA) were cultured in RPMI 1640 (Gibco, Burlington, ON, CA) supplemented with 10 mM HEPES (Gibco, Burlington, ON, CA), 1 mM sodium pyruvate (Gibco, Burlington, ON, CA) and 10% FBS. Y79-Luc cells were kindly donated by Dr. Andrew Davidoff (St. Jude Children's Research Hospital, TN, USA) and cultivated similarly Y79 cells. Human RB tumor samples were obtained from the primary-site intra-ocular RB of a young patient at CHU Sainte-Justine (Montreal, QC, Canada), in accordance with the Ethic Committee of CHU Sainte-Justine. The primary cells were obtained during a surgical procedure and no information about patient's previous chemotherapy treatment was available. Primary human RB cells were processed and cultured as previously described (122, 187). Cells were incubated at 37°C under a water-saturated atmosphere supplemented with 5% CO<sub>2</sub>.

#### **2.4.6. Cell transfection**

Switchable LNP and survivin siRNA were complexed at N/P ratio of 4 for a final siRNA concentration of 10, 20 or 40 nM per well. siLNP were diluted in Opti-MEM then added to trypsinized cells or suspension cells diluted in their culture media. Cells were finally incubated for 48 hours at 37°C under a water-saturated atmosphere supplemented with 5% CO<sub>2</sub>. As a positive

control, cells were treated with Lipofectamine RNAiMAX (Thermo Scientific, Waltham, MA, USA) according to the manufacturer's reverse transfection protocol with minor modifications. Briefly, 0.1875  $\mu\text{L}$  of Lipofectamine RNAiMAX (LF) was mixed in sterile dextrose 5% with 20 nM of siRNA for a single well followed by 5 minutes incubation at RT and dilution in Opti-MEM. Reagents were scaled up accordingly to the number wells, type of plate and siRNA concentration. For the negative control, cells were transfected with scramble siRNA following the same protocol described herein.

#### **2.4.7. Relative quantification of target genes by RT-qPCR**

For the RNA extraction and qPCR assay,  $10 \times 10^4$  cells were plated in a 12 well-plate and transfected according to the procedure previously described. The extraction of total RNA of transfected cells or cells treated with cytotoxic was performed using the Total RNA Purification kit (NorgeneBiotek, Thorold, ON, CA) or RNeasy mini kit (Qiagen, Hilden, Germany) according to the manufacturer protocol. Total RNA was quantified by nanodrop (Thermo Scientific, Waltham, MA, USA) by measuring the absorbance at 260 nm. The RNA purity was determined with same instrument by calculating 260/230 and 260/280 ratios. A ratio of 1.8 is acceptable for pure DNA and 2.0 for pure RNA. The RNA integrity was evaluated by the ratio of 28S/18S ribosomal RNA using the Agilent BioAnalyzer 2100 (Agilent Technologies, Mississauga, ON) following the manufacturer's protocol. Several RNA extracts from transfected cells were checked before RT-qPCR to confirm that the transfection by the switchable LNP and the extraction method preserved RNA integrity.

RNA extracts were reverse transcribed into cDNA using the High Capacity cDNA Reverse Transcription Kit (Applied Biosystems, Waltham, MA, USA) following the manufacturer protocol. A noRT control (no reverse transcriptase) was added to check any genomic DNA contamination.

PCR reactions were done in 384-well plate using 1.5  $\mu\text{L}$  of diluted cDNA samples, 5  $\mu\text{L}$  of 2X Taqman Fast qPCR MasterMix (Applied Biosystems, Waltham, Ca, USA) 0.05  $\mu\text{L}$  of mix oligos specific for each gene (50  $\mu\text{M}$ , Applied Biosystems, refer to Table 2 for full sequences), 1  $\mu\text{L}$  of specific Universal Probe Library (1  $\mu\text{M}$ , Roche, Basel, Switzerland) and 2.45  $\mu\text{L}$  of RNase-free water (Thermo Scientific, Waltham, ON, CA). No Template Control was added by replacing cDNA with water to check any contamination in qPCR products.

Real-Time PCR System (Applied Biosystems® ViiA™ 7, Waltham, CA, USA) was programmed in Fast mode with an initial step of 3 minutes at 95°C followed by 40 cycles of 5 seconds at 95°C and 30 seconds at 60°C. The Ct (cycle threshold) was used for quantification.  $\beta$ -actin (ACTB) was used as endogenous control (Table 3).

The relative expression (RQ) of target genes was determined using the  $\Delta\Delta$ CT method ( $RQ=2^{(-\Delta\Delta CT)}$ ,  $\Delta\Delta CT= \Delta Ct \text{ Sample}- \Delta Ct \text{ Calibrator}$ ). Real time PCR data were analyzed using Expression Suite Software.

	<b>Forward 5'–3'</b>	<b>Reverse 5'–3'</b>	<b>UPL Probe</b>
ACTB <sup>1</sup>	attggcaatgagcggttc	tgaaggtagtttcgtggatgc	11
BIRC5 <sup>2</sup>	gccagtgtttcttctgctt	ccggacgaatgctttttatg	11
CASP3 <sup>3</sup>	tttggaattgatgcgtgat	ggctcagaagcacacaaaca	68

<sup>1</sup>*b-actin*; <sup>2</sup>*survivin*; <sup>3</sup>*caspase-3*

Table 3. – The sequence of oligos used in PCR analysis.

#### 2.4.8. Western blot assay

Protein profile expression was evaluated by Western immunoblotting assay. For the Western blot assay,  $1.2 \times 10^6$  cells were plated in a 6-well plate and transfection was carried as described above. Briefly, transfected cells and/or cytotoxic treated cells were collected at different time points and treated with M-PER (Thermo Scientific, Waltham, MA, USA) containing 1X protease inhibitors (Thermo Scientific, Waltham, MA, USA) to obtain whole cell lysate. Proteins concentration were quantified using the Bradford assay (Thermo Scientific, Waltham, MA, USA). Equivalent amounts of proteins (40  $\mu$ g) were denatured in 4X laemmli buffer (Bio-Rad laboratories, Hercules, CA, USA) for 5 min at 95°C and, then, electrophoretically separated on 15% polyacrylamide gel for 1 hour before transferring to Immun-Blot PVDF membranes (Bio-Rad Laboratories, Hercules, CA, USA) overnight at 30V in a cold room. Membranes were blocked with either 3% bovine serum albumin (BSA, Sigma Aldrich) for survivin detection or 5% skimmed milk for the other proteins for

1 hour and then incubated overnight at 4°C with either rabbit anti-survivin (1:500 in 3% BSA, #2803, Cell Signalling Technology, Danvers, MA, USA), rabbit anti-p21 (1:400, #2947, Cell Signalling Technology), mouse anti-p53 (1:500, sc-126, Santa Cruz Biotechnology, Santa Cruz, CA, USA) or mouse anti-B-actin (1:5000, sc-8432, Santa Cruz Biotechnology, Santa Cruz, CA, USA) antibodies. Membranes were washed thrice with TBST (0.15M NaCl, 0.02M Tris-HCl pH 7.4, 0.1% Tween 20 (v/v)) and then incubated with either anti-rabbit (1:5000, sc-2004, Santa Cruz Biotechnology) or anti-mouse (1:5000, sc-2005, Santa Cruz Biotechnology, Santa Cruz, CA, USA) secondary horseradish peroxidase-conjugated antibodies at room temperature for 1 hour followed by washing with TBST and incubation with either Clarity max ECL substrate (Bio-Rad Laboratories, Hercules, CA, USA) for survivin detection or Western Lightning Plus-ECL, Enhanced Chemiluminescence Substrate (PerkinElmer, Waltham, MA, USA) for all other proteins for 5 minutes before imaging. Proteins were visualized using the ECL Western blotting detection system (Perkin Elmer). Digital images were treated using ImageJ software. Chemicals for buffer preparation were obtained from Sigma-Aldrich (Oakville, ON, Canada).

#### **2.4.9. Viability assay**

For the viability assay,  $4 \times 10^4$  cells were plated in a 96-well plate for subsequent transfection and/or drug treatment. The viability of transfected Y79, Y79-luc, ARPE-19 and/or cytotoxic treated Y79, Y79-luc and ARPE-19 was assessed 96 hours after seeding using a resazurin-based cell viability assay (PrestoBlue, Thermo Scientific, Waltham, ON, CA). Briefly, 48 hours after incubation with siLNP or scrLNP, cells were treated with solutions of different concentrations of either carboplatin, Teniposide, Topotecan, Melphalan or a combination of carboplatin and topotecan. Non-treated cells received media only and were used as negative control. Thereafter drug treatment, 20  $\mu$ L of PrestoBlue was added per well and cells were incubated for 24 hours at 37°C and 5% CO<sub>2</sub>. Fluorescence was measured at  $\lambda_{ex/em} = 570/600$  nm using a Safire microplate reader (Safire, Männedorf, Zürich, Switzerland). Cellular viability was normalized to the negative control. When indicated, cells were incubated from the day of seeding until viability measurement with a 2 nM solution of survivin inhibitor YM155. The drug concentration required to reduce cell viability down to 50% after 48 hours of drug incubation (IC<sub>50</sub>), with or without prior survivin silencing, was calculated using GraphPad 7 software (La Jolla, CA, USA).

#### **2.4.10. Synergistic effect**

The effect of survivin silencing followed by carboplatin, topotecan, melphalan or Teniposide treatment was evaluated by combination index (CI) theorem proposed by Chou and Talalay (188) using the CompuSyn software (Paramus, NJ, USA). CI values were calculated when the combined siRNA and drug treatment decreased the cells' viability more than 50% compared to drug only treated cells. A CI lower than 1 indicates synergism, whilst CI = 1 or CI > 1 indicate additive or antagonistic effect, respectively. When calculated, CI are presented above each viability chart bar for a specific drug concentration-siRNA treated cells.

#### **2.4.11. Statistical analysis**

Experiments were carried at least in triplicate unless stated otherwise and expressed as mean  $\pm$  standard deviation (SD). Data were plotted in Prism Software (GraphPad Software, La Jolla, CA, USA) and statistical significance was calculated by Student t-test and expressed as: \* ( $p < 0.5$ ), \*\* ( $p < 0.05$ ), \*\*\* ( $p < 0.005$ ) or \*\*\*\* ( $p < 0.0001$ ).

### **2.5. Results**

#### **2.5.1. Preparation of switchable lipid nanoparticles**

The cationic switchable lipid (CSL), previously reported for siRNA transfection *in vitro* and *in vivo* (121, 122) was evaluated in this project for survivin silencing. Switchable lipid nanoparticles (switchable LNP) were prepared as previously described, using CSL, DSPC, Cholesterol and DSPE-PEG<sub>2000</sub>, either by microfluidics or by manual extrusion (Table 4). Both methods yielded nanometric particles, with narrow distribution, cationic surface zeta potential and high siRNA encapsulation efficiency, as assessed by fluorescence intercalation assay. As previously observed (121), microfluidics yielded smaller particles than manual extrusion, with or without siRNA. This difference can be attributed to the precipitation method involving nucleic acids and lipid precipitation in one step, rather than post incubation of liposomes with siRNA (189). Nevertheless, we have previously shown that switchable LNP retain their pH-sensitive properties and transfection ability whatever the preparation method (121). In this project, extrusion method was used for cancer cell screening. Microfluidics was preferred for further investigation on

retinoblastoma *in vitro* and *in vivo* models, thanks to its scalable and reproducible properties (190).

Liposome composition	Zave ± SD	PDI ± SD	Zeta ± SD	EE % ± SD	CSL dosage ± SD (mM)
<b>Microfluidic method</b>					
CSL/DSPC/Chol/PEG*	59 ± 1	0.18 ± 0.01	49.9 ± 2.7	N/A	0.85 ± 0.04
CSL/DSPC/Chol/PEG* + siSurvivin (N/P = 4) †	133 ± 2	0.17 ± 0.02	31.5 ± 4.06	96.37 ± 1.35	0.85 ± 0.04
<b>Extrusion method</b>					
CSL/DSPC/Chol/PEG*	146 ± 2	0.10 ± 0.01	34.3 ± 1.3	N/A	0.95 ± 0.05
CSL/DSPC/Chol/PEG* + siSurvivin (N/P = 4)	162 ± 1	0.13 ± 0.03	31.6 ± 1.0	ND	ND

\* 50:10:37.5:2.5 molar proportions of lipids †N/P : number of amino groups (CSL) / number of phosphate groups (siRNA); N/A: not applicable; ND: not determined

Table 4. – Physicochemical characteristics of switchable LNPs, through two preparation methods

### 2.5.2. *In vitro* survivin silencing by switchable LNP

The versatility of the switchable LNP to silence survivin was assessed on 13 cell lines standing for breast, colon, lung, cervix, ovary and retinoblastoma cancer models by RT-qPCR (Figure 26, Table S5).

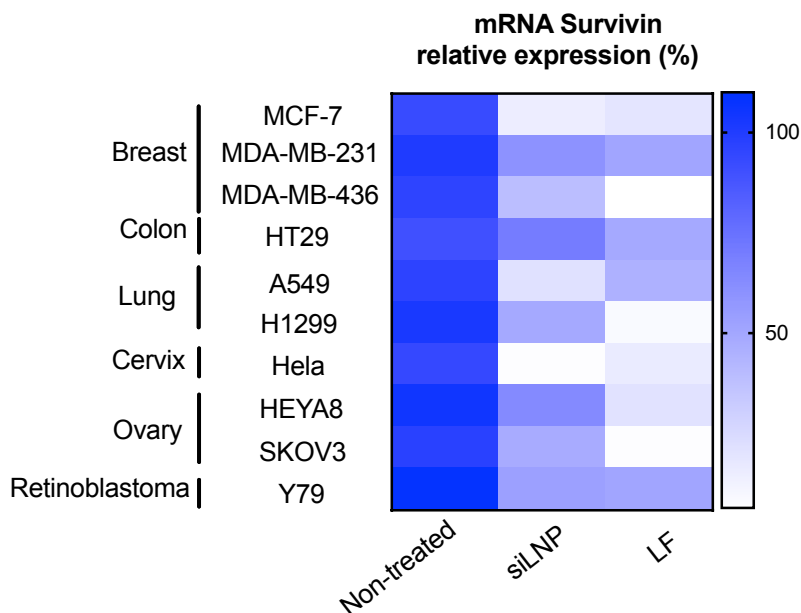


Figure 26. – Heat map of survivin downregulation on a range of cancer cells using siSurvivin switchable LNP. siRNA against survivin was used at 40 nM and prepared by manual extrusion for all cell lines, except for retinoblastoma cells (Y79), which were transfected with microfluidics-formulated switchable LNP and 20 nM siRNA. Lipofectamine® RNAiMAX (LF) reagent was prepared using 40 nM siRNA. Untreated cells were used as controls. Gene downregulation was assayed by RT-qPCR 48 h after incubation (n = 3). *B-actin* mRNA (ACTB) was used as endogenous control. The relative expression of target gene was determined using the  $\Delta\Delta CT$  method (see materials and methods). Image was processed using GraphPad 7 software (La Jolla, CA, USA) from full data presented on Table S5.

The results show a significant variability according to the cell lines. The switchable system silenced survivin to a better extent than Lipofectamine (LF) in MCF7 (84 %), A549 (78 %) and HeLa cells (92 %) and similar in MDA-MB-231 (60 %), and Y79 (34 %). The lineage-specific survivin silencing might suggest particular endocytic processes ruling internalization process of siRNA-cationic switchable lipid nanoparticle. As for our project, we selected retinoblastoma cancer model since both switchable LNP silenced survivin to a comparable extent than LF (Fig 27A) and since we previously developed an *in vitro* and *in vivo* model of this disease (122). Since mRNA silencing not necessarily reflects protein downregulation, we assessed the survivin protein downregulation in Y79 cells over time (Fig 27B).



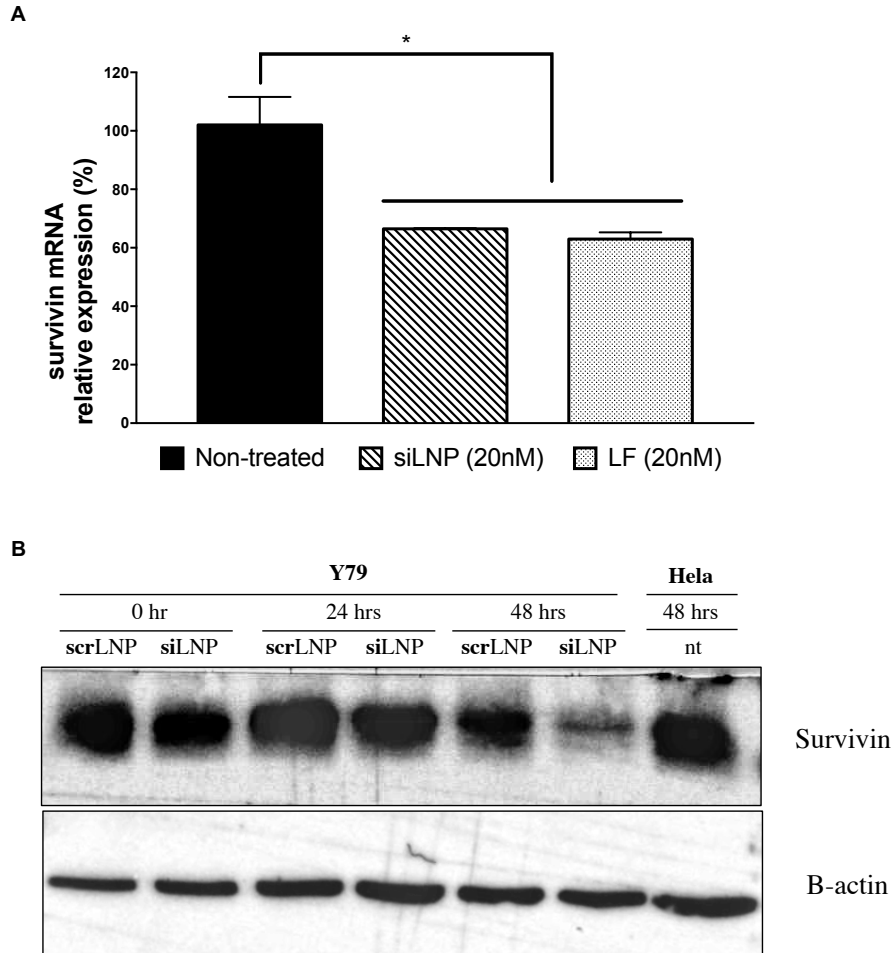


Figure 27. – *In vitro* survivin downregulation in Y79 cells with switchable LNP. (A) mRNA relative expression was assayed by RT-qPCR 48 h after transfection (n = 3). ACTB was used as endogenous control, Lipofectamine® RNAiMAX (LF) reagent at 20 nM and non-treated cells were used as positive and negative controls, respectively. The relative expression of target gene was determined using the  $\Delta\Delta\text{CT}$  method (see materials and methods). (B) Downregulation of survivin protein in Y79 cells was assessed by western blot. Cells were harvested at 0, 24 and 48 hours after transfection with either siRNA survivin (siLNP) or siRNA scramble (scrLNP) at 20 nM. Non-treated Hela cells were used as positive control of survivin expression.

A 48 h delay was required to observe a significant decrease in survivin protein level in Y79 cells. Similar results were obtained using LF to silence survivin in Y79 and in a Y79-luciferase cell line (Figure S33), used in orthotopic *in vivo* RB model to measure tumor growth non-invasively. Importantly, siRNA was specific to survivin since scramble siRNA did not silence survivin at the

protein level (Figure 27B). Therefore, in subsequent combination studies, cells were pretreated with switchable LNP for 48 h before addition of chemotherapeutics. This order, although the most rational, was not always observed in combination studies with survivin inhibitors (180).

### **2.5.3. Drugs used in the RB protocol induce survivin expression differently**

Several drugs are currently administered by intravitreal injection in retinoblastoma clinical setting. The most used is melphalan, which has shown a success rate of 83% in retinoblastoma with recurrent vitreous seeds (27). Melphalan is a DNA alkylating agent, promoting crosslinking intra- and inter- DNA strands, preventing from DNA transcription. Topoisomerase inhibitors (*e.g.* topotecan, teniposide) or platinum-based antineoplastic (*e.g.* carboplatin) are also administered, alone or in combination, through intraarterial injection (27). We first determined IC<sub>50</sub> of those drugs in Y79 cell line (Figure S34). Y79 cells were found to be sensitive to topotecan and melphalan, which was consistent with previous studies (122, 191), but highly resistant to carboplatin (IC<sub>50</sub> = 282 μM) (192) and teniposide (IC<sub>50</sub> not determined).

In order to investigate the synergy of survivin silencing with current chemotherapeutics, we first examined the impact of drug treatment on survivin mRNA and protein levels (Figure 28). Caspase 3 levels were also determined, since survivin is known to interfere with Caspase-3 apoptotic pathway (52). Thus, a chemotherapeutic that upregulated survivin and downregulated Caspase 3 could be identified as a suitable candidate for further testing with survivin downregulation.

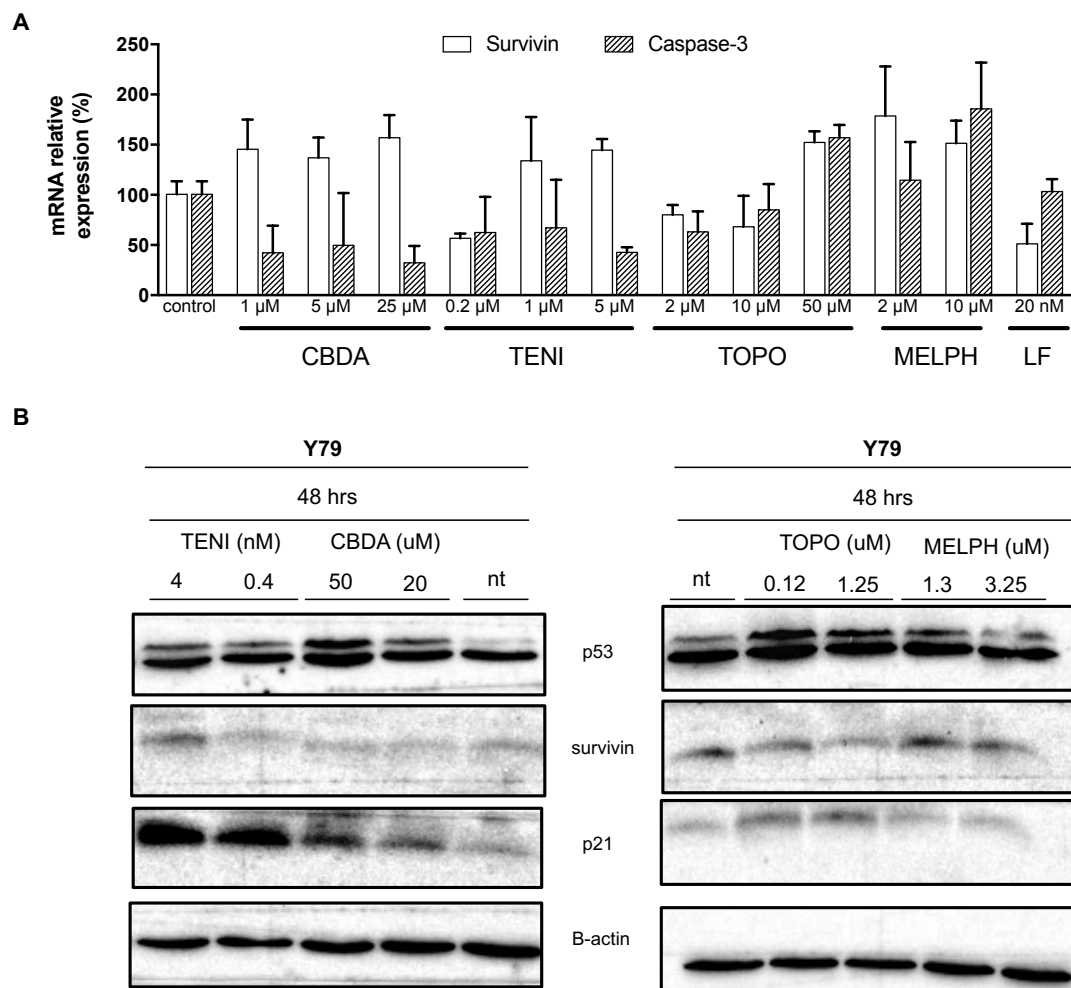


Figure 28. – RT-qPCR and western blot of Y79 cells after 48 h incubation with different chemotherapeutics. (A) mRNA relative downregulation was assayed by RT-qPCR 48 hours after incubation with drugs ( $n = 3$ ). *B-actin* mRNA (*ACTB*) was used as endogenous control. Non-treated cells were used to normalize mRNA values. CBDA: Carboplatin; TENI: Teniposide; TOPO: topotecan; MELPH: Melphalan. (B) Western blotting profile of Y79 cells treated with different chemotherapeutics.

Regarding the qPCR assessment, two behaviors could be distinguished: carboplatin (25  $\mu$ M) and teniposide (5  $\mu$ M) both upregulated survivin and downregulated caspase-3 mRNA levels by 1.5 and 2-fold, respectively, suggesting a resistance to apoptotic pathways, consistently with their  $IC_{50}$  values (Figure S34). On the other side, topotecan and melphalan upregulated both survivin and caspase-3 mRNA levels by 1.5-fold at the highest concentrations. Considering protein

expression, survivin was mildly expressed after the treatments, but no significant change could be concluded before and after drug treatment at a protein level. On the contrary, all drugs upregulated the proapoptotic proteins p53 and p21 in comparison to non-treated cells after 48 hours of drug incubation, which confirmed the cytotoxic activity of drugs.

Considering that all drugs tested upregulated survivin at mRNA levels but could not be discriminated based on their protein expression profile, we pursued our combination investigation with all four drugs. Our working hypothesis was that survivin downregulation prior drug treatment could lead to a better cytotoxicity of chemotherapeutics in Y79 cells.

#### 2.5.4. Survivin downregulation followed by drug treatment on Y79 cells

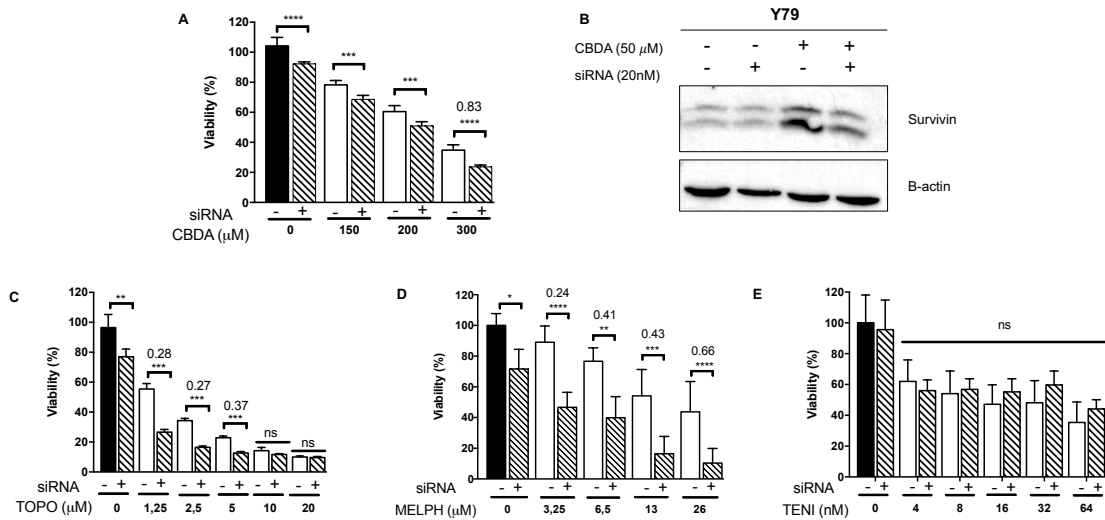


Figure 29. – Viability of Y79 cells after survivin downregulation by siRNA/LF for 48 h followed by treatment with either (A) carboplatin, (B) topotecan, (D) melphalan or (E) teniposide for 48 h. (C) Y79 survivin protein expression of cells treated with siRNA/LF (48 h) followed by 50  $\mu$ M CBDA (48 h). Non-treated cells and siRNA/LF (48 h) or 50  $\mu$ M CBDA (48 h) only following the same time sequencing were used as control. Cells were harvest 96 h from seeding for western blotting assay. Black bars represent non-treated cells. Synergistic effect was expressed as combination index (CI) and indicated above each graph. Statistical analysis was performed using student t-test, where \* ( $p < 0.05$ ), \*\* ( $p < 0.005$ ), \*\*\* ( $p < 0.0005$ ), \*\*\*\* ( $p < 0.0001$ ) and ns means no significant difference.

The synergy of survivin downregulation with chemotherapeutics was first screened using LF loaded with siRNA targeted against survivin (Figure 29). Three out of four drugs benefitted from survivin downregulation. Carboplatin, topotecan and melphalan exhibited a higher cytotoxicity after siRNA treatment when compared to drug alone (Figure 29). As a result, the  $IC_{50}$  of these drugs was decreased when survivin silencing preceded drug treatment: both melphalan and topotecan encountered a 77% decrease in their  $IC_{50}$  value and CBDA's  $IC_{50}$  decreased by 23%, which is substantial for a resistant behavior (Figure S34). Only Teniposide toxicity was not significantly impacted by survivin downregulation at any concentration tested (Figure 29E). The synergistic effect of siRNA pretreatment was also quantified when the fraction affected was higher than 0.5 (more than 50% of cell death) using the combination index (CI) theorem proposed by Chou and Talalay (188), where CI lower than 1 indicates synergism. Survivin silencing prior drug treatment synergistically improved carboplatin, topotecan and melphalan's cytotoxicity at specific concentrations (Fig 29A, B, and D). CI values ranged from 0.83, when siRNA was combined with carboplatin at 300  $\mu$ M, to a maximum effect of 0.24, when siRNA synergistically improved melphalan's cytotoxicity at 3.25  $\mu$ M. The involvement of survivin into carboplatin's resistance mechanism was confirmed by western blot (Figure 29C). Pretreatment of Y79 cells with survivin-targeted siRNA attenuated the increase in survivin protein level raised by carboplatin exposure. In this assay, survivin increase induced by carboplatin was more obvious than in Figure 28B. This is in agreement with previous reports, which showed similar restoration of survivin levels using YM155 and carboplatin (68).

Moreover, survivin silencing was investigated with a ternary drug combination of carboplatin and topotecan (Figure S35). After survivin pretreatment, 50% cell viability was reached with only 30  $\mu$ M and 0.25  $\mu$ M of carboplatin and topotecan respectively, as compared to 191  $\mu$ M and 0.5  $\mu$ M when the drugs were used individually.

Taken together, the findings confirm that survivin silencing resulted in reduced therapeutic dose of carboplatin, melphalan and topotecan, alone or in combination, but not teniposide.

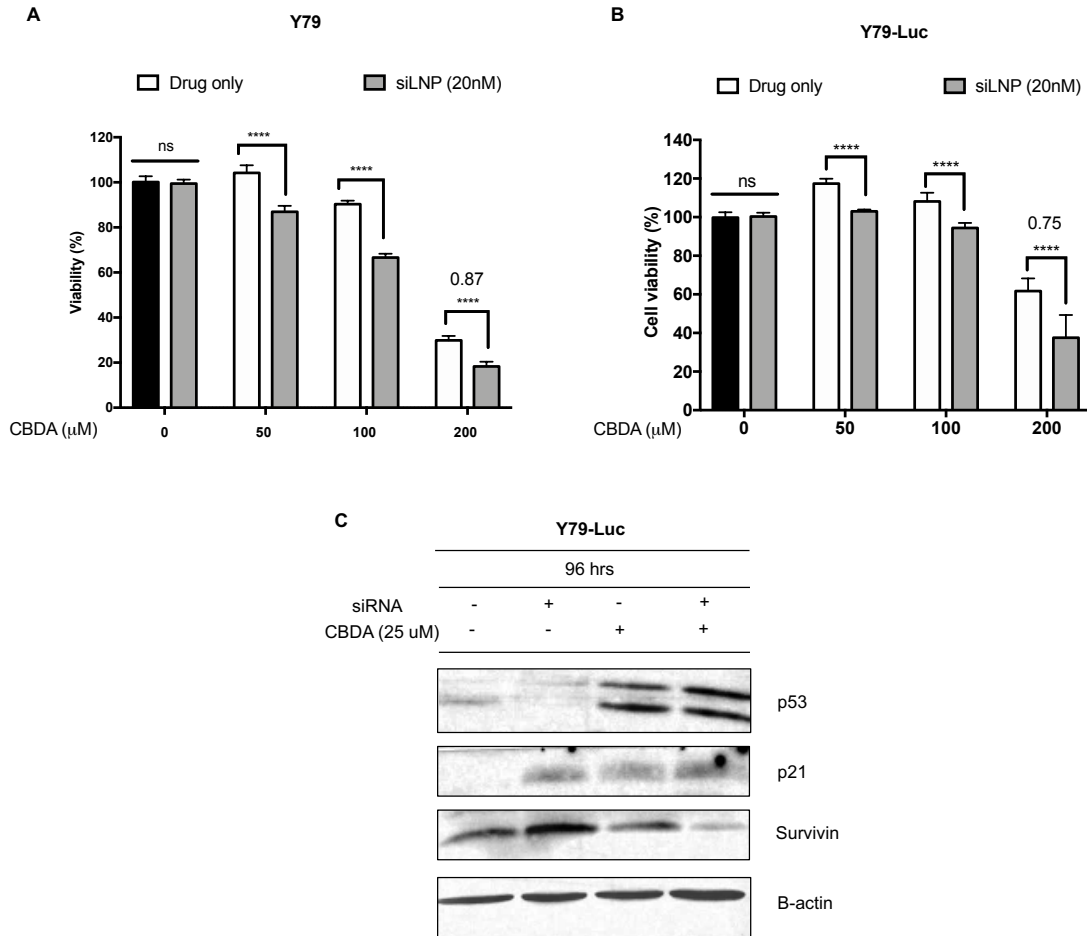


Figure 30. – Viability of (A) Y79 and (B) Y79-luc cells 96 hours after siSurvivin delivery by switchable LNP (48 h, siLNP) followed by carboplatin incubation (48 h). (C) Western blot of Y79-Luc cells treated or not with siSurvivin (LF, 20 nM siRNA) and/or Carboplatin (25 μM). Black bars represent non-treated cells. Synergistic effect was expressed as combination index (CI) and indicated above each graph. Statistical analysis was performed using student t-test, where \* ( $p < 0.05$ ), \*\* ( $p < 0.005$ ), \*\*\* ( $p < 0.0005$ ), \*\*\*\* ( $p < 0.0001$ ) and ns means no significant difference.

Since these results were obtained with LF, we further assessed switchable LNP ability to trigger such a synergy between survivin silencing and CBDA in retinoblastoma cancer model (Figure 30). When compared to LF, switchable LNP performed as efficiently and siRNA survivin pretreatment significantly improved carboplatin toxicity in both Y79 (Figure 30A) and Y79-Luc (Figure 30B) cells. Survivin silencing followed by CBDA at 200 μM treatment resulted in synergistic interaction with combination indexes of 0.87 and 0.75 in Y79 or Y79-luc cells, respectively. Y79-Luc cells behaved

similarly to its non-luciferase counterpart with regards to upregulation of apoptosis-related proteins, p53 and p21, and abrogation of survivin re-expression upon drug treatment (compare Fig 30C and 29C). Altogether, these results yielded robust evidence that pretreatment with survivin silencing siRNA carried by either LF or switchable LNP sensitizes retinoblastoma cells to carboplatin.

### 2.5.5. Specificity of survivin downregulation

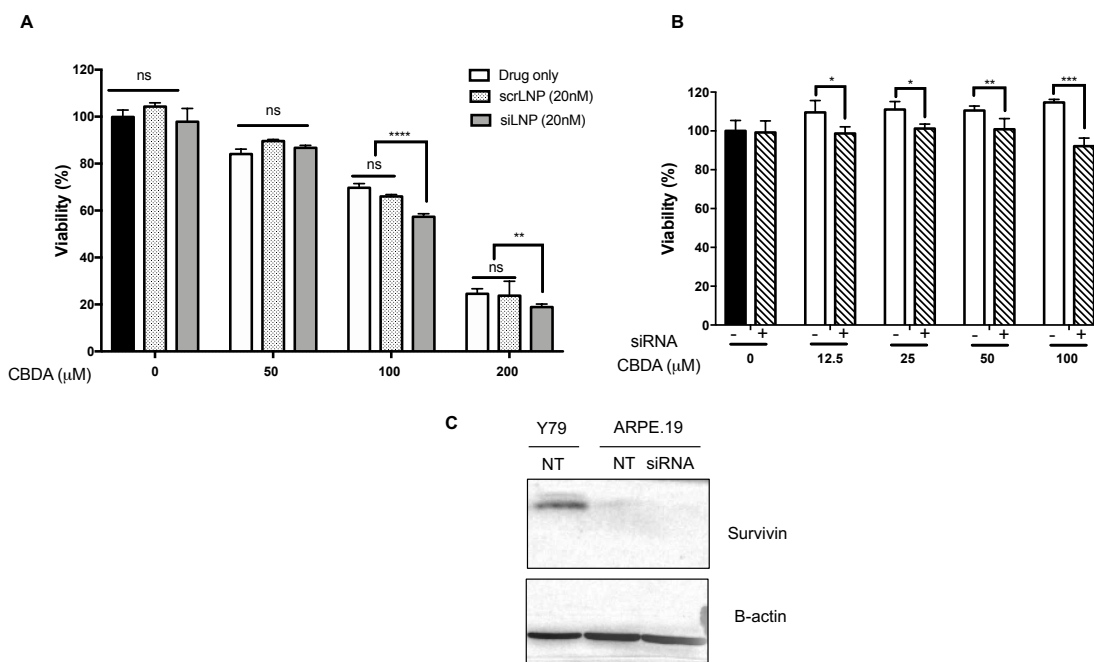


Figure 31. – Carboplatin cytotoxicity in (A) Y79 cells transfected with scramble (scrLNP, 20nM siRNA) or survivin-targeted siRNA switchable LNP (siLNP, 20 nM siRNA) and in (B) ARPE.19 cells transfected with siSurvivin (LF, 20 nM siRNA). (C) Survivin immunoblotting of non-treated Y79 and ARPE.19 prior and after survivin silencing (LF, 20 nM siRNA). Black bars represent non-treated cells.. Statistical analysis was performed using student t-test, where \* ( $p < 0.05$ ), \*\* ( $p < 0.005$ ), \*\*\* ( $p < 0.0005$ ), \*\*\*\* ( $p < 0.0001$ ) and ns means no significant difference.

Specificity of treatment is a crucial issue in cancer treatment. The specificity of the transfection of siLNP was assessed using siRNA scramble (Figure 31A) and the specificity of the treatment for retinoblastoma cancer cells was evaluated in a noncancer cell line (ARPE.19, Figure 31B).

As expected, scramble siRNA did not enhance CBDA toxicity since no difference can be seen between non treated cells and cells treated with scramble siRNA, as opposed to siRNA targeted against survivin (Figure 31A). This result confirmed that the selected siRNA sequence is specific to survivin, and that switchable LNP did not yield further toxicity on Y79 cells, which was consistent with our previous report (122). In addition, survivin silencing did not impact cell viability nor carboplatin toxicity (Figure 31B, striped bars). By reducing the  $IC_{50}$  of carboplatin, the survivin pretreatment also minimized the concomitant toxicity observed on healthy cells. For instance, survivin treatment followed by carboplatin 100  $\mu$ M induced 40% cell toxicity in Y79 cells (Figure 31A) but only 10% in ARPE.19 cells (Figure 31B). This could be rationally explained since ARPE.19 cells did not overexpress survivin (Figure 31C). These results confirm that survivin is a relevant and specific target for retinoblastoma, and that siRNA treatment improved the treatment selectivity. The specificity of survivin silencing as an adjuvant for targeting retinoblastoma cells was further confirmed as the siRNA treatment did not impact Y79 nor ARPE.19 cell's viability, as opposed to the highly cytotoxic activity of survivin inhibitor YM155 on both cell lines (Figure S36).

The same experiments were conducted on melphalan and topotecan using switchable LNP, since both drugs also exhibited improved efficacy with survivin silencing with lipofectamine (Figure 29). As expected, melphalan benefited from survivin silencing through switchable LNP, enhancing the toxicity of the drug treatment at 26 and 52  $\mu$ M (Figure 32A). At the latter concentration, siLNP followed by melphalan treatment killed more than 50% of Y79 at a calculated CI of 0.71, indicating a synergistic cooperation. Here again, the scramble version of siRNA did not yield any improvement of melphalan's activity, confirming the selectivity of siRNA targeted against survivin. Surprisingly, this effect was not observed for topotecan (Figure 32B). In this experiment, neither scramble nor switchable LNPs impacted the efficacy of topotecan, although lipofectamine was able to yield a significant effect in a previous experiment (Figure 29B). This suggested that even if survivin is downregulated, this effect was not significant to reduce cell viability.

Finally, we validated this combination strategy transfecting primary human RB cells with siLNP prior to treatment with carboplatin and melphalan, the two drugs selected from cytotoxicity screening with RB immortalized cells. As observed with Y79 cells, survivin downregulation by switchable LNP sensitized primary cells to carboplatin and melphalan (Figure 32C). The viability



of primary RB cells treated with siLNP followed by carboplatin at 200  $\mu$ M or melphalan at 52  $\mu$ M was reduced to 61 and 49%, whilst the viability of cells transfected with scrLNP and treated with either drug at the same concentration was not impacted. Interestingly, primary RB cells were resistant to carboplatin at 100  $\mu$ M and 200  $\mu$ M and melphalan at 26 and 52  $\mu$ M, behaving differently from their immortalized counterpart (compare Figures 31 and 32A and B with Figure 32C). This result suggests that the stepwise strategy of downregulating survivin with switchable LNPs followed by drug treatment can revert the resistance to melphalan and carboplatin in a closely related clinical model of retinoblastoma.

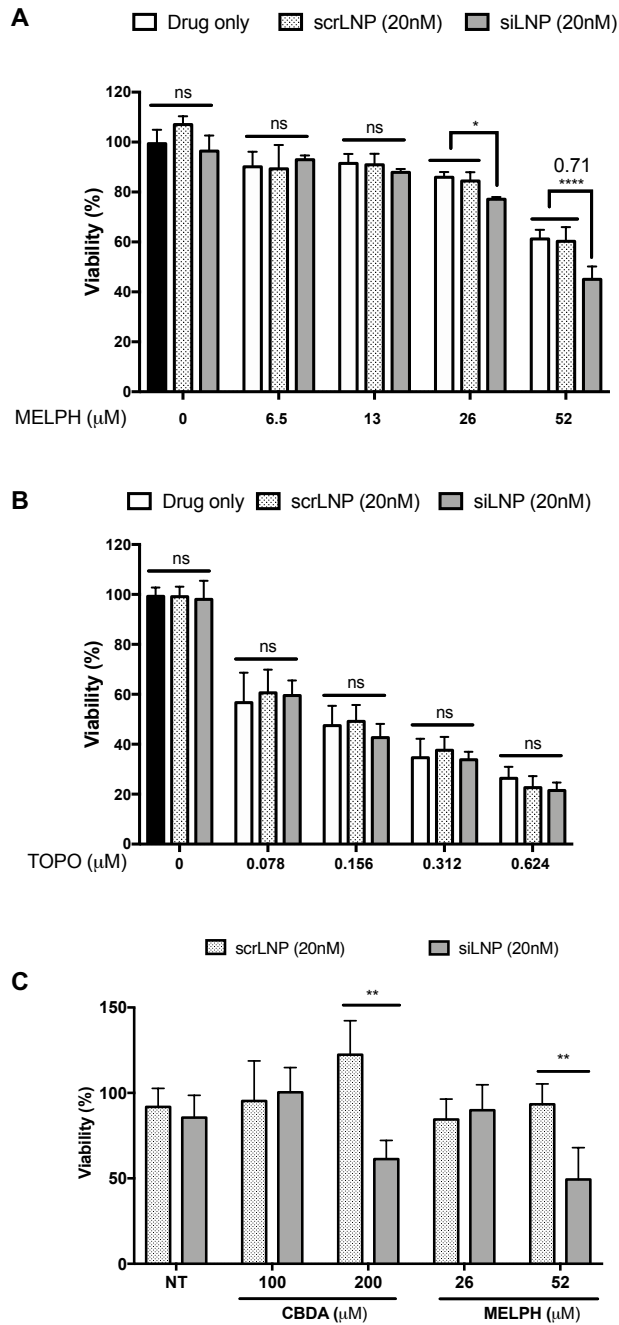


Figure 32. – Viability of Y79 (A and B) and primary RB cells (C) after siLNP or scrLNP transfection followed by chemotherapeutics. Y79 cells were treated with (A) melphalan or (B) topotecan. Primary RB cells were treated with either carboplatin or melphalan. Black bars represent non-treated cells. Viability of primary Statistical analysis was performed using student t-test, where \* ( $p < 0.05$ ), \*\* ( $p < 0.005$ ), \*\*\* ( $p < 0.0005$ ), \*\*\*\* ( $p < 0.0001$ ) and ns means no significant difference.

## 2.6. Discussion

Retinoblastoma treatment has encountered major advances in the last decade. Understanding of the molecular biology of cancer enabled more targeted therapies, and have improved the survival rates in developed countries (27). Survivin has been identified as one of the most specific cancer targets, due to its high difference of expression in cancer vs. healthy cells. Survivin was found to be overexpressed in RB tumor samples and positively correlated to RB staging (43, 90). In our studies, we indeed confirmed that retinoblastoma cells Y79 overexpressed survivin whereas healthy cells ARPE.19 did not (Figure 31). Therefore, the latter were not affected by the silencing treatment, with or without CBDA treatment (Figures 31 and S36A). This major advantage justifies the development of survivin-targeted treatments for retinoblastoma.

In this project, we used siRNA targeted against survivin to downregulate survivin before chemotherapy. Previous reports have reported the use of YM155, a small molecule inhibitor of survivin. Its mechanism of action was further revised for a DNA-damage inducing agent that led to survivin inhibition, but not specifically (61). YM155 has reached clinical trials but unfortunately failed because of low efficacy as a single agent. Its use in combination is explored in several preclinical cancer models (180, 193), including retinoblastoma (68). In our study, we observed that YM155 was cytotoxic regardless of the survivin expression level, as YM155 significantly reduced cell viability in both Y79 and ARPE.19 cells as compared to siRNA treatment (Figure S36). Therefore, siRNA treatment is seen as a more specific treatment, limiting the toxicity on healthy cells. As far as we know, this study is the first report on survivin-targeted siRNA for retinoblastoma (180).

Several delivery strategies have been explored for siRNA delivery. In particular, survivin-targeted siRNA has been delivered by polymeric nanoparticles, micelles, or liposomes (88, 180). In this project, we focused on the switchable lipid nanoparticles, previously developed for miRNA delivery to retinoblastoma *in vivo* (122).

We confirmed that switchable LNP were as efficient as lipofectamine for siRNA delivery on several cancer cell lines (Figures 26, 27, 29, 30) and can be used as a reliable transfection agent for immortalized and primary retinoblastoma cells. Caution must be exercised when interpreting the

results of survivin downregulation. Both qPCR (several cell lines transfected) and Western blot (Y79 and Y79-Luc) demonstrated that survivin knockdown was not achieved after treatment with siRNA against survivin. In Y79 cells, survivin protein was still detected following transfection with either siLNP (Figure 27B) or lipofectamine RNAiMAX (Figure 29C). As discussed earlier, survivin is a multifunctional protein intersecting with cell death and cell division pathways (51). Furthermore, survivin is distributed in different subcellular localizations, where each subpopulation can play a key role in survivin's nodal activity (51, 52). Therefore, we may hypothesize that protein knockdown was not observed due to subcellular populations detected by Western blot and qPCR 48 hours following transfection of 20 nM of siRNA against survivin. Although the confirmation of this hypothesis is beyond the scope of this investigation, our results are in agreement with other investigations where survivin downregulation, but not a knockdown, was identified by Western blot following transfection of siRNA or short hairpin RNA (shRNA) against survivin (88, 89, 194).

Nonetheless, the protein downregulation mediated by siLNP or LF was sufficient to significantly improve the cytotoxicity of carboplatin and melphalan in Y79 cells. Only the result of combination studies with topotecan differed between both agents (Figures 29 and 32). Cell viability could be reduced after lipofectamine/survivin treatment but not significantly by switchable LNP. Since cell viability is not a direct measurement of transfection efficiency, and alike results were observed for the two other drugs, we might hypothesize that survivin silencing through LNP might not be sufficient to impact topotecan's activity and result in viability decrease in these conditions. This mitigated effect was also observed by Ferrario *et al.* (68). Incubation with YM155 and topotecan induced apoptosis and reduced viability, but this effect was not significant in Y79 cells. In another study, Sato *et al.* reported the same range of viability for topotecan in combination with survivin-targeted siRNA/lipofectamine in a renal cancer model (195). Since topotecan is a topoisomerase I inhibitor and acts on the apoptotic cascade (196), further studies on apoptotic cascade intermediates could reveal potential interferences between topotecan and survivin mechanisms. The cytotoxic drugs selected in this study (melphalan, carboplatin, teniposide, topotecan) were inspired from the clinical guidelines of retinoblastoma management (27). In order to select the candidate exhibiting the best synergy with survivin silencing, we conducted a stepwise evaluation

of four drugs. Although all drugs impacted mRNA survivin levels, they behaved very differently on this retinoblastoma model. Y79 were found to be resistant to teniposide, and survivin silencing did not reverse this phenomenon, suggesting that resistance in this cell line was not involving survivin. Resistance to teniposide has been reported to involve altered topoisomerase II levels associated to multidrug resistance in leukemic cells (197). Y79 were also found to be resistant to carboplatin, but its IC50 could be reduced by a third after survivin downregulation (Figure S34). This synergy was also observed in Y79 cells for YM155 and carboplatin by Ferrario *et al.* (68).

Finally, melphalan was also potentialized by survivin downregulation, cutting by two third the required dose to kill retinoblastoma cells. This would alleviate the toxicity burden on healthy cells surrounding retinoblastoma in the eye. In a recent report, survivin inhibition was reported to reverse melphalan resistance in myeloma cells (198). Since melphalan is the most used chemotherapeutics in local administration of retinoblastoma in clinics (27), we believe that this strategy would significantly improve the tolerance of chemotherapy. In addition, we confirmed the cooperation between survivin silencing and carboplatin or melphalan on primary human RB cells. Similarly to immortalized Y79 cells, survivin silencing by switchable LNPs significantly enhanced the cytotoxicity of both drugs at the highest concentration tested.

To further improve the therapeutic effect, encapsulation of drugs into liposomes could be envisaged, as it enhanced melphalan efficacy in RB primary cells and might help overcoming multidrug resistance. In this case, the temporal sequence of siRNA and melphalan should be carefully studied (sequential or simultaneous) to optimize the synergy, as previously reported (180).

## **2.7. Conclusion**

In this study, we explored the ability of switchable lipid nanoparticle to silence survivin in several cancer *in vitro* models. This ability was confirmed in retinoblastoma model, establishing its potential as a transfection agent *in vitro*. Further studies are required to understand the variability between cell lines and potential prediction. In addition, we have explored the synergy between survivin silencing and chemotherapeutics in two retinoblastoma *in vitro* models: immortalized Y79 cells and primary RB human cells. The distinct behavior of the drugs demonstrated that the

survivin strategy cannot be applied to any cytotoxic agent and that a diligent screening should be envisioned when looking for synergy with survivin. Teniposide and topotecan were not significantly impacted by survivin downregulation, whereas carboplatin and melphalan were. The benefit of survivin downregulation by switchable LNPs on the cytotoxicity of melphalan and carboplatin was confirmed in human RB primary cells. The efficacy of this combination in a closer to the clinics model provides extra support for translating this strategy to *in vivo* assays. Further studies will be focused on survivin silencing prior to chemotherapy with melphalan and/or carboplatin in a rat model of retinoblastoma. Monitoring of the colocalization with the tumor cell (Y79-luc), regression of the tumor size, and biocompatibility studies will be envisaged. The selectivity of survivin siRNA treatment is a promising strategy to reduce the therapeutic dose of drugs and alleviate toxicity on healthy cells.

## 2.8. Supporting information

**Table 5:** Relative (%) survivin mRNA expression in different cancer cell lines after switchable LNP transfection

**Figure 33:** Lipofectamine RNAiMAX carrying siRNA survivin (20nM) downregulates survivin protein in both Y79 and Y79-luc cell

**Figure 34:** Y79 cells viability 48 hours upon (A) carboplatin, (B) topotecan, (C) melphalan or (D) teniposide treatment. (E) IC<sub>50</sub> before and after survivin silencing treatment with siRNA/LF (20nM)

**Figure 35:** Effect of survivin silencing on carboplatin and topotecan combined therapy in Y79 cells.

**Figure 36:** Viability of Y79 (A) and ARPE.19 (B) cells 48 hours after treatment with LF carrying siSurvivin (20 nM) or chemical inhibitor YM155 (2 nM).

Model	Cells	relative survivin mRNA expression				
		Non treated	LNP			Lipofectamine
			10 nM	20 nM	40 nM	40 nM
Breast	MCF7	92.87 ± 8.82	31.6 ± 4.75	16.53 ± 9.29	15.63 ± 5.09	19.86 ± 5.10
	MDA-MB-231	100.93 ± 7.54	78.01 ± 6.47	51.43 ± 11.45	60.30 ± 8.90	51.30 ± 7.56
	MDA-MB-436	93.53 ± 10.98	52.43 ± 2.11	34.03 ± 1.62	39.16 ± 2.99	6.43 ± 0.83

	BT474	103.80 ± 6.67	67.85 ± 4.45	81.01 ± 15.87	48.16 ± 8.79	9.96 ± 1.10
Colon	HT29	90.30 ± 13.71	70.36 ± 3.21	66.40 ± 2.82	70.43 ± 5.16	49.66 ± 6.98
Lung	A549	96.50 ± 14.69	82.50 ± 2.97	60.01 ± 3.11	21.56 ± 1.65	45.33 ± 5.97
	H460	91.15 ± 12.51	66.75 ± 29.91	79.95 ± 16.61	72.56 ± 8.41	26.10 ± 15.96
	H1299	102.36 ± 5.82	61.90 ± 17.58	76.60 ± 16.31	49.60 ± 11.33	8.96 ± 0.90
Cervix	HeLa	93.45 ± 7.30	22.03 ± 5.05	11.10 ± 2.12	7.56 ± 0.58	16.93 ± 1.07
	ME180	92.93 ± 6.95	91.70 ± 5.65	80.00 ± 6.42	80.36 ± 5.05	24.33 ± 1.51
Ovary	OV90	96.76 ± 4.36	101.00 ± 10.95	103.20 ± 4.17	91.46 ± 11.19	31.96 ± 11.39
	HEYA8	104.70 ± 6.64	95.55 ± 2.90	79.65 ± 14.35	63.73 ± 13.36	21.10 ± 4.59
	SKOV3	97.73 ± 10.09	72.16 ± 7.37	67.26 ± 6.88	48.30 ± 9.32	6.50 ± 1.15

Table 5. – Relative (%) survivin mRNA expression in different cancer cell lines after switchable LNP transfection. siRNA against survivin was used at 10, 20 or 40 nM and prepared by manual extrusion for all cell lines. Lipofectamine® RNAiMAX (LF) reagent was prepared using 40 nM siRNA. Untreated cells were used as controls. Gene downregulation was assayed by RT-qPCR 48 h after incubation (n = 3). *B-actin* mRNA (ACTB) was used as endogenous control. The relative expression of target gene was determined using the  $\Delta\Delta CT$  method (see materials and methods).

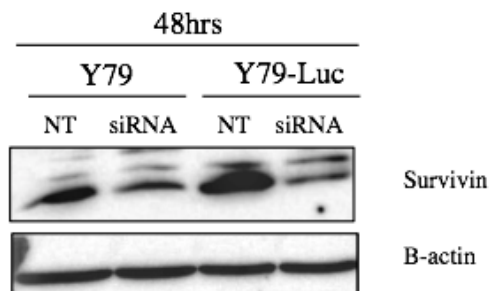
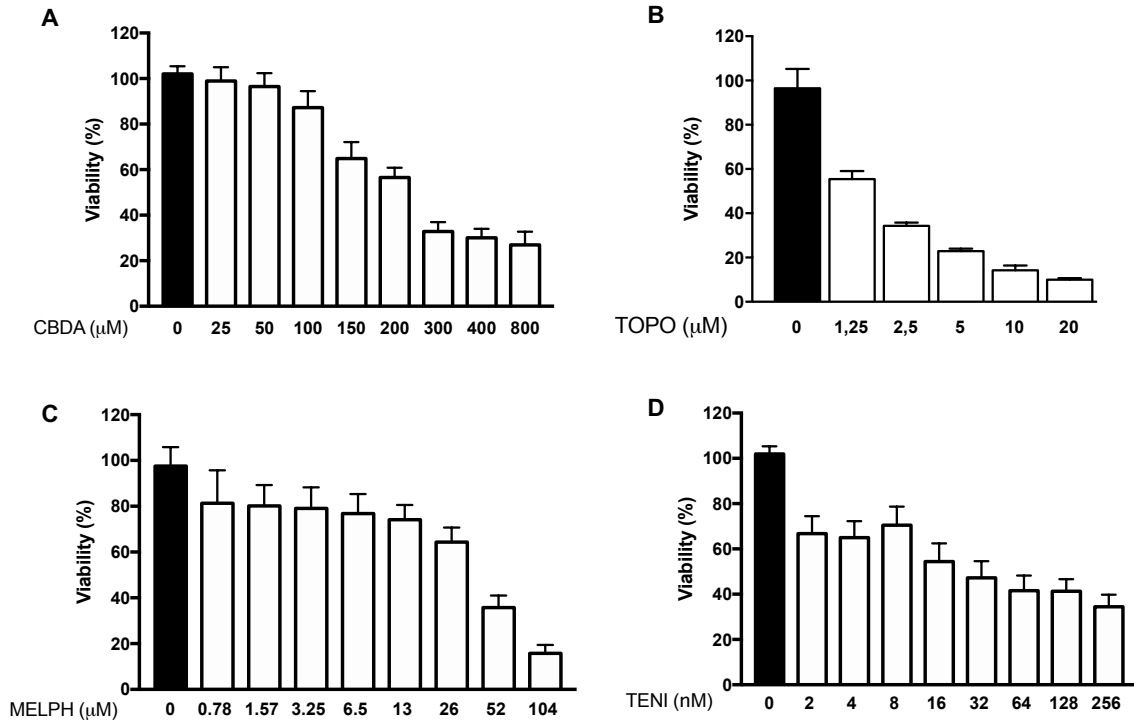


Figure 33. – Lipofectamine RNAiMAX carrying siRNA survivin (20nM) downregulates survivin protein in both Y79 and Y79-luc cells. Cells were harvested at 48 hours after transfection with siRNA/LF. Non-treated cells were used as control of survivin expression.



**E**

Y79	Carboplatin ( $\mu\text{M}$ )		Melphalan ( $\mu\text{M}$ )		Topotecan ( $\mu\text{M}$ )		Teniposide
	NT	siSurvivin	NT	siSurvivin	NT	siSurvivin	
	$282.5 \pm 32.39$	$191 \pm 22.39$	$14.83 \pm 2.42$	$3.43 \pm 0.61$	$1.48 \pm 0.07$	$0.52 \pm 0.09$	ND

Figure 34. – Y79 cells viability 48 hours upon (A) carboplatin, (B) topotecan, (C) melphalan or (D) teniposide treatment. (E) IC<sub>50</sub> before and after survivin silencing treatment with siRNA/LF (20nM).



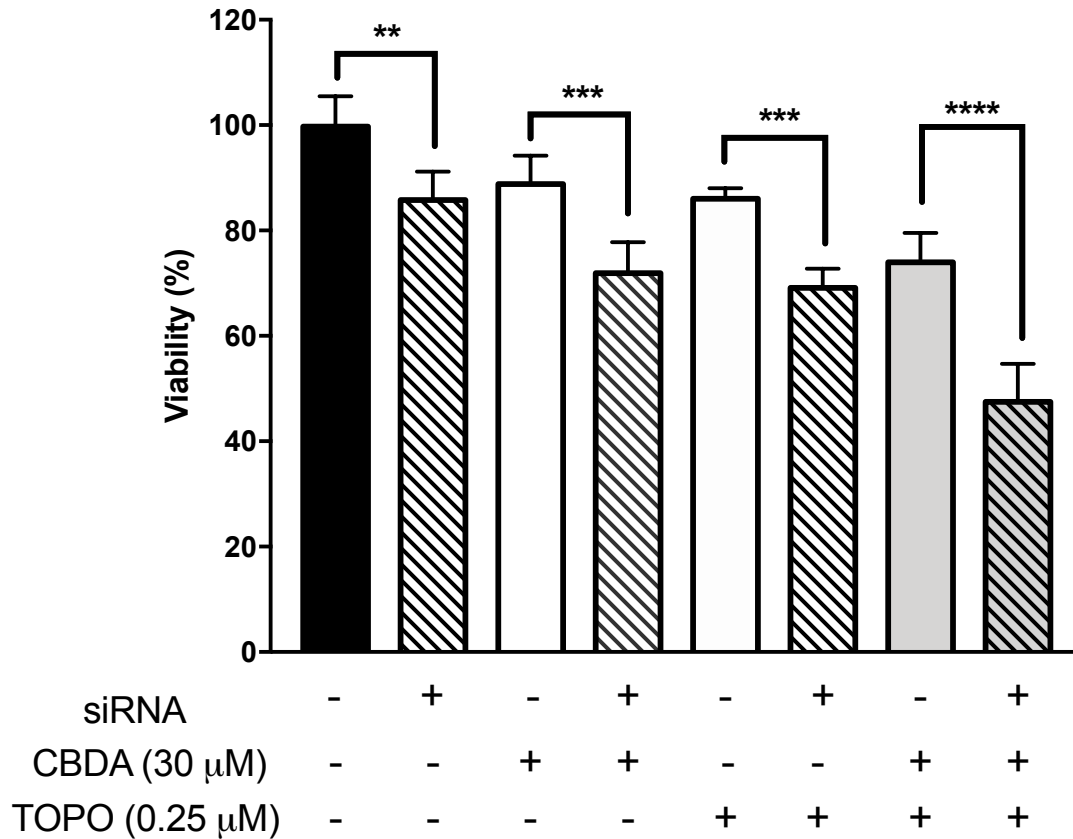
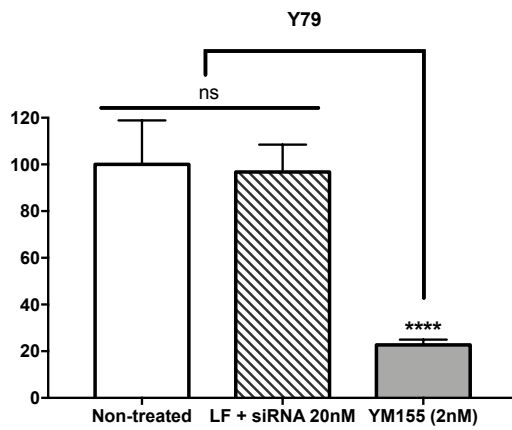


Figure 35. – Effect of survivin silencing on carboplatin and topotecan combined therapy in Y79 cells. Viability of Y79 cells after survivin downregulation by siRNA/LF (20nM) for 48 h followed by concomitant treatment with carboplatin (30 $\mu$ ) and topotecan (0.25  $\mu$ M). Non-treated cells, cells treated with CBDA or TOPO only, or siRNA/LF only for 48 h following the same sequencing regimen were used as control. Cell's viability was measured 96 hours from seeding using PrestoBlue fluorescence assay. Statistical analysis was performed using student t-test, where \* (p < 0.05), \*\* (p < 0.005), \*\*\* (p < 0.0005), \*\*\*\* (p < 0.0001) and ns means no significant difference.

A



B

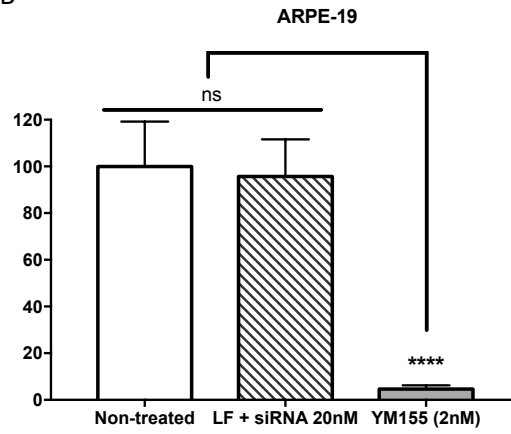


Figure 36. – Viability of Y79 (A) and ARPE.19 (B) cells 48 hours after treatment with LF carrying siSurvivin (20 nM) or chemical inhibitor YM155 (2 nM). Statistical analysis was performed using student t-test, where \* ( $p < 0.05$ ), \*\* ( $p < 0.005$ ), \*\*\* ( $p < 0.0005$ ), \*\*\*\* ( $p < 0.0001$ ) and ns means no significant difference.

## Chapter 3 – Paper published in the journal *Polymers*

Published. The electronic version of the paper can be found at <https://doi.org/10.3390/polym12030637>.

### 3.1. Title page

Title: Switchable lipid provides pH-sensitive properties to lipid and hybrid polymer/lipid membranes

Authors: Victor Passos Gibson <sup>1</sup>, Martin Fauquignon <sup>2</sup>, Emmanuel Ibarboure <sup>2</sup>, Jeanne Leblond Chain <sup>3,\*</sup> and Jean-François Le Meins <sup>2,\*</sup>

<sup>1</sup> Gene Delivery Laboratory, Faculty of pharmacy, University of Montréal, Montréal, QC, Canada; victor.passos.gibson@umontreal.ca

<sup>2</sup> Laboratoire de Chimie des Polymères Organiques LCPO Université de Bordeaux CNRS Bordeaux INPUMR 562916 Avenue Pey Berland F-33600 Pessac France; lemeins@enscbp.fr

<sup>3</sup> ARNA Laboratory, INSERM U1212, CNRS UMR 5320, University of Bordeaux, Faculty of pharmacy, F-33016 Bordeaux, France. Jeanne.leblond-chain@inserm.fr.

\* Correspondence: Jeanne.leblond-chain@inserm.fr; lemeins@enscbp.fr

### 3.2. Abstract

Blending amphiphilic copolymers and lipids constitutes a novel approach to combine the advantages of polymersomes and liposomes into a new single hybrid membrane. Efforts have been made to design stimuli-responsive vesicles, in which the membrane's dynamic is modulated by specific triggers. In this investigation, we proposed the design of pH-responsive hybrid vesicles formulated with poly(dimethylsiloxane)-*block*-poly(ethylene oxide) backbone (PDMS<sub>36</sub>-*b*-PEO<sub>23</sub>) and cationic switchable lipid (CSL). The latter undergoes a pH-triggered conformational change and induces membrane destabilization. Using confocal imaging and DLS measurements, we interrogated the structural changes in CSL-doped lipid and hybrid polymer/lipid unilamellar

vesicles at the micro- and nanometric scale, respectively. Both switchable giant unilamellar lipid vesicles (GUV) and hybrid polymer/lipid unilamellar vesicles (GHUV) presented dynamic morphological changes, including protrusions and fission upon acidification. At the submicron scale, scattered intensity decreased for both switchable large unilamellar vesicles (LUV) and hybrid vesicles (LHUV) under acidic pH. Finally, monitoring the fluorescence leakage of encapsulated calcein, we attested that CSL increased the permeability of GUV and GHUV in a pH-specific fashion. Altogether, these results show that switchable lipids provide a pH-sensitive behavior to hybrid polymer/lipid vesicles that could be exploited for the triggered release of drugs, cell biomimicry studies, or as bioinspired micro/nanoreactors.

**Keywords:** hybrid polymer/lipid membrane; pH-sensitive liposomes; switchable lipid

### 3.3. Introduction

Liposomes were initially developed as simplified cell membrane analogs and rapidly recognized as promising vesicles for a wide range of pharmaceutical applications (125), especially as drug delivery carriers (199). More than fifteen liposomal-based drug formulations have reached the market (200) (*e.g.* AmBisome<sup>®</sup>, Doxil<sup>®</sup>/Caelyx<sup>®</sup>, and DepoCyt<sup>®</sup>), and, recently, lipid nanoparticles enabled the delivery of the first RNAi-based drug (OnPattro<sup>®</sup>), a milestone for gene therapy (201). Nonetheless, liposomes still suffer from short shelf-life due to low stability and poor control over membrane leakage. On the other end, polymersomes have been developed to overcome these limitations. Such vesicles are composed of amphiphilic copolymers able to self-assemble into vesicles similarly than liposomes, exhibiting more robust properties, such as a more stable and less permeable membrane (133).

Recently, it became possible to combine the advantages of both polymersomes and liposomes into a new single hybrid unilamellar vesicle. Hybrid polymer/lipid vesicles combine the stiffness and stability of polymersomes with the biocompatibility and chemical functionality of phospholipids (134). Modulation of the structuration of the hybrid membrane is possible by playing with the nature of polymer and lipids used and the polymer-to-lipid molar ratio (144). However, the membrane permeability remains an issue, as passive diffusion or membrane disruption are the main methods of payload release (137). Therefore, efforts have been made to

formulate “smart” hybrid polymer/lipid vesicles, which would be able to change their membrane properties in response to specific triggers (202). In particular, pH-sensitive vesicles allow specific drug delivery at acidic conditions, as present at certain pathological microenvironment, e.g. cancer (159), inflammation (203) and ischemia (204, 205), or upon vesicle endocytosis in early endosomes. We have recently developed pH-sensitive lipids that undergo a conformational switch at acidic pH (130). Incorporated into lipid nanoparticles, they destabilize the lipid membrane in a pH-responsive fashion through a mechanism involving fusion. Thanks to their endosomal escape ability, they massively release their cargo in less than 30 min, resulting in good *in vitro* and *in vivo* transfection of siRNA, for cancer (122) and hypercholesterolemia applications (121).

In polymersomes, stimuli-responsive materials have been explored thanks to the versatility of polymer chemistry (137). Chen *et al.* formulated pH-sensitive polymersomes based on a PEG-moiety-grafted acid-labile polycarbonate able to encapsulate both paclitaxel and doxorubicin hydrochloride (DOX.HCl) and promote their release upon acid-triggered hydrolysis (163). Similarly, Liu *et al.* encapsulated DOX and DOX.HCl in pH-sensitive polymersomes based on poly(D,L-lactide)-block-poly(2-methacryloyloxyethyl phosphorylcholine) (164). However, in both cases, only partial drug release was obtained after 24 hours of incubation. Quicker responding systems would be desired to trigger burst drug release at the target site or to match the time course of endosomal maturation, which is under 1 h.

In this study, we hypothesized that doping polymeric membranes composed of poly-(ethylene oxide)-grafted poly(dimethylsiloxane) (PDMS-PEO) with switchable lipids would provide pH-sensitive properties to the resulting hybrid polymer/lipid vesicles. PDMS-*b*-PEO was selected because both blocks are biocompatible and PDMS exhibits flexible chains, which is required to prepare giant vesicle by the hydration process. In addition, such PDMS-*b*-PEO polymersomes have demonstrated their ability to form stable hybrid edifices. We exploited the development of giant unilamellar vesicles (206) to investigate the dynamic behavior of switchable lipids in either lipid or hybrid polymer/lipid unilamellar membranes (GUV and GHUV) at an acidic environment using confocal imaging. We compared the results with DLS measurements of micrometer large unilamellar lipid or hybrid polymer/lipid vesicles (206) (LUV and LHUV) at acidic pH. Lastly, we

analyzed, qualitatively and quantitatively, the influence of switchable lipids on membrane's permeability of calcein-loaded GUV and GHUV in acidic microenvironment.

### 3.4. Materials and methods

All organics solvents and chemicals were purchased from Sigma-Aldrich (Sigma-Aldrich Chimie, Saint Quentin Fallavier, France) and Thermo Scientific (Waltham, MA, USA). 1-Palmitoyl-2-oleoyl-sn-glycero-3-phosphocholine (POPC) and 1,2-dioleoyl-sn-glycero-3-phosphoethanolamine-N-(lissamine rhodamine B sulfonyl) (Rhodamine-PE) were obtained from Avanti Polar Lipids Inc. (Alabaster, AL, USA). PDMS-NBD and Poly-(ethylene oxide)-grafted poly(dimethylsiloxane) backbone (PDMS<sub>36</sub>-*b*-PEO<sub>23</sub>, M<sub>n</sub> 4000 g.mol<sup>-1</sup>) were synthesized as previously described (Polymers, 2019, submitted) and is known to spontaneously form polymersomes with a membrane thickness of 9.9 nm. Cationic switchable lipid (CSL) was synthesized as previously described (121). Sucrose and all other chemicals were purchased from Sigma-Aldrich (Saint Quentin Fallavier, France). Liquid nuclear magnetic resonance was acquired on a Bruker AVANCE 400 MHz spectrometer, using residual CHCl<sub>3</sub> for peak calibration.

#### 3.4.1. GUV and GHUV preparation

Giant Unilamellar Vesicles (GUV) and Giant Hybrid Unilamellar Vesicles (GHUV) were prepared by the electroformation method proposed by Angela *et al.* (207). Briefly, a 1.4 mg.mL<sup>-1</sup> solution of lipids (POPC or a mixture of POPC:CSL at a ratio 80:20 or 50:50 %mol) in chloroform or a mixture of polymer (PDMS<sub>36</sub>-*b*-PEO<sub>23</sub>) and lipid (POPC or CSL) at specific ratio (polymer:lipid 80:20 or 50:50 %mol) was deposited thrice in each side of ITO-coated slide (Sigma Aldrich, Saint Quentin Fallavier, France) using a capillary tip. For confocal visualization, two probes were added to the appropriate lipid or polymer/lipid organic solution: Rhodamine-PE at 0.1% w/w for lipid bilayer visualization and/or PDMS-NBD at 1% w/w for polymer visualization. The electroformation chamber was set by connecting both ITO-covered slides using a rubber O-ring, which were, then, dried under vacuum overnight. The next day, samples were connected to an AC generator and an alternative voltage (10 Hz, 2 V) was applied, followed by immediate addition of 200 µL of 100 mM sucrose solution. GUV or GHUV were collected after 45 minutes using a syringe with 21-gauge needle. Samples were prepared the same day as experimentation.

### 3.4.2. LUV and LHUV preparation

Large unilamellar vesicles (LUV) and large hybrid unilamellar vesicles (LHUV) were prepared using the lipid film hydration method. A lipid or a polymer/lipid solution in chloroform at the desired ratio (for LUV, 80:20 or 50:50 %mol POPC:CSL; for GHUV, 80:20 or 50:50 %mol PDMS<sub>36</sub>-*b*-PEO<sub>23</sub>:CSL) was added in a 25 mL round-bottom flask, dried under reduced pressure in a rotary evaporator and further dried under vacuum for at least 2 hours before hydration with 10 mL of ultrapure water at room temperature without any agitation to yield a 1.4 mg.mL<sup>-1</sup> lipid suspension. Afterwards, the suspension was extruded 11 times through a 1 μm polycarbonate membrane (Avanti Polar Lipids Inc., Alabaster, AL, USA) for DLS measurement.

### 3.4.3. <sup>1</sup>H NMR measurement

For <sup>1</sup>H NMR measurements only, LUV or GHUV were prepared by the hydration of the lipid film as mentioned above for LUV and LHUV, in order to get the sufficient amount of particles. After hydration, vesicles were not extruded but rather transferred to another 150 mL round-bottom flask for further freeze-drying. Then, the powder was resuspended in 500 μL of deuterated chloroform for <sup>1</sup>H NMR analysis to reach a final CSL concentration of 7 mg mL<sup>-1</sup>. Other components were calculated according to the POPC:CSL ratio, in LUV, or PDMS<sub>36</sub>-*b*-PEO<sub>23</sub>:CSL in GHUV. Samples were analyzed the same day as preparation.

### 3.4.4. Dynamic and static light scattering

Hydrodynamic diameter and ζ-potential of LUV or LHUV suspension were measured at 20°C using a Malvern Zetasizer Nano ZS (Malvern, Worcestershire, UK). Samples were diluted in Milli-Q water (1:2 v/v) to a final volume of 1 mL. Size measurements were performed with a scattered angle of 173° and reported as Z-average (intensity). The voltage for ζ-potential was set automatically by the equipment. In order to evaluate the effect of pH change on the LUV or LHUV properties, samples were acidified with HCl 0.01 mM and monitored using pH-meter until a drop of pH from 6.8 to 2.8. When applicable, equivalent amount to HCl of NaCl at the same molarity was added to vesicles suspension as a control. Measurements were performed at least in triplicate. Graphs were plotted using GraphPad (Prism 7, GraphPad Software Inc., San Diego, CA, USA).

### 3.4.5. Confocal imaging

All images were acquired on a Leica TCS SP5 (Leica Microsystems CMS GmbH, Mannheim, Germany) inverted confocal microscope (DMI6000). A 50- $\mu$ L aliquot of 100 mM sucrose suspension of GUV or GHUV was added into 150  $\mu$ L iso-osmolar (100 mOsm L<sup>-1</sup>) glucose solution containing in an eight-well  $\mu$ -Slide (Ibidi, Martinsried, Germany). Vesicles were allowed to sediment for at least 2 min before imaging. It is important to stress that vesicles were formulated in sucrose 100 mM and allowed to sediment in a glucose solution prepared at same concentration to avoid osmolarity shock. In order to evaluate the morphological and/or loaded-calcein intensity changes upon acidification, 39  $\mu$ L of an iso-osmolar HCl solution in glucose (100 mOsm L<sup>-1</sup>,  $4 \times 10^{-4}$  mM) was added directly in the well chamber. This volume of HCl was sufficient to, within 2 min, drop the pH down to 4.7, which was a value lower than the pH of the CSL conformation switch [16]. As a control, the same volume of an iso-osmolar sucrose solution of NaCl was added to the vesicles-containing chamber. PDMS-NBD/calcein and rhodamine-PE were stepwisely imaged using an argon laser line with an excitation/range of emission of 488 nm/500–530 nm (PDMS-NBD/calcein) and 514 nm/600–700 nm (Rhodamine-PE). Images were processed using Fiji/ImageJ software.

To calculate the overall fluorescence intensity of loaded calcein immediately before and after (2 min) HCl treatment, 13 images per condition were processed by ImageJ software on the same Region of Interest (ROI). Fluorescence intensity ranged from 0 to 250 and the number of pixels for each intensity was normalized by the total amount of pixels measured. A normal distribution of fluorescence intensity was plotted using GraphPad (Prism 7, GraphPad Software Inc., San Diego, CA, USA).

## 3.5. Results

### 3.5.1. CSL was successfully inserted into LUV or LHUV

In order to assess the incorporation of cationic switchable lipid (CSL) in lipid and hybrid polymer/lipid membranes, we prepared a series of vesicles and assessed their hydrodynamic diameter and polydispersity index (PDI) by DLS, their surface charge by electrophoretic light



scattering (ELS), and their composition by  $^1\text{H}$  NMR. CSL was incorporated (0, 20, 50 mol %) into POPC large unilamellar vesicles (LUV) or into PDMS<sub>36</sub>-*b*-PEO<sub>23</sub> large hybrid unilamellar vesicles (LHUV) formed by the hydration method (Table 1). Their non-switchable counterparts (POPC only and PDMS<sub>36</sub>-*b*-PEO<sub>23</sub>:POPC 80:20 and 50:50 mol %) were prepared in a similar fashion and used as control throughout the experiments (Table 6).

Name	Composition (% w/w)	Measured Molar Ratio ( $^1\text{H}$ NMR)	Hydrodynamic Diameter (nm)	PDI	$\zeta$ Potential (mV)
LUV-POPC	POPC	n/a	687 ± 6	0.254	-26 ± 1
LUV-CSL	POPC:CSL 80:20	80:20	101 ± 24	0.279	+29 ± 1
	POPC:CSL 50:50	54:46	245 ± 3	0.338	+38 ± 1
LHUV-POPC	PDMS <sub>36</sub> - <i>b</i> -PEO <sub>23</sub> :POPC 80:20	N/D	234 ± 0	0.339	-14 ± 1
	PDMS <sub>36</sub> - <i>b</i> -PEO <sub>23</sub> :POPC 50:50	N/D	165 ± 9	0.290	-8 ± 1
LHUV-CSL	PDMS <sub>36</sub> - <i>b</i> -PEO <sub>23</sub> :CSL 80:20	83:17	228 ± 2	0.354	+31 ± 1
	PDMS <sub>36</sub> - <i>b</i> -PEO <sub>23</sub> :CSL 50:50	51:49	320 ± 1	0.340	+35 ± 1

N/D: not determined

Table 6. – Physico-chemical properties of LUVs and LHUVs.

The ratio of  $^1\text{H}$  NMR aromatic peaks of CSL and methyl of POPC (CSL/POPC) and CSL and methyl of PDMS<sub>36</sub>-*b*-PEO<sub>23</sub> (CSL/ PDMS<sub>36</sub>-*b*-PEO<sub>23</sub>) was used to determine actual ratio amount of CSL after preparation in LUV and LHUV, respectively (Figures S40-S43). The values, close to the initial feeding ratio, indicate that switchable lipid was successfully incorporated into LUV and LHUV. After extrusion using a 1  $\mu\text{m}$  size filter, surprisingly, the vesicles exhibited a submicron size, which was characteristic of LUV and LHUV (206). The incorporation of CSL into LUV reversed the  $\zeta$ -potential, which was due to the cationic character of CSL. The  $\zeta$ -potential varied according to the CSL amount within LUV or LHUV, accounting for the incorporation of CSL into the membranes. Regarding the hydrodynamic diameter, a strong decrease is observed upon incorporation of CSL into LUV, while the evolution is less clear for LHUV and depends on the amount of CSL incorporated.

### 3.5.2. Acid-related morphological modifications

#### 3.5.2.1. DLS and $\zeta$ -measurements

CSL have been reported to undergo a conformational change upon acidification (predicted  $pK_a \approx 5.39$ ), destabilizing liposomes membrane and promoting fast cytosolic delivery of siRNA if incorporated at 50% mol (121). In this study, the hydrodynamic size distribution and derived count rate (DCR), accounting for the number of particles detected, were examined before and after global decrease of pH from 6.8 to 2.8 (Figure 37, Figure S44 and Table S8).

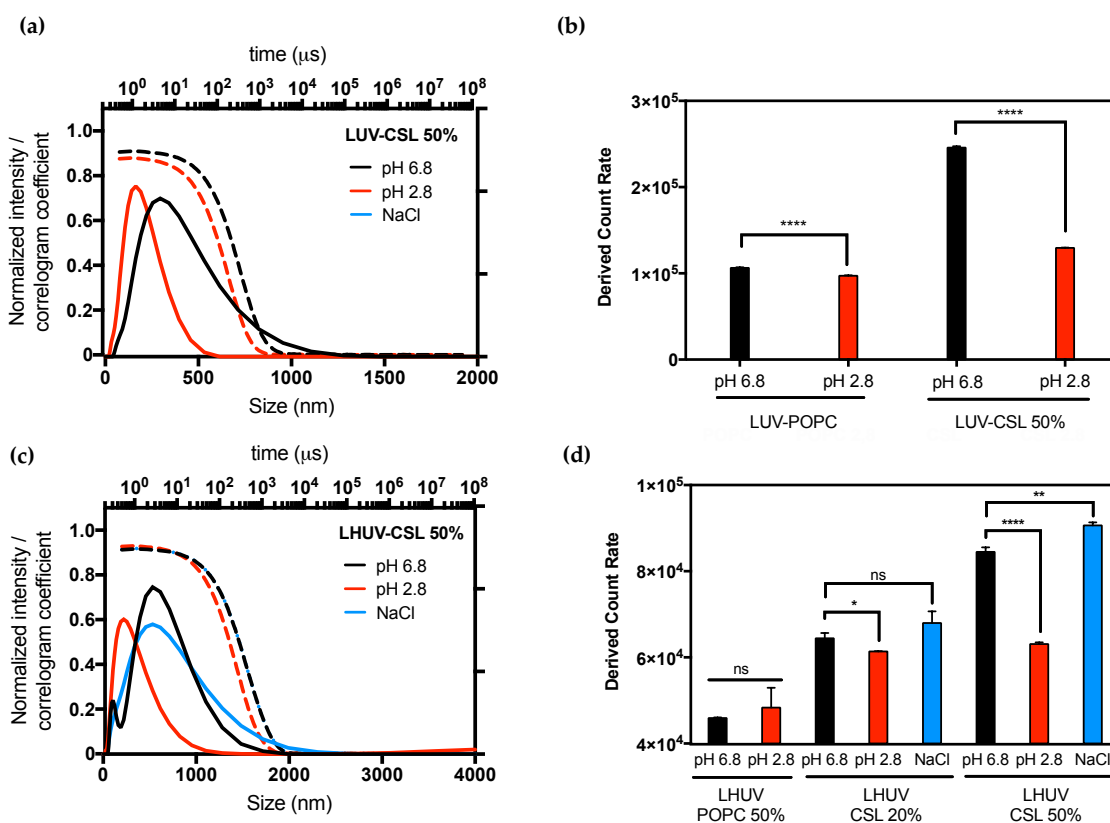


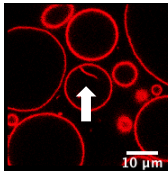
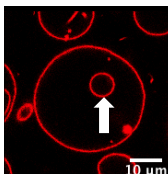
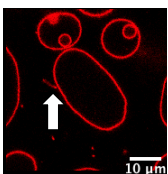
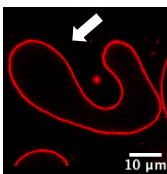
Figure 37. – DLS and zeta potential measurements of LUV and LHUV at pH 6.8 and 2.8. (a) Size distribution and correlogram of LUV-CSL 50%; (b) Derived count rate and zeta potential of both LUV-POPC and LUV-CSL 50% at both pHs; (c) Size distribution and correlogram of LHUV-CSL 50% at both pHs and after NaCl addition; (d) Derived count rate and zeta potential of LHUV-POPC 50%, LHUV-CSL 20% and 50% at both pHs and after NaCl addition. Data represents mean  $\pm$  SD ( $n = 3$ ). Student's t-test, where \* ( $p < 0.05$ ); \*\* ( $p < 0.005$ ) and \*\*\*\* ( $p < 0.0001$ ).

The presence of CSL strongly impacted the properties of both LUV and LHUV as compared to non-switchable vesicles. Upon acidification, LUV-CSL 50% became smaller (from 245 to 126 nm, Table S1) and presented a 2-fold decrease in the derived count rate, whilst exhibiting a suitable correlogram profile (Figure 37A and B). In comparison, LUV-POPC did not show any significant change upon acidification (Figure 37B, S44 and Table S8). This observation confirms the presence of CSL into the lipid bilayer and suggests a rearrangement of the vesicles, that might involve fusion as previously reported (121). Interestingly, similar behavior was observed for hybrid vesicles. Acidification significantly decreased LHUV-CSL size (Figure 1c for LHUV-CSL 50% and Figure S5 for LHUV-CSL 20%) and DCR (Figure 1d and Table S1). The more CSL incorporated into the LHUV, the more marked these effects (Figure 37D). In comparison, LHUV-POPC 20% was not impacted by acidification, neither in size (Figure S44) nor DCR (Figure 37D). LHUV-POPC 50% showed a slight increase in size (Figure S44 and Table S8) but not in DCR (Figure 37D). This increase could result from aggregation when the remaining negative charges of POPC-based vesicles were eventually neutralized. Notably, the lowering in size and DCR at CSL-containing LHUV were not caused by osmotic changes, as addition of same volume of NaCl at similar molarity did not impact hydrodynamic diameter and only slightly DCR at the highest CSL concentration (Figure 37D, and Table S8). Altogether, those results attest that LUV-CSL and LHUV-CSL exhibit pH-dependent modifications, which are due to the presence of switchable lipid embedded in vesicles' membrane.

#### 3.5.2.2. Confocal observations

We further investigated the pH-triggered modifications in membranes bearing switchable lipid by macroscopic observations using confocal microscopy. We incorporated CSL into Giant Unilamellar Vesicles (GUV-CSL) or Giant Hybrid Unilamellar Vesicles (GHUV-CSL) prepared by electroformation, since their micrometric size is better adapted to confocal microscopy. Their morphological alterations upon global decrease of pH was experimentally examined under confocal microscopy and posteriorly categorized as vesicles with inward or outward structures (tubular protrusions, membrane attached aggregation), internalized vesicles or membrane fluctuation (non-round shaped vesicles) (208) and assembled in a table with values presented as relative percentage of total vesicles counted (Table 7). As previously, non-switchable Giant

Unilamellar Vesicles (GUV-POPC) or Giant Hybrid Unilamellar Vesicles (GHUV-POPC) were used as control. It has to be noted that we failed to harvest switchable GHUV containing 50% of CSL after 45 minutes of electroformation. Therefore, we assessed the acid-induced modifications on GUV-POPC, GUV-CSL 20% (Figure S45) and GUV-CSL 50% (Figure S46), GHUV-CSL 20% (Figure S47) and GHUV-POPC 20% (Figure S47).

	Number of Vesicles Analyzed	Vesicles with Inward Structures <sup>1</sup>	Internalized Vesicles	Vesicles with Outward Structures <sup>1</sup>	Membrane Fluctuation <sup>2</sup>
					
GUV-POPC	64	15%	5%	1.5%	0
GUV-POPC+ NaCl	77	18%	5%	6.5%	0
GUV-POPC + HCl	79	18%	4%	1%	0
GUV-CSL 20%	125	11%	13%	3%	16%
GUV-CSL 20% + HCl	130	11%	16%	20%	4.6%
GUV-CSL 50%	140	9%	6%	6%	9%
GUV-CSL 50% + NaCl	254	6%	6%	2%	8%
GUV-CSL 50% + HCl	208	14.5%	7%	14%	4%
GHUV-POPC 20%	135	14%	28%	4%	0
GHUV-POPC 20% + HCl	183	11.5%	13%	2%	0

GHUV-CSL 20%	43	28%	37%	0	0
GHUV-CSL 20% + HCl	112	11%	40%	14%	7%

<sup>1</sup> nanotube, aggregations; <sup>2</sup> fluidity, non-rounded vesicles

Table 7. – Morphological changes in GUV and GHUV upon HCl or NaCl treatment.

The most remarkable observation concerned outward structures after acidification. GUV-CSL 20% and GUV-CSL 50% vesicles responded to acidification by projecting outward tubular protrusions, since 20% and 14% of the vesicles analyzed presented such structures, respectively (Table 7). Membrane-derived structures pointing outward are commonly referred as positive curvatures (208), whilst negative curvature denotes membrane-arisen structures pointing inward. In the images, we could observe a positive membrane curvature in GUV-CSL 20% and 50% as a result of treatment with HCl but not NaCl (Figures S45 and S46). Nevertheless, it is difficult to correlate the number of outward structures to the proportion of CSL in the lipid composition, since our preparation method does not guarantee the incorporation of similar amount of lipids in each vesicle.

Interestingly, this phenomenon was concomitant with a relative decrease in membrane fluctuation (Table 7), which could be associated to a transition from irregular shaped-vesicles towards more spherical shaped-vesicles after acid treatment (Figure S45, S46). Those effects were not observed in non-switchable vesicles, which did not show any substantial changes upon acidification (GUV-POPC, Table 7). Here again, these effects were not due to osmotic shock, since NaCl treatment did not impact CSL-GUV morphology (Table 7, Figure S45). Finally, In HCl-treated GUV-CSL 50%, the number of inward vesicles increased after acidification. This could be attributed to the further rearrangement of irregular-shaped vesicles, dividing into two daughter vesicles, as shown in the video S1 (Centre left, frame 1 to 8, Figure S46 and Video S1).

Regarding the hybrid polymer/lipid structures, similar observations could be drawn, although exhibiting a different morphology. Whilst GHUV-POPC 20% exhibited spherical and isolated vesicles in agreement with previous reports (209), the presence of CSL in the membrane resulted

in aggregated multilamellar structures (Figure S47). Interestingly, the dual labeling of lipids (Rhodamine-PE) and polymers (PDMS-NBD) indicated that polymers and lipids were mixed homogeneously within the membrane (Figure S47). Quantitatively, 28% of GHUV-CSL 20 % displayed inward structures and 37% of population had internalized vesicles under confocal observation, but no outward protruding tubes or membrane fluctuation were observed before acidification. After a global decrease of pH, up to 14% of switchable GHUV projected outward tubes, in a similar fashion than switchable GUV (Table 7, Figure S47). Such quantitative observations, as well as qualitative observations (Figure S48 and video S2), demonstrate that positive curvature of membranes is a pH-triggered response due to CSL, regardless the membrane's composition. For GHUV-CSL, this process was accompanied by an increase in the membrane fluidity (from 0 to 7%) and a reduction of the inward structures (Table 7). Furthermore, pH-triggered membrane distortions, leading to hybrid vesicles fission, was another similarity between CSL-bearing GUV and GHUV (GHUV-CSL 20%, frame 1-8, central left vesicle, Figure S48 and Video S2).

### **3.5.3. Study of the pH-Triggered Membrane Permeability to GUV and GHUV**

#### **3.5.3.1. pH-triggered calcein release from GUV**

Since CSL provided membrane modifications to both lipid-based and hybrid lipid/polymer-based vesicles, we wondered if this behavior could result in pH-triggered permeability and/or drug release ability. Calcein (10  $\mu$ M) was successfully encapsulated into GUV-CSL 50% and GUV-POPC 50% using the electroformation method. GUV-CSL 20% were not studied since morphological changes were less significant than for GUV-CSL 50% (Table 7). Calcein was homogeneously distributed in the core of GUV-POPC vesicles (Figure S49). Notably, calcein was not so evenly encapsulated into GUV-CSL 50%, which exhibited aggregation and calcein distribution within the core and the membrane of the vesicles (Figure S50). The permeability of calcein-loaded GUV was monitored by confocal microscopy upon acid treatment and the overall fluorescence intensity of vesicles was quantified before and after acidification (Figure 38)

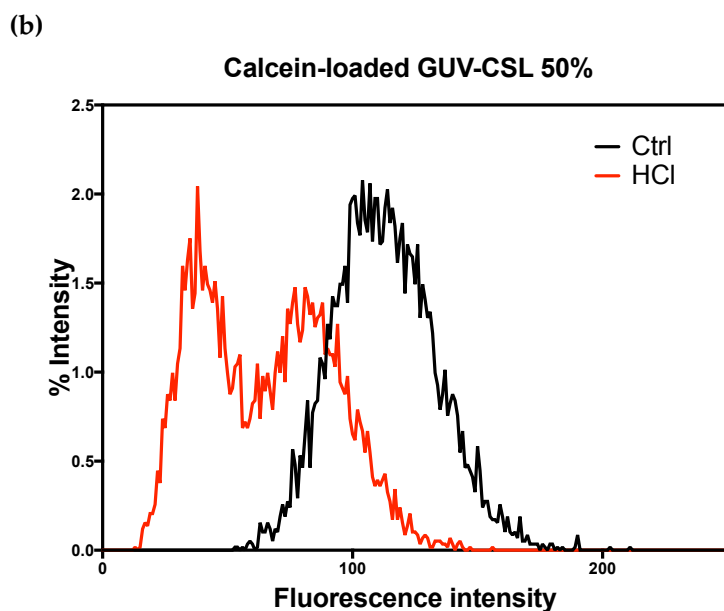
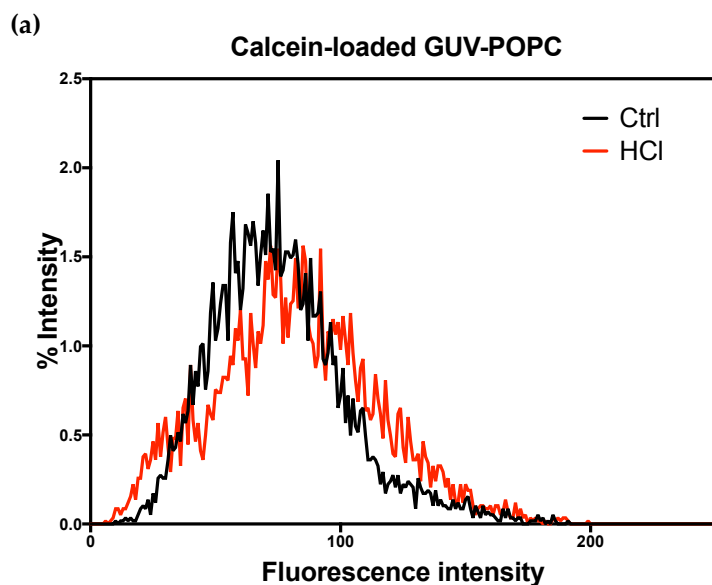


Figure 38. – Overall calcein fluorescence intensity in GUVs before and after acidification (pH 6.8 and 4.8). (a) Calcein loaded GUV-POPC and (b) calcein-loaded GUV-CSL 50%.

Acidification did not change the morphology (Figure S49) nor the fluorescence intensity (Figure 2a) of the GUV-POPC vesicles. Conversely, GUV-CSL 50% lost their fluorescent content (Figure 38B), demonstrating the release of calcein (Figure S50), qualitatively and quantitatively. These results confirm the pH-triggered release of hydrophilic probes reported for switchable lipids previously (130). In addition, the time course of these experiments (analysis after 2 min acidification) agree with the fast conformational switch of the lipids (130). Remarkably, an uneven

distribution of calcein intensity inside GUV-CSL 50% population was observed after acidification (Figure 38). This suggests that all the vesicles did not incorporate the same amount of CSL, since we previously reported that magnitude of release was related to the proportion of CSL in the lipid composition (130).

#### 3.5.3.2. pH-triggered calcein release from GHUV

The impact of CSL incorporation on the behavior of hybrid lipid/polymer vesicles was monitored the same way. Calcein was incorporated successfully into all hybrid lipid/polymer vesicles, yielding homogeneous spherical vesicles, even for GHUV-CSL 50%, which were not harvested without calcein (Figure 39 and S51). GHUV-CSL 20% were also much less aggregated and more unilamellar than their empty counterparts (compare Figure S8 and 39B). We could hypothesize that the presence of calcein at the interface, due to its amphiphilic nature, might modify surface properties and prevent membrane collapse and vesicle aggregation.

Global decrease of pH slightly impacted the intensity of GHUV-POPC 20% vesicles, but not the regular round morphology (Figure 39A). In contrast, GHUV-CSL 20% drastically lose their fluorescent content in few minutes, resulting in mostly empty vesicles (Figure 39B). Video recording demonstrated that the rate of release could vary according to the particles (Video S3). As previously checked, this release was not due to osmotic shock, since NaCl treatment did not trigger any release from the GHUV-CSL 20% (Figure 39C). Importantly, significant morphological changes were observed in GHUV-CSL 20% and 50% (Figure 39B and S51, respectively). Protruding and membrane fluidity (Figure 39B and Video S3) was observed at acidic pH, consistently with unloaded GHUV-CSL (Figure S9). In addition, vesicles became multilamellar and more aggregated (Figure S12), similarly to unloaded GHUV-CSL vesicles (Figure S48). In the case of calcein-loaded GHUV-CSL 50%, only a few aggregated vesicles were visualized after HCl treatment (Figure S51), as the hybrid system disrupted with global acidification (Video S4).



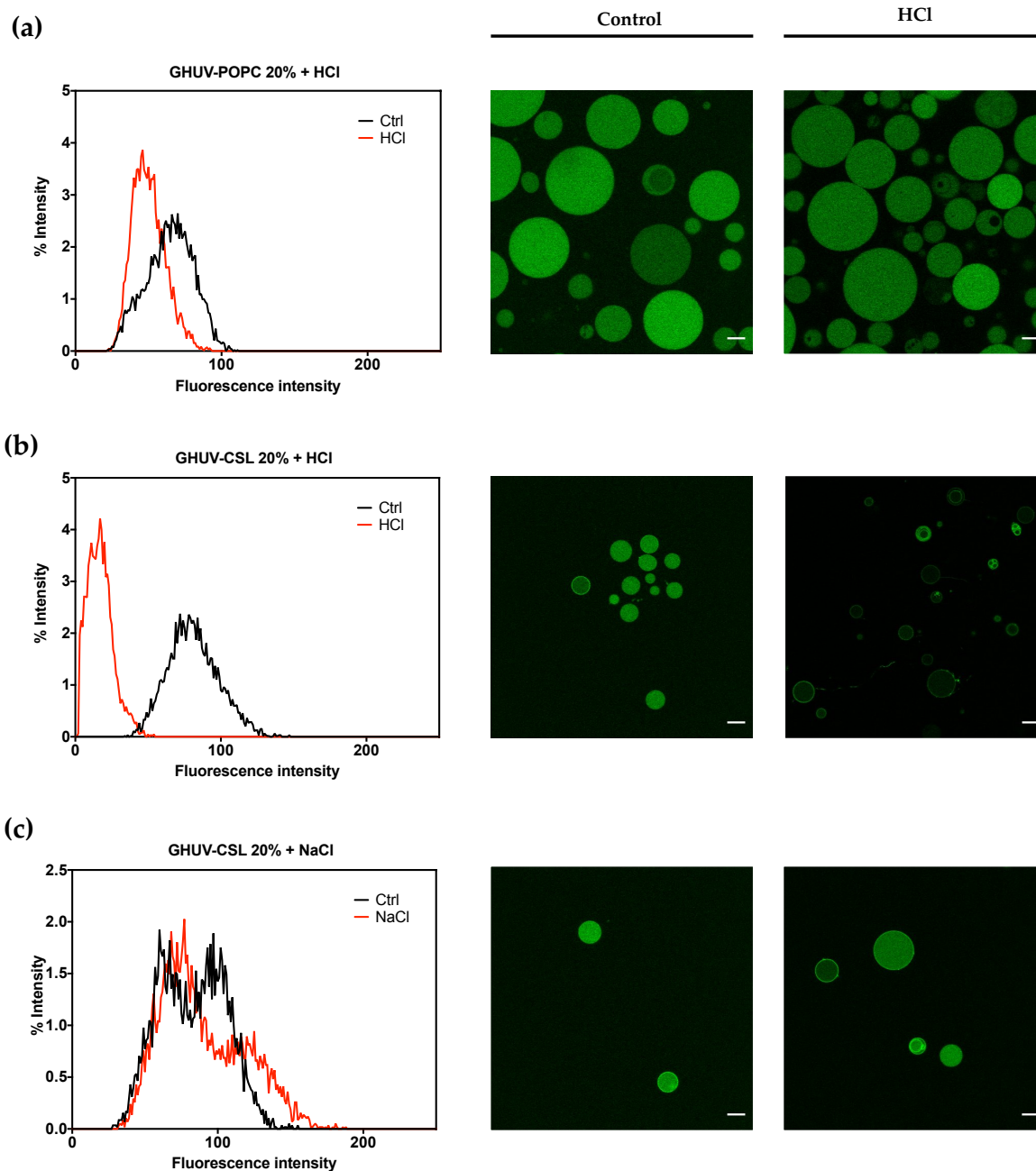


Figure 39. – Overall calcein fluorescence intensity distribution in GHUVs before and after acidification. (a) overall intensity in GHUV-POPC 20% followed by confocal pictures before and after acidification; (b) overall intensity of loaded-calcein in GHUV-CSL3 20% followed by representative pictures before and after acidification or (c) NaCl treatment. Scale bar: 10  $\mu\text{m}$ . Calcein filter.

### 3.6. Discussion

Molecular tweezers have been recently explored for pharmaceutical applications (129). Their defined molecular structure allows a fine-tuned control over their conformation, which can be monitored by external stimuli, such as pH, ions, or light (210). We have previously developed switchable lipids, which exploit a pH-triggered conformational change in order to destabilize a lipid membrane and release hydrophilic drugs and oligonucleotides in the cytoplasm of cells (121, 130). Although the microscopic mechanism of membrane destabilization by CSL is not yet elucidated, we demonstrated that fusion occurred in a pH-responsive fashion and could explain endosomal escape (121). In this study, we investigated further the biophysical behavior of the lipid membrane upon acidification, to understand deeper the membrane deformation upon acidification. Although different types of vesicles were examined (LUV and GUV composed of POPC and CSL, on the one hand, and hybrid polymer lipid, LHUV and GHUV composed of PDMS-*b*-PEO diblock copolymer, POPC and CSL, on the other hand), several common features were observed and could be attributed to the presence of the switchable lipid. Firstly, the pH-triggered release of calcein confirmed the fluorescence studies of sulforhodamine B release from switchable liposomes according to the pH (130). In latter study, 88% of the content was released in less than 15 min. The amplitude of release was related to the amount of the switchable lipid in the lipid composition, and to the pH. In addition, the confocal live observations were consistent with a fast responding system leading to quick release (less than 15 min). Secondly, we show for the first time that CSL-containing LUV undergo a size change (Table S8) under acidic treatment and that CSL-containing GUV present morphological alterations (Figure S45 and Table 7). Therefore, this study brings additional evidence that pH-triggered macroscopic changes of the lipid membranes are due to the conformational switch of the CSL. Remarkably, the difference between neutral and acidic conditions demonstrates the pH selectivity, which ensures biocompatibility with biological membranes at pH 7.4.

Then, such properties were then exploited for hybrid lipid/polymer membranes, in order to provide pH-responsive ability to polymersomes. Hybrid lipid/polymer vesicles have been designed with the idea of overcoming the drawbacks of each component (leakage and mechanical

instability for liposomes, low permeability for polymersomes) and combining the benefits of each component (biocompatibility and permeability of liposomes, toughness of polymersomes) (134)

Some studies comment about their potential use as nano/micro reactors (211) and/or as drug delivery agents (212), where membrane permeability is of prime importance. Without stimuli-responsive properties, payload release is only achieved by passive diffusion. In this study, we selected PDMS-*b*-PEO diblock copolymers, as they are able to form hybrid vesicles in association with POPC (213). We used lipid/polymer composition leading to a homogenous phase distribution and the pH-sensitive properties were maintained in GHUV, demonstrating the potential of the switchable lipid.

Macroscopically, GUV-CSL 50% and GHUV-CSL 20% shared a remarkable feature when submitted to HCl treatment: both lipid and hybrid polymer/lipid vesicles underwent morphological changes after global acidification (Table 7, Figure S45 and S47). In particular, the observation of outward structures upon acidification were specific to CSL-containing vesicles, since POPC-containing vesicles did not exhibit such deformations, and they were not due to osmotic changes. Another interesting observation shared among minimal membrane system and hybrid polymer/lipid vesicles was intense membrane fluctuation leading to vesicles fission (Figure S46 and S48).

Altogether, the morphological changes observed in this study at a nanometer (LHUV) or micrometer scale (GHUV) are due to the presence of the switchable lipid, which is able to destabilize polymer membranes, reported to be much stiffer than lipid membranes (133, 135, 214) . To our knowledge, the morphological changes reported here are the first report of pH-sensitive lipid/polymer hybrid vesicles (LHUV or GHUV).

### **3.7. Conclusion**

In this study, we show how a cationic switchable lipid (CSL) impacts the membrane dynamics of a lipid or hybrid lipid/polymer membrane in a pH-responsive manner. At a nanometer scale (LUV and LHUV), the incorporation of CSL resulted in decreased size and count rate, which was not observed for non-responsive vesicles. At a micrometer scale (GUV and GHUV), CSL incorporation resulted in pH-triggered membrane morphological changes and increased membrane permeability. This study gives additional insight to the biological behavior of CSL-based lipid

nanoparticles previously reported and open new perspectives in hybrid lipid/polymer vesicle design. In future studies, it would be important to screen different polymers or lipid/polymer blends to investigate the possibility of domains formation, which could lead to a pH-responsive gate in synthetic vesicles. In this case, we need to further develop a fluorescent-tagged switchable lipid to address their distribution within lipid and hybrids polymer/lipid membranes. Moreover, anisotropic NMR could unveil whether the tweezer-like structure arisen from pH-triggered conformational change are responsible for a bilayer incompatible polymorphism.

### **3.8. Supporting information**

**Figure 40** :  $^1\text{H}$  NMR of GUV-CSL 20% in  $\text{CDCl}_3$

**Figure 41** :  $^1\text{H}$  NMR GUV-CSL 50% in  $\text{CDCl}_3$

**Figure 42** :  $^1\text{H}$  NMR GHUV-CSL 20% in  $\text{CDCl}_3$

**Figure 43** :  $^1\text{H}$  NMR GHUV-CSL 50% in  $\text{CDCl}_3$

**Figure 44**: Size distribution and correlogram fit of LUV and LHUV at pH 6.8 and 2.8

**Table8**: Physico-chemical properties of LUVs and LHUVs before and after treatment with HCl or NaCl.

**Figure 45**: Morphological changes of GUVs upon HCl or NaCl treatment.

**Figure 46**: Snapshots of morphological changes in GUV-CSL 50% treated with HCl.

**Figure 47**: Morphological changes of GHUVs upon HCl treatment.

**Figure 48**: Snapshots of morphological changes in GHUV-CSL 20% treated with HCl.

**Figure 49**: Permeability of calcein-loaded GUV-POPC 50% treated with HCl.

**Figure 50**: Snapshots of morphological changes in GUV-CSL 50% treated with HCl.

**Figure 51**:. Snapshots of calcein-loaded GHUV-CSL 50% treated with HCl.

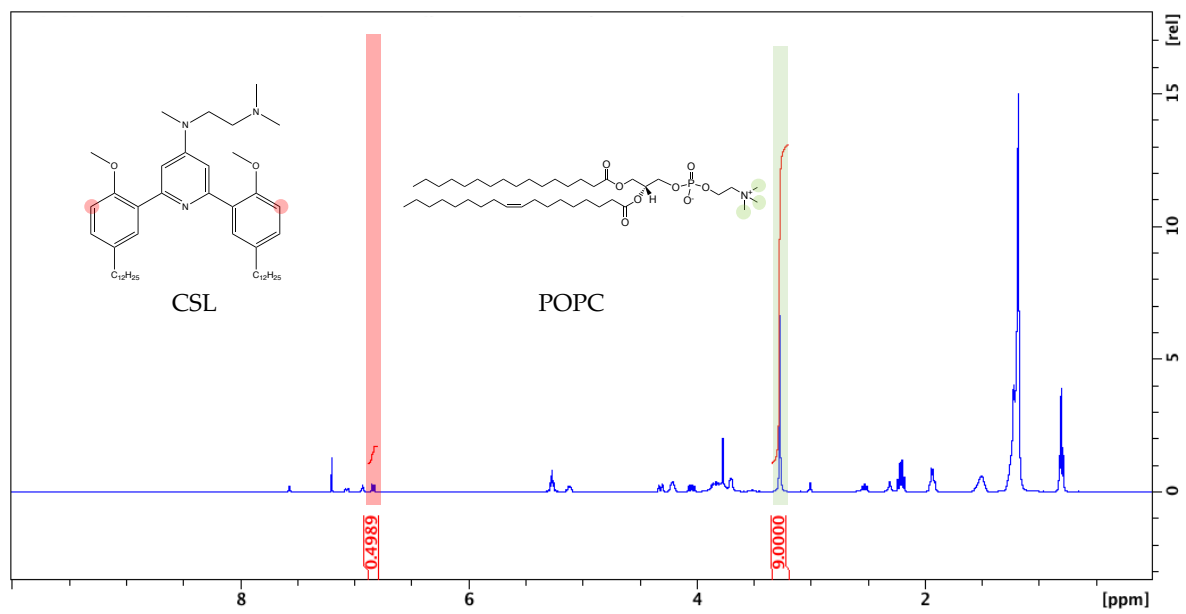


Figure 40. – <sup>1</sup>H NMR spectrum of GUV-CSL 20% in CDCl<sub>3</sub>

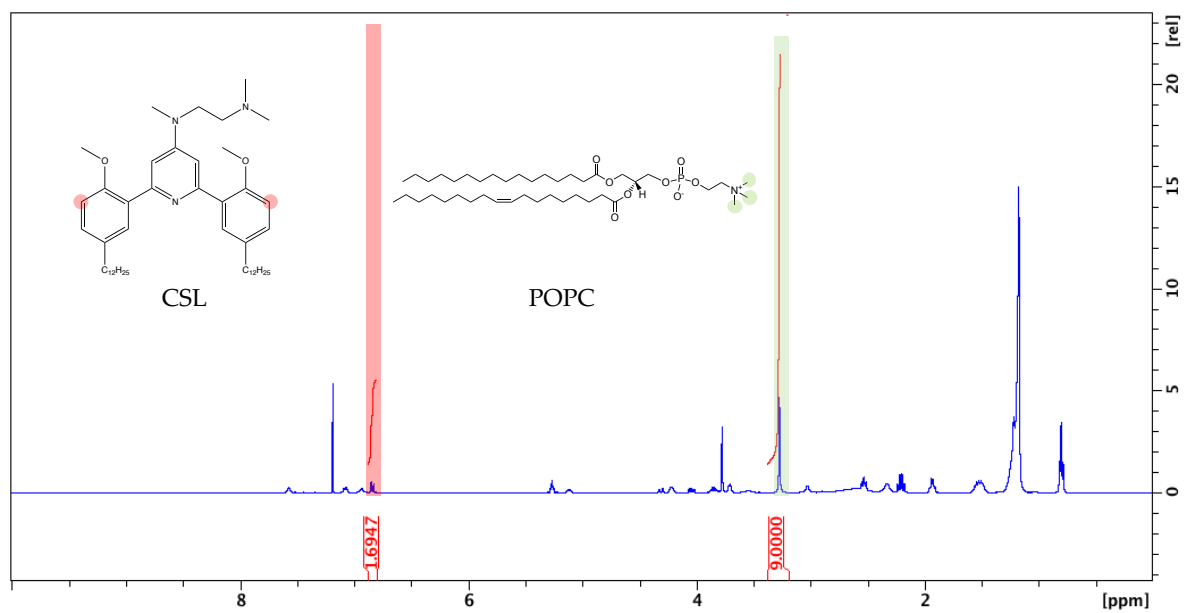


Figure 41. – <sup>1</sup>H NMR spectrum of GUV-CSL 50% in CDCl<sub>3</sub>

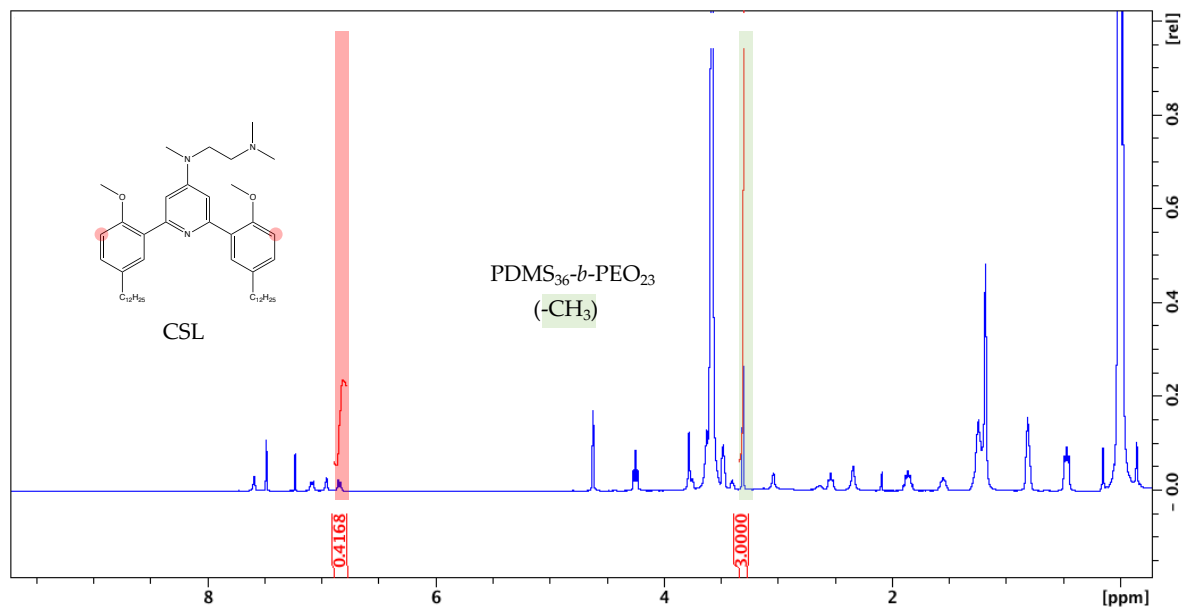


Figure 42. – <sup>1</sup>H NMR spectrum of GHUV-CSL 20% in CDCl<sub>3</sub>

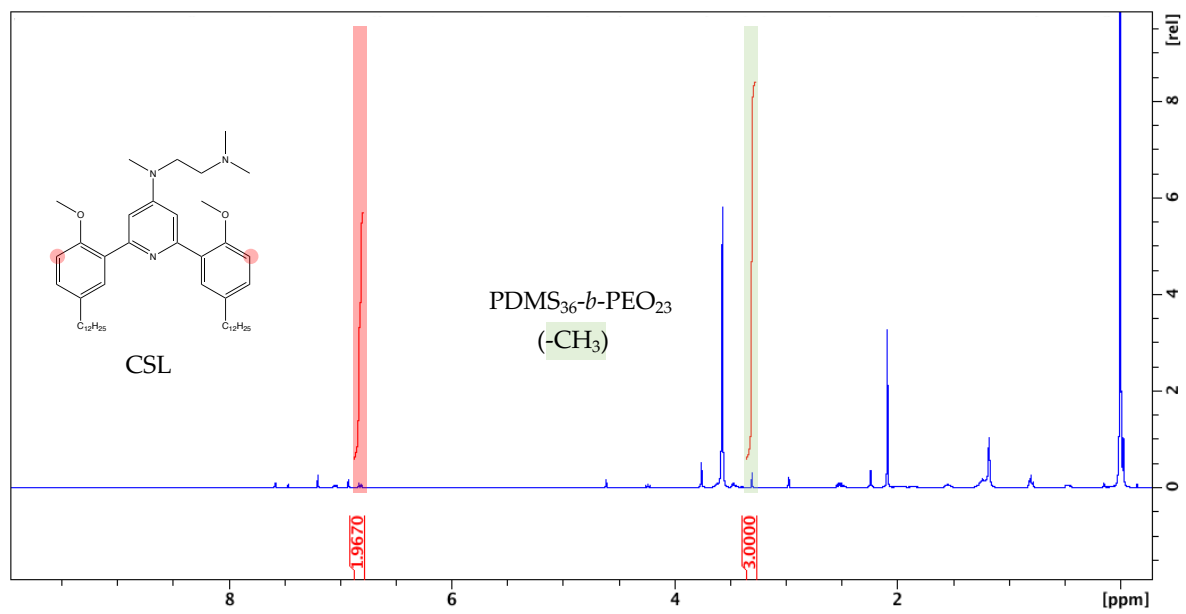


Figure 43. – <sup>1</sup>H NMR spectrum of GHUV-CSL 50% in CDCl<sub>3</sub>

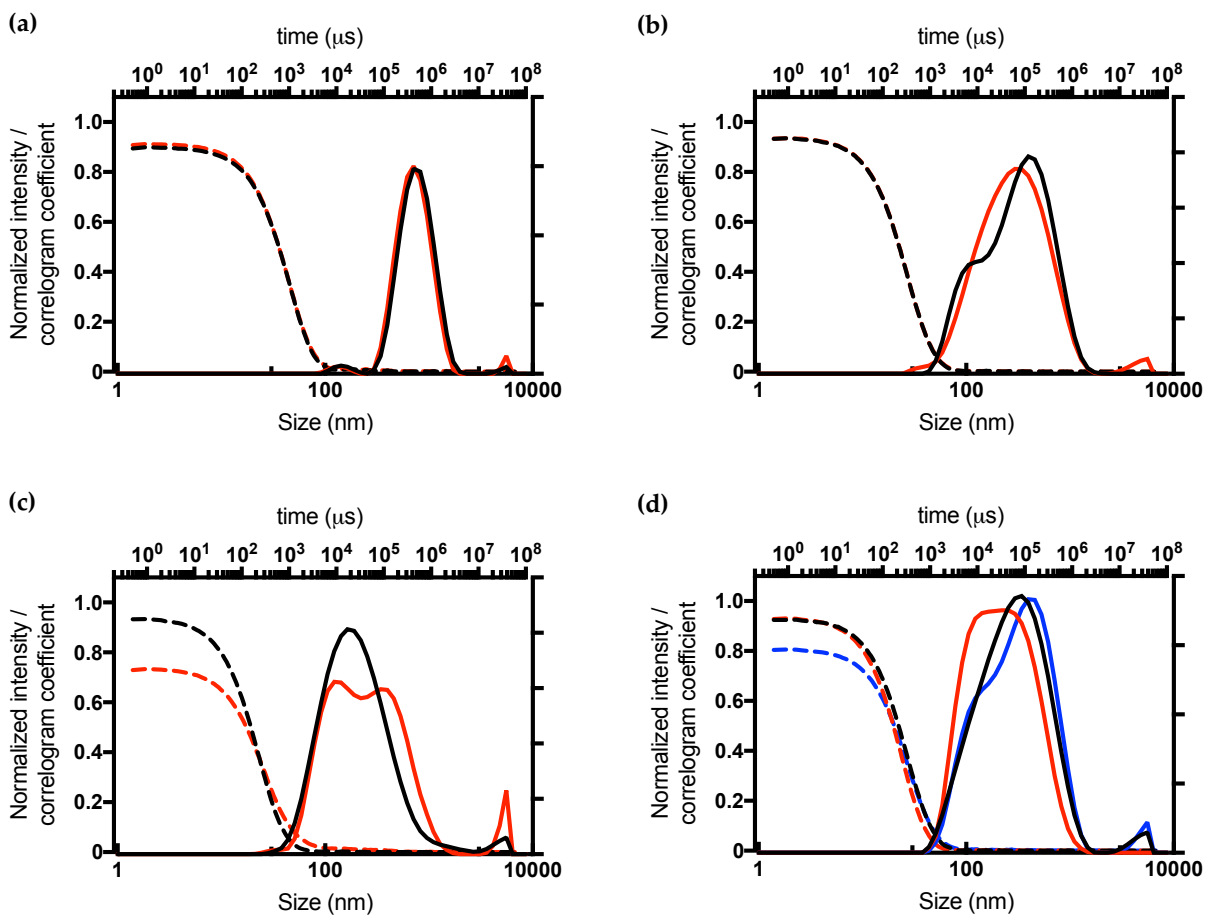


Figure 44. – Size distribution and correlogram fit of LUV and LHUV at pH 6.8 and 2.8. (a) LUV-POPC, (b) LHUV-POPC 20%, (c) LHUV-POPC 50%, (d) LHUV-CSL 20%.

Name	Composition (% mol)	Hydrodynamic diameter (nm)			DCR (Derived count rate)		
		pH 6.8	pH 2.8	NaCl	pH 6.8	pH 2.8	NaCl
LUV-POPC	n/a	687 ± 6	657 ± 9	ND <sup>1</sup>	1.0 × 10 <sup>5</sup> ± 0.6 × 10 <sup>3</sup>	0.9 × 10 <sup>5</sup> ± 0.4 × 10 <sup>3</sup>	ND
LUV-CSL	POPC:CSL 50:50	245 ± 3	126 ± 1	ND	2.4 × 10 <sup>5</sup> ± 1.3 × 10 <sup>3</sup>	1.2 × 10 <sup>5</sup> ± 0.2 × 10 <sup>3</sup>	ND
LHUV-POPC	PDMS <sub>36</sub> - <i>b</i> -PEO <sub>23</sub> : POPC 80:20	234 ± 1	232 ± 3	ND	6.1 × 10 <sup>4</sup> ± 0.2 × 10 <sup>3</sup>	6.1 × 10 <sup>4</sup> ± 0.1 × 10 <sup>3</sup>	ND
	PDMS <sub>36</sub> - <i>b</i> -PEO <sub>23</sub> : POPC 50:50	165 ± 2	216 ± 1	ND	4.5 × 10 <sup>4</sup> ± 0.1 × 10 <sup>3</sup>	4.8 × 10 <sup>4</sup> ± 3.7 × 10 <sup>3</sup>	ND
LHUV-CSL	PDMS <sub>36</sub> - <i>b</i> -PEO <sub>23</sub> : CSL 80:20	228 ± 2	177 ± 1	242 ± 8	6.4 × 10 <sup>4</sup> ± 1.0 × 10 <sup>3</sup>	6.1 × 10 <sup>4</sup> ± 0.07 × 10 <sup>3</sup>	6.7 × 10 <sup>4</sup> ± 2.2 × 10 <sup>3</sup>
	PDMS <sub>36</sub> - <i>b</i> -PEO <sub>23</sub> : CSL 50:50	320 ± 1	183 ± 1	312 ± 10	8.4 × 10 <sup>4</sup> ± 0.8 × 10 <sup>3</sup>	6.3 × 10 <sup>4</sup> ± 0.3 × 10 <sup>3</sup>	9.0 × 10 <sup>4</sup> ± 0.5 × 10 <sup>3</sup>

<sup>1</sup>Not determined

Table 8. – Physico-chemical properties of LUVs and LHUVs before and after treatment with HCl or NaCl.



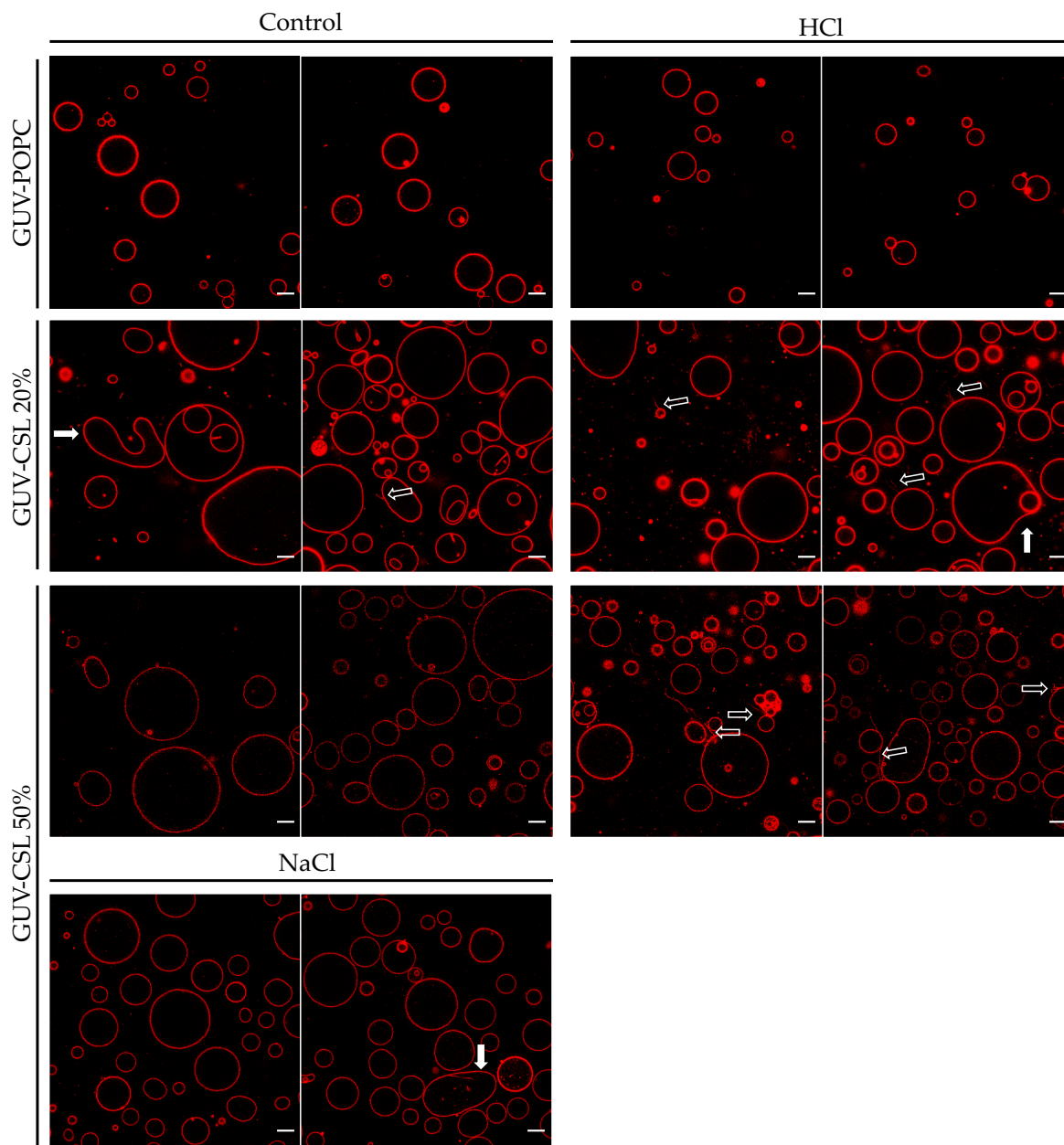


Figure 45. – Morphological changes of GUVs upon HCl or NaCl treatment. Open arrows: vesicles with outward projections. Full arrows: membrane fluctuation events. Scale bar: 10 μm.

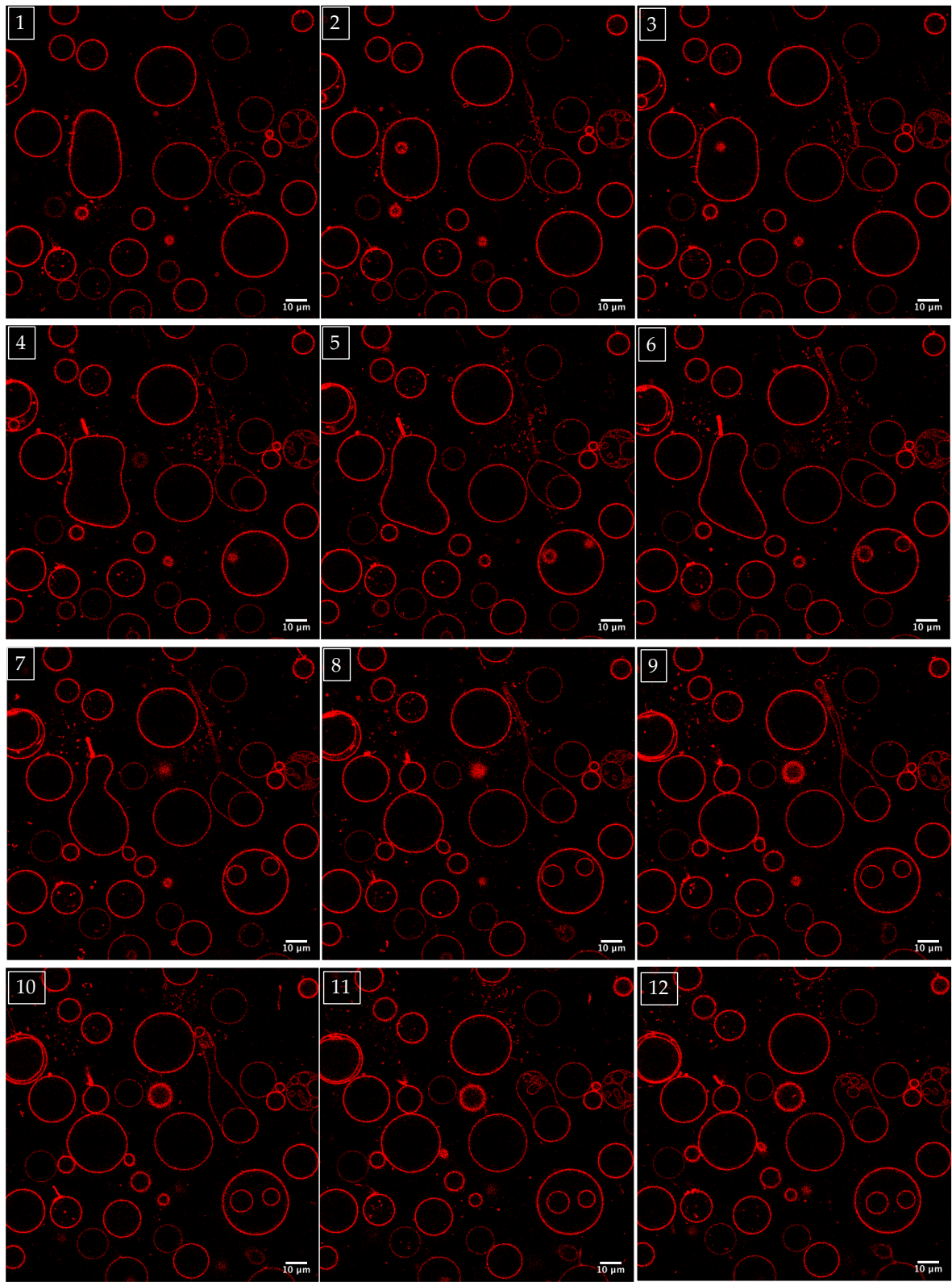


Figure 46. – Snapshots of morphological changes in GUV-CSL 50% treated with HCl. White boxes in the upper left corner indicate frame order. Scale bar: 10  $\mu\text{m}$ . Time-lapse between pictures is 0.143 second; total time-lapse is 1.86 seconds. Scale bar: 10  $\mu\text{m}$ .

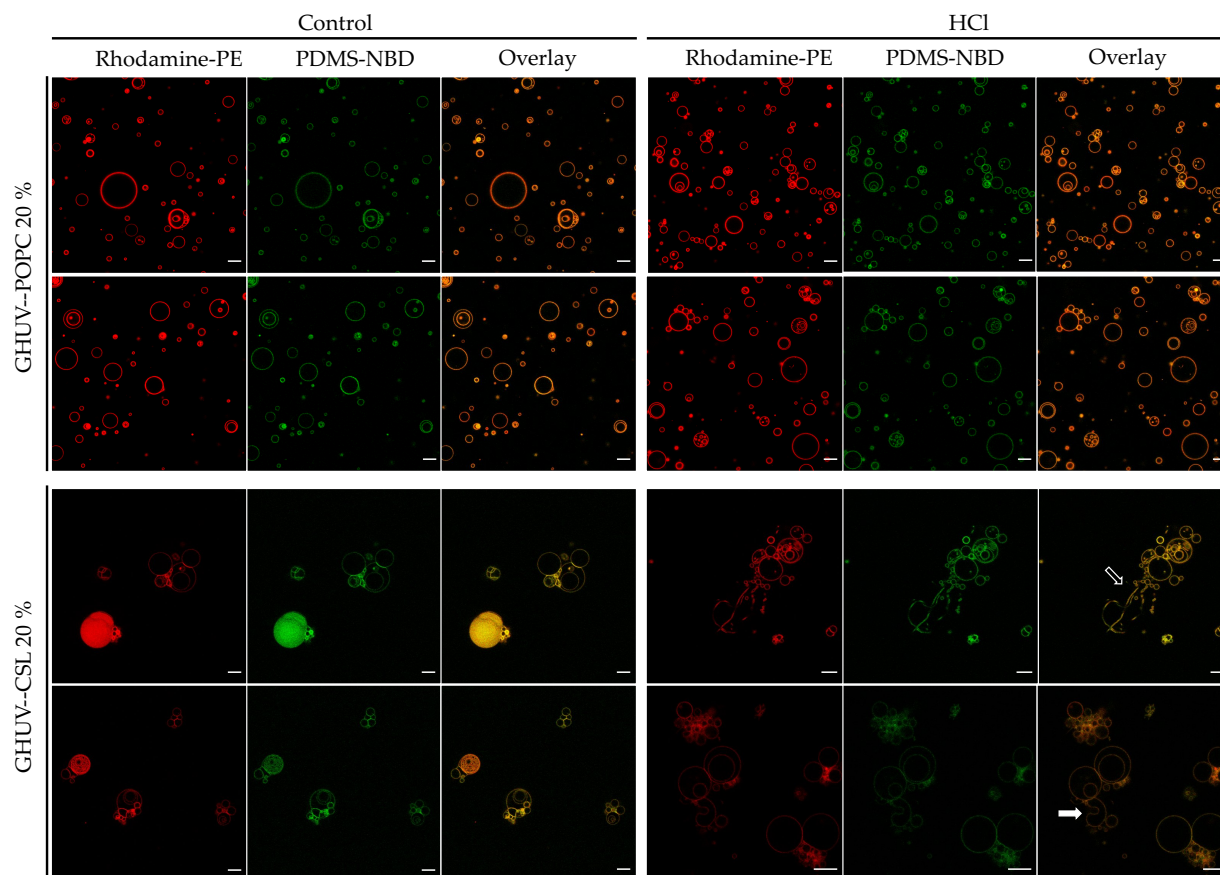


Figure 47. – Morphological changes of GHUVs upon HCl treatment. Open arrows: vesicles with outward projections. Full arrows: membrane fluctuation events. Scale bar: 10  $\mu\text{m}$ .

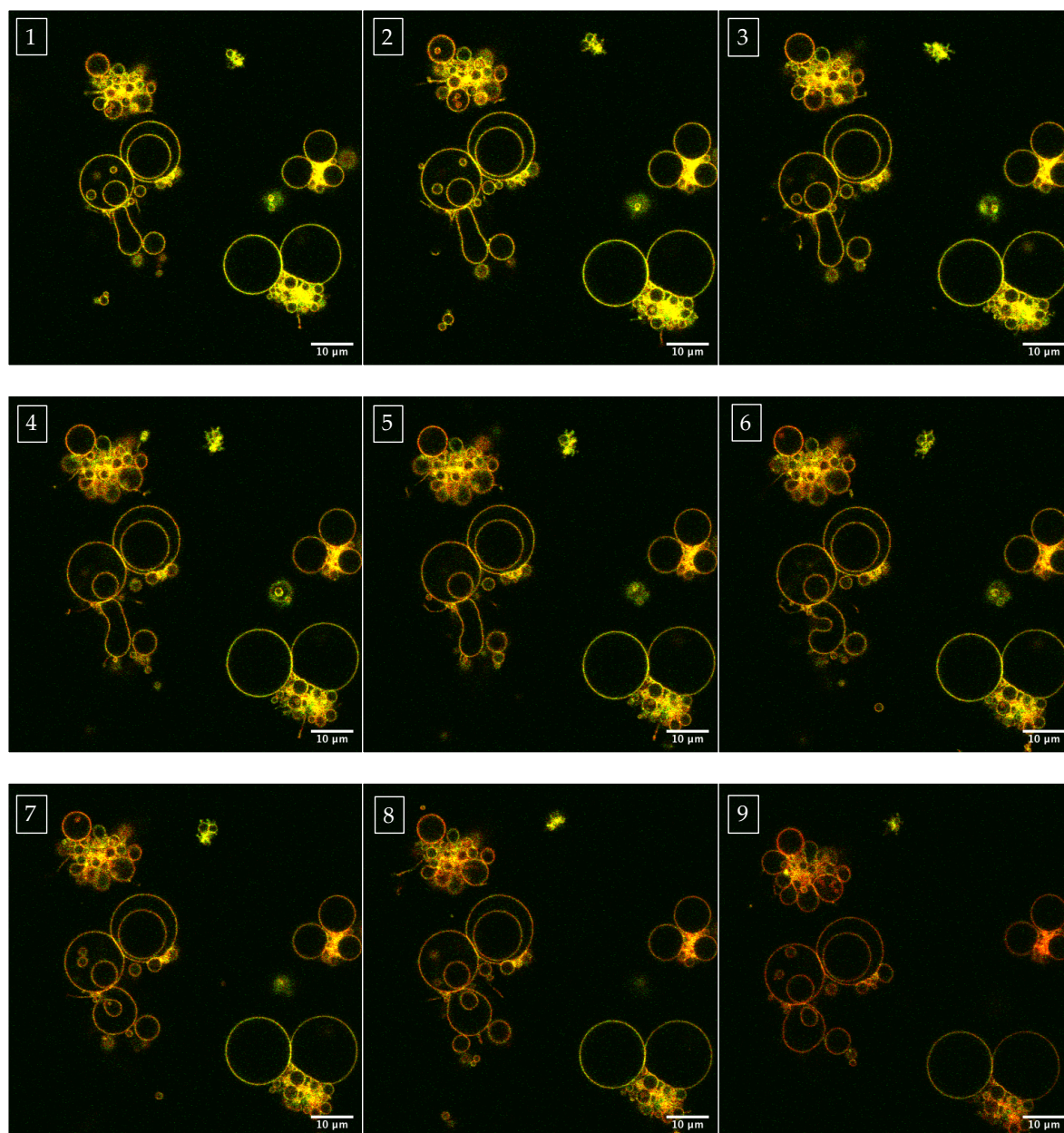


Figure 48. — Snapshots of morphological changes in GHUV-CSL 20% treated with HCl. Merged PDMS-NBD and Rhodamine-PE filters. Scale bar: 10  $\mu\text{m}$ . Time-lapse between pictures is 0.694 second; total time-lapse is 6.25 seconds. Scale bar: 10  $\mu\text{m}$ .

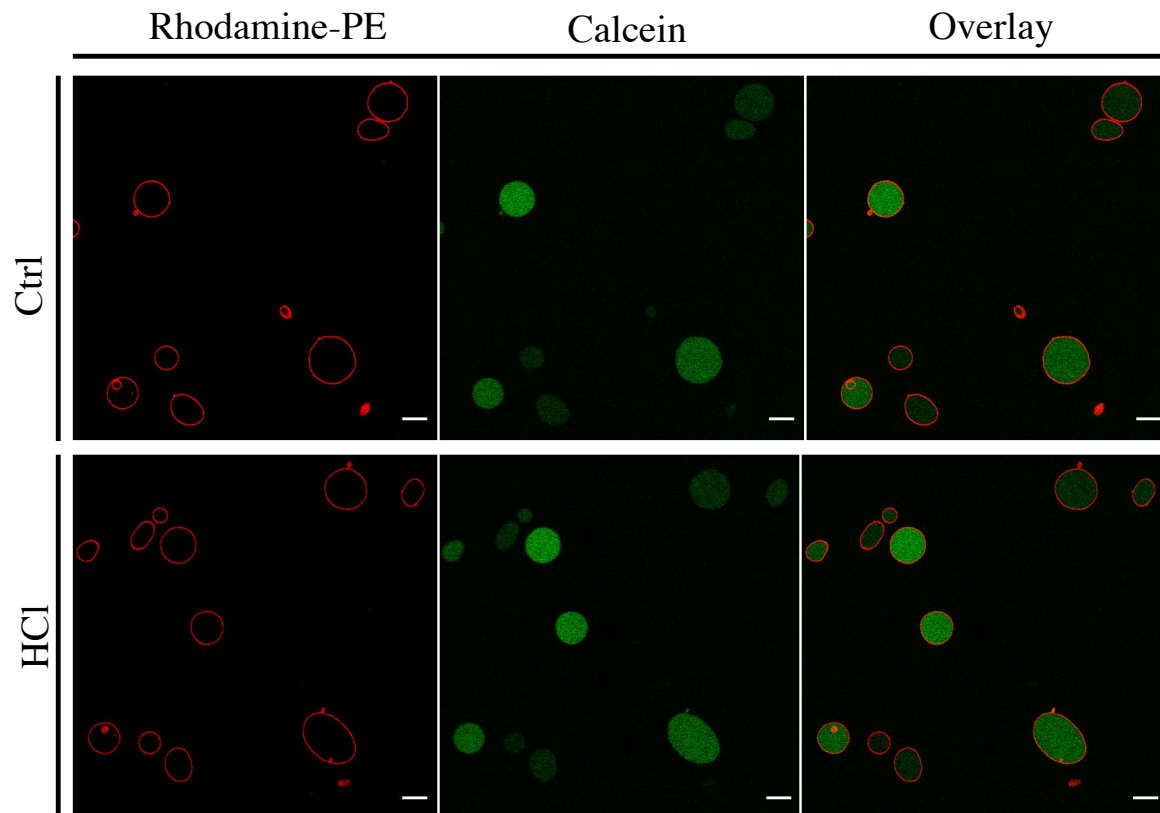


Figure 49. – Permeability of calcein-loaded GUV-POPC 50% treated with HCl. Snapshots of morphological changes in GUV-POPC 50% treated with HCl. Rhodamine, calcein and merged filters. Scale bar: 10  $\mu\text{m}$

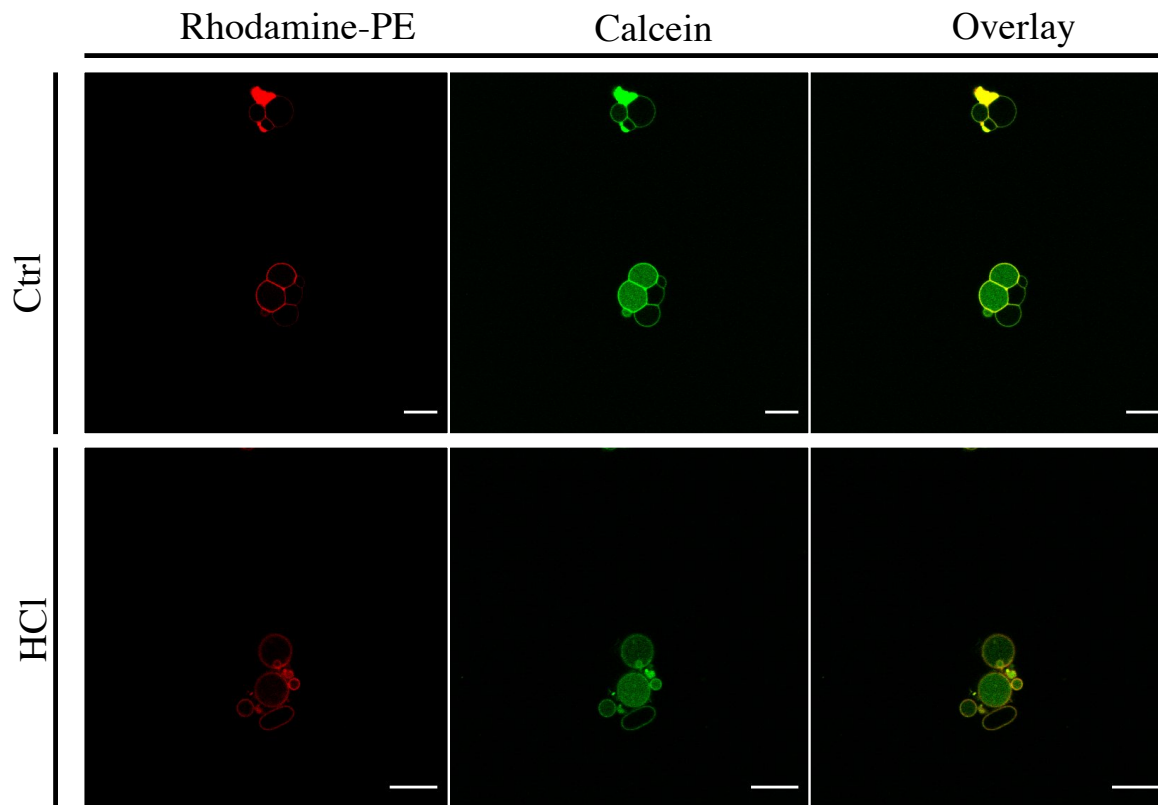


Figure 50. – Snapshots of morphological changes in GUV-CSL 50% treated with HCl. Rhodamine, calcein and merged filters. Scale bar: 10  $\mu\text{m}$

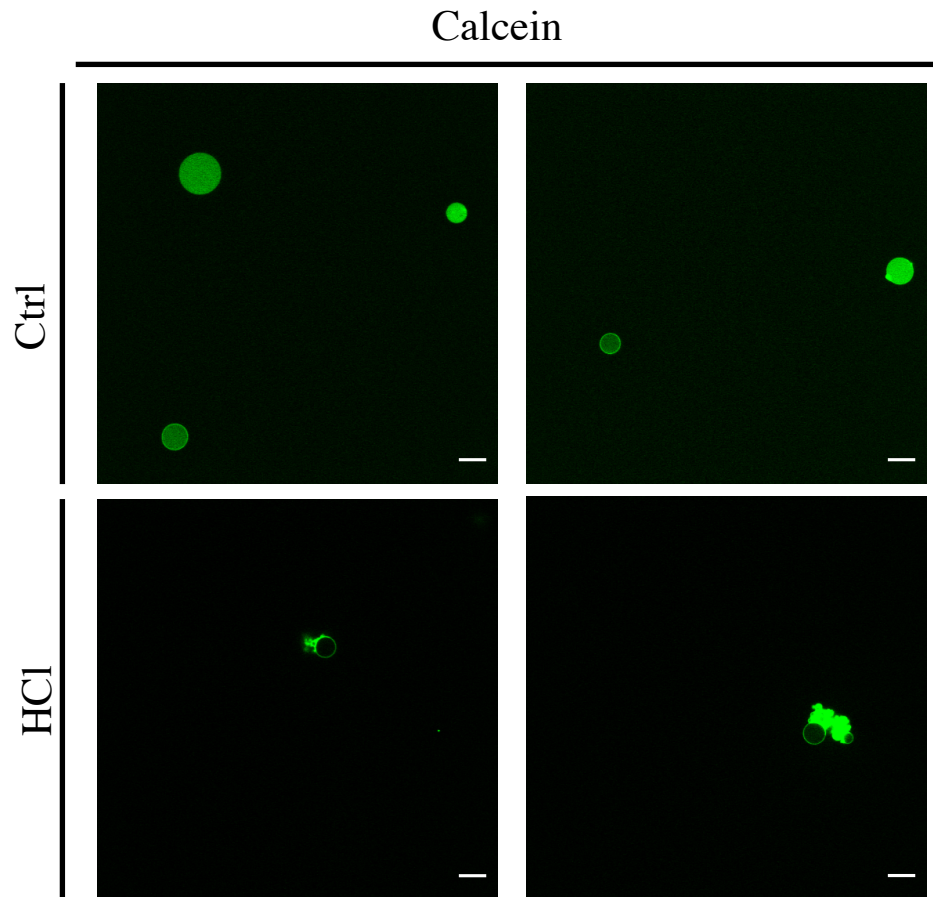


Figure 51. – Snapshots of calcein-loaded GHUV-CSL 50% treated with HCl. Calcein filters.  
Scalebar: 10  $\mu\text{m}$ .





## Chapter 4 – Discussion and perspectives

### 4.1. Switchable lipids : a robust delivery platform

The general objective of this investigation was to gather more scientific evidence about the cationic switchable lipid (CSL). This structure has emerged in our research team from a technology transfer from molecular tweezers into pharmaceutical sciences (129). Molecular tweezers are biomimetic recognition hosts, displaying a spatial cavity defined by two arms and a linker (210). Such structures allow fine control over the conformation of the molecules and their potential interactions. Dynamic tweezers could be obtained by introducing a stimulus-responsive unit, controlling a conformational change upon a stimulus. In our project, the pH-sensitive unit was composed of anicole-pyridine-anisole motif. This unit allowed the pH-triggered binding and release of an anticancer drug model (215). When introduced into a lipid structure, it provided pH-responsive drug release properties to the lipid particles. Since the first proof-of-concept of cytosolic delivery (130), two generations of lipids have been identified: a non-cationic lipid (C12diMe,(130)), yielding negatively charged lipid nanoparticles, and a cationic counterpart, CSL, used in this study, designed for nucleic acid delivery (121). Interestingly, this lipid has now been assessed in various applications, gathered in Table 9:

Lipid	Formulation	Drug/gene	Application Cell/animal model	Vitro/vivo	ref
C12diMe C12COOH C12NH2	C12diMe/DSPC /DSPE-PEG	Sulforhodamine B	Endosomal escape HeLa	In vitro	(130)
CSL1 CSL2 CSL3 CSL4	CSL/Chol/DSPC /DSPE-PEG	siRNA GFP siRNA PCSK9 siRNA FVII	HeLa Liver targeting: Hypercholesterolemia (Huh-7) Coagulation cascade	In vitro in vivo	(121)

CSL3	CSL/Chol/DSPC /DSPE-PEG	Melphalan miR-181a	Retinoblastoma (Y79)	In vitro In vivo	(122)
CSL3	CSL/Chol/DSPC /DSPE-PEG	Poly (I/C)	Pulmonary administration (bronchial cells submerged/well- differentiated)	In vitro	(216- 218)
CSL3	CSL/Chol/DSPC /DSPE-PEG	siRNA	Placenta cells (human primary villous cytotrophoblasts) Macrophages	In vitro	(219)
CSL3	CSL/Chol/DSPC /DSPE-PEG	siRNA survivin	Lung, breast, colon, cervix, ovary, retinoblastoma	In vitro	<sup>1</sup>
CSL3	POPC/CSL3 PDMS-PEO	calcein	GUV, GHUV	In vitro	<sup>1</sup>
CSL3 C12diMe	CSL/Chol/DSPC /DSPE-PEG C12diMe/DSPC /DSPE-PEG	Blank LNP	Zebrafish toxicity	In vivo	<sup>2</sup>

<sup>1</sup>This M.Sc. <sup>2</sup>Not published

Table 9. – Applications of switchable LNP as a drug/gene carrier.

Therefore, based on the scientific evidence accumulated to the present moment, including the results provided in this M.Sc thesis, we add more evidence to switchable LNP as a robust platform for drug and gene delivery, when nanovectors are formulated with C12diMe or CSL3 as the switchable lipid component, respectively. Furthermore, LNP containing the cationic switchable lipid (CSL) has demonstrated to be a versatile carrier for gene transfection, as show by: miRNA (122), Poly (I/C) (mimic of viral double-stranded RNA) (216-218), siRNA (121) and pDNA (ongoing investigation). Notably, the composition of switchable LNP designed for gene delivery was

inspired from the OnPattro formulation. Tailoring the composition of switchable LNP for each variety of genetic cargo (*e.g.* mRNA) could be envisaged to improve the potency of switchable LNP as transfection carrier (126, 220). The optimization might include varying the excipients formulated alongside the CSL to afford switchable LNP or structural modifications in the cationic lipid but preserving the switchable unit responsible for the fast pH-triggered release of cargo.

Several cancer cell models have been assessed. This investigation has demonstrated that switchable LNP display a variable activity in downregulating survivin at the mRNA level. Cells reported as “easy-to-transfect” (HeLa, MCF-7, A549) exhibited good transfection in this investigation, corroborating with data obtained in previous studies, where switchable LNP efficiently transfected HeLa (121) and macrophages (217). Importantly, switchable LNP also delivered cargo to hosts reported as difficult to transfect by non-viral vectors, such as primary cells (218, 219). Further work should focus on explaining the variability of survivin mRNA levels among cell lines after siLNP transfection encountered in this work. Potential points to be addressed in a cell-specific fashion include, but not limited to LNP-cell interaction, cell uptake, endosomal escape rate and intracellular fate of switchable lipid.

Interestingly, the transfection efficiency of switchable LNP can be compared with commercial agents. *In vitro*, we have previously demonstrated that switchable LNP promoted GFP knockdown in stable GFP expressing HeLa cells similarly to lipofectamine (121). In this investigation, we demonstrated that switchable LNP silenced survivin and synergistically enhanced the cytotoxicity of CBDA and MELPH as did lipofectamine. *In vivo*, switchable LNP silenced Factor VII (FVII) in values compared with that to the 1st generation of ionizable cationic lipid (DLinDMA) (Figure 52), which was the precursor that paved the way to the synthesis of DLin-MC3-DMA, the major component of OnPattro formulation.

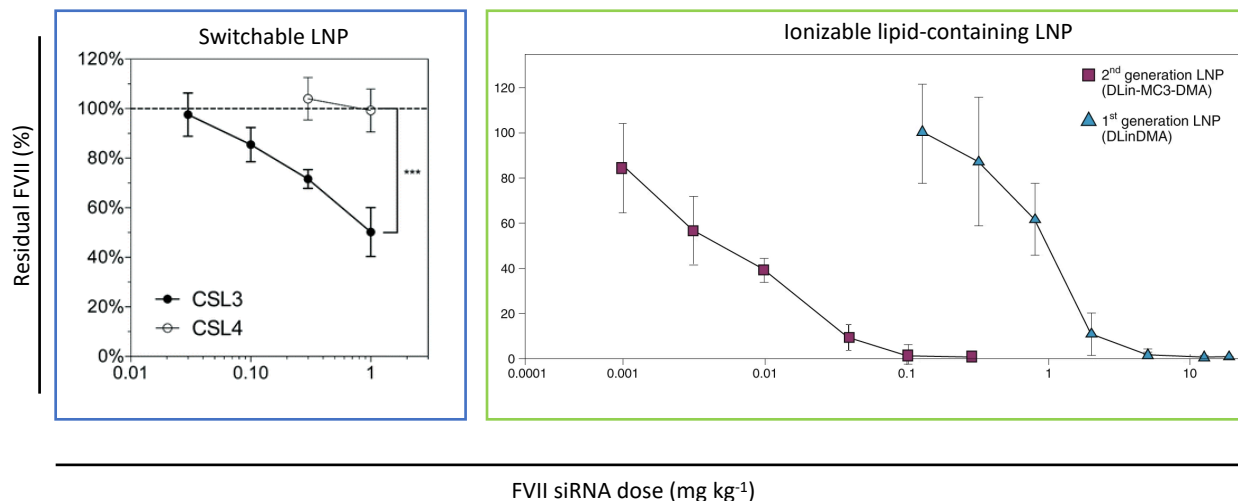


Figure 52. – Comparison of *in vivo* dose-dependent silencing of FVII by switchable LNP (CSL3, filled circles, left) or ionizable lipid-containing LNP (1<sup>st</sup> and 2<sup>nd</sup> generations, right). Adapted from (121, 221)

Finally, in chapter 3, we developed a new hybrid switchable lipid/polymer vesicle. The compatibility of switchable lipids with a diblock copolymer (PDMS<sub>36</sub>-*b*-PEO<sub>23</sub>) adds more evidence into the robustness of switchable lipids as building blocks for responsive vesicles. This opens new possibilities of vesicle formulations or biomimetic synthetic cells. Overall, the transfection ability of switchable LNP was assessed in several cell lines. The good performance observed encourage us, in the future, to seek further potential applications of switchable LNP as delivery vectors. Possible applications will involve an extensive investigation of stability and transfection efficiency of switchable LNP as a carrier for different cargos, *e.g.* mRNA and CRISPR/Cas-9.

#### 4.1.1. Targeting survivin : advantages and limitations

To explore the opportunity of switchable LNP in cancer, we selected a target that was common to several cancers: survivin. This study allowed us to discern the advantages and limitations of this target.

##### Advantages of survivin targeting

- The relationship between survivin and cancer, as the implications thereof, has been largely reported in the literature. Although its mechanism is still not fully elucidated, much

evidence sustain the involvement of survivin in cancer resistance to apoptosis. Therefore, anti survivin strategies could be envisaged to ameliorate the cytotoxicity of virtually any drug that encountered resistance;

- Survivin is virtually expressed in all malignancies, becoming a universal cancer target. As we demonstrated that survivin silencing in retinoblastoma synergistically improved the cytotoxicity of selected chemotherapeutics, we could translate this strategy to other cell lines. As the survivin intracellular network is deeply implicated in many signaling pathways (Figure 4), some cell lines might rely more on survivin as an apoptosis guardian, thus combining survivin silencing with anti-cancer drugs in such lineages would result in a better cytotoxicity efficiency;
- Survivin stands out as a cancer-specific target: it is overexpressed in malignancies, but silenced in healthy and well-differentiated adult cells. We have confirmed that survivin was not expressed in healthy cells. This opportunity reflected in a targeted treatment with a better benefit to risk ratio with that of YM155 for instance (Figure 36).

#### Limitations of survivin targeting

- Survivin protein levels are not uniformly expressed. Survivin is a cell cycle-dependent protein (222). It is important that experiments are carried out with synchronized cells to assure a homogeneous level of survivin to discriminate the role of survivin in preventing apoptosis followed by treatment with chemotherapeutics. Furthermore, it is unknown whether survivin level varies upon cell passage. As an example: cells originating from the same source, such as Y79 and Y79 stably expressing luciferase (Y79 Luc), did not show the same mRNA survivin levels after siLNP transfection (Figure 30). Different cell passage or intracellular pathways altered by lentiviral modification might perturb the phenotypic response of survivin silencing. Those factors add difficulty in the reproducibility of experiments and raise precaution before translating assumptions of survivin benefits to chemotherapeutics to in vivo experimentation;
- Interconnexion with drug mechanism: the lesson from this study is that not any drugs can be combined with anti-survivin strategies. The straightforward thinking that survivin silencing will synergistically improve the cytotoxicity of drugs is not always valid. To

rationally choose a good candidate, one must perform experiments that interrogate the relationship between survivin and the drug candidate differently. For example, we assessed the survivin and caspase-3 mRNA levels in Y79 cells after the incubation with the 4 drugs under investigation. We expected to select our candidate based on the survivin overexpression, accompanied by a downregulation of caspase 3, as a response to DNA damage-inducing agents. That was not the case as no drug presented such a pattern clearly. In the cytotoxicity study, we confirmed that survivin silencing as an adjuvant therapy synergistically ameliorated the cytotoxicity of carboplatin and melphalan, but not teniposide. Therefore, more experiments are necessary to clarify the interaction between melphalan and survivin, or carboplatin and survivin (*e.g.* survivin and/or drug treatment at different cell-cycle phase, investigation of apoptosis by flow cytometry using annexin/PI co-staining, caspase activity by immunoassays, blockage of p53/p21 prior survivin/drug incubation). To this end, we have observed that transfection with siRNA prior drug treatment abrogated survivin overexpression in carboplatin-treated Y79 cells (Figure 20C). Moreover, carboplatin induces p21 and p53 protein expression in luciferase-expressing Y79 cells (Figure 29C). Blocking p53 or p21 activity could add more data to the hypothesis that survivin is overexpressed in Y79 cells as a defense mechanism against carboplatin-induced apoptosis and that the synergistic effect observed is mediated by the p53/p21 axis. Other experiments were envisaged in this study, but must be cautiously considered due to reproducibility (n=1). Among those experiments, we observed that transfection of siRNA survivin (20 nM) arrested Y79 cells in the G2/M phase 96 hours after transfection and delayed cells' proliferation during the 10-days course of the experiment as compared with that of non-treated cells (Figure 53).

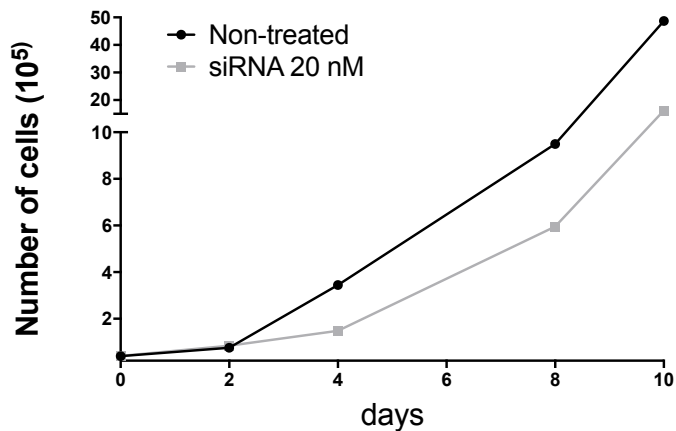
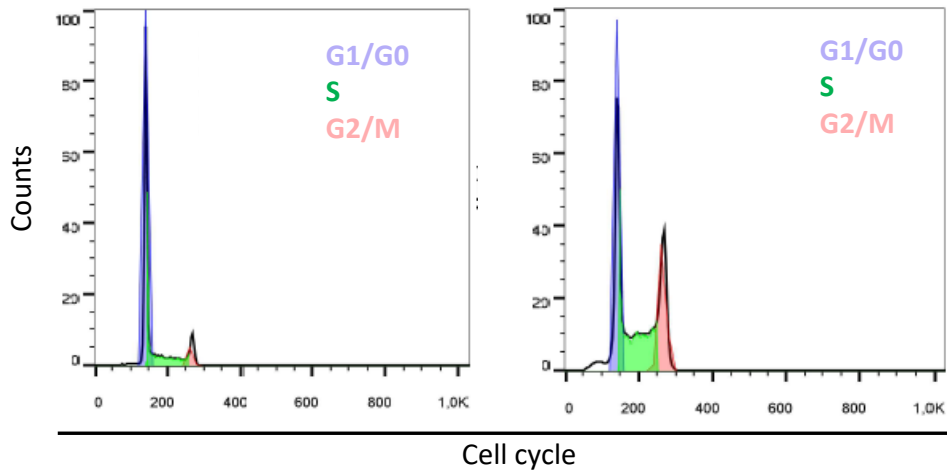


Figure 53. – Effects of transfection of siRNA survivin (20 nM) on cell cycle and proliferation in Y79 cells. N=1

Other considerations into survivin targeting strategies

- Co-delivery of siRNA and drugs. Here we demonstrated that the incubation of chemotherapeutics with Y79 cells 48 hours after transfection of the siRNA against survivin led to better cytotoxicity of drugs. By Western blotting, we observed that 48 hours was required for protein downregulation after LF or switchable LNP siRNA survivin transfection (compare Figure 27 (siLNP) with 33 (LF)). Temporal investigation of drug and siRNA adjuvant therapy might help to elucidate the best kinetics to observe synergism between the two treatments;

- Drugs that target survivin pathway. As a nodal protein involved in cell division and cell death, cancer cells might strongly depend on survivin for proliferation. Liu *et al.* (89) and Samuel *et al.* (90) transfected Y79 cells with 100 nM of siRNA against survivin and observed that survivin downregulation induced apoptosis and impaired cells' proliferation and viability. We did not observe such effects when we transfected 20 nM of siRNA against survivin in Y79 cells, although this amount of siRNA was enough to ameliorate drugs cytotoxicity. To improve this effect, one might combine a dual-targeting strategy (*e.g.* targeting proliferation signaling, SYK, and apoptosis regulator, survivin) inspired by the synthetic lethality approach. See further consideration of this proposal in the perspective section;
- A final general comment relies upon the prospective applicability of the survivin-targeted siRNA compared with the survivin-suppressant molecule, YM155. The later did not achieve its primary endpoints in clinical trials, although it was generally well tolerated (51, 73). Two reasons might justify the failure of YM155 in reaching the bedside: the molecule is chemically unstable, as serum concentration of YM155 rapidly decreased once the drug infusion stopped (223); secondly, YM155 was first believed to mediate specific survivin silencing through inhibition of its promoter region (60). Further studies put that into question and the exact mechanism whereby the molecule mediates survivin silencing is not fully elucidated (61). As recently advocated by Lin *et al.* (224), numerous anticancer candidates might be failing in achieving clinical benefits due to a misconceived mechanism of action. YM155 may fall into that category. Strategies based on siRNA technology might circumvent this issue by specifically inhibiting the mRNA target. Here we put forward more *in vitro* evidence that switchable LNP stands out as a promising non-viral siRNA carrier. However, caution must be exercised as a single siRNA is not sufficient to ascertain specificity because of possible off-target effects; 2 or more different siRNA against the same target would reinforce the results obtained.

In conclusion, we show more evidence that survivin is a promising target but its mechanism within the cancer model under investigation should be better understood. Otherwise, results might fail on reproducibility or significance. Although significant, the results drawn in this study might not



be sufficient to go on *in vivo* experimentation. Drug concentration is still high and further clarification on survivin mechanism might help to rationally select a better drug candidate and/or treatment protocol. Under the light of good animal care handling, our studies could still be optimized before *in vivo* testing.

### **4.3. pH-triggered switch : a selective fluidity modulation**

The driving hypothesis of the switchable lipid was that the pH-triggered switch could occur in diverse environments. The various applications in this study and previous ones showed that it is indeed the case. In particular, it is important to note that the switch could overcome the hydrophobic stacking of lipids in bilayers. Here we demonstrated that this is also the case when CSL is embedded in the hybrid polymer/lipid membrane. This is a major asset to develop further the portfolio of formulations involving CSL.

Several mechanisms could be proposed to explain cytosolic release of cargo by pH-sensitive lipids (225, 226): (A) non-endosomal processes, which would include fusion of liposomes with cytoplasmatic membrane and thus cargo release and (B) processes involving endosomal escape pathways. The later could more better detailed into (i) fusion between liposomal and endosomal membranes, (ii) active cargo transport via endosomal membrane proteins or liposomal destabilization and passive diffusion of cargo across endosome membrane, (iii) transient disruption of endosomal membrane and (iv) lysis of endosome and cytosolic delivery of cargo (Figure 54).

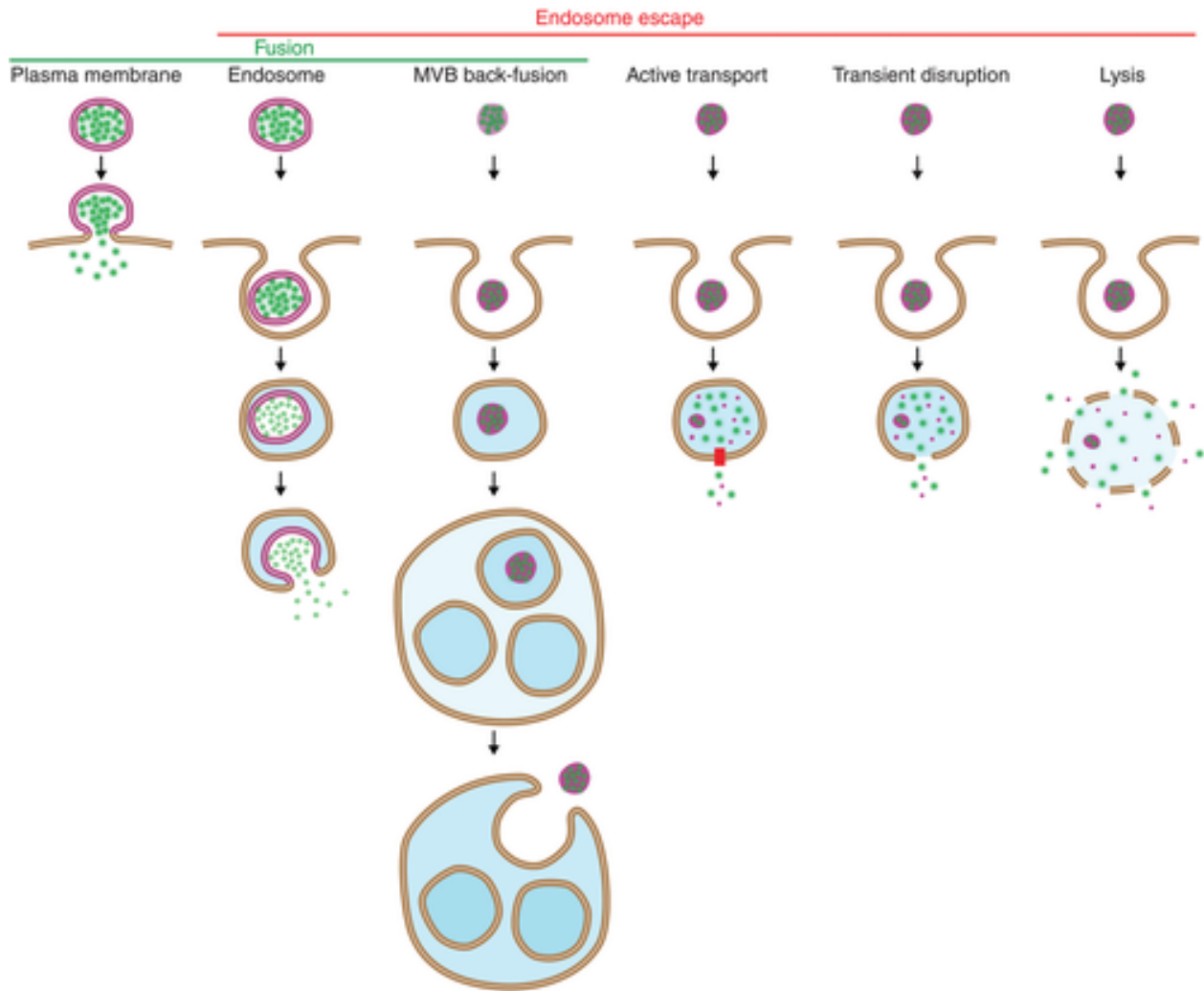


Figure 54. – Endosomal escape pathways mediated by pH-sensitive liposomes. Adapted from (118)

Since the first proof-of-concept of switchable LNP as a platform for cytosolic delivery of drugs (130), we have gathered several evidences that:

- Endosomal pathway is involved. Switchable LNP mediates cargo release via endosomal destabilization. Fluorescence co-visualization of endosomal pathway and encapsulated cargo demonstrated that switchable LNP are internalized through the endosomal pathway (130). Moreover, blockade of the endosomal acidification with Bafilomycin A1 or formulating an LNP containing a non-switchable CSL-analog abrogated siRNA silencing, confirming the acidification is a key trigger in the endosomal escape process (121).

- Fusion is involved in the pH-triggered release. Lipid mixing assay confirmed that fusion events were observed for C12DiMe and CSL3 at the nanoscale (121, 130). We might then hypothesize that this lipid mixing is occurring with the endosomal membrane. In our study, we indeed confirmed high membrane fluidity leading to intermembrane fusion and fission events in GUV (Figure 46) and GHUV (Figure 48). Further experiments using fluorescence resonance energy transfer (FRET) can investigate both switchable lipid and siRNA fate within the cell upon internalization; lipid colocalization with early/late endosomes would clarify whether CSL is transferred to the endosomal membrane after destabilization event; finally, a dual-labeled switchable lipid would unravel the integrity and fate of CSL after endocytosis and endosomal destabilization.
- Vesicles are maintained after acidification (no lysis). At the nanoscale, the mixing and fusion events that were reported in previous investigations could be correlated with a decrease in derived count rates observed in our studies (Figure 37D). Here we also observed that vesicles were preserved in the acidic environment, as reflected by the correlogram fit and particle distribution (DLS measurements, Figure 37C). Moreover, at the microscale, giant vesicles were maintained after acidification. Such observations were valid whether switchable lipids were formulated in giant liposomes or hybrid polymer/lipid vesicles. Properties observed at the micrometer scale must be cautiously investigated before translating to vesicles at the nanoscale (206). Therefore, further physicochemical analyses are still needed to understand the role of CSL in mediating endosomal disruption and cytosolic delivery of siRNA. Such clarification is of utmost importance in the development of more efficient switchable lipid-based formulations. To this end, we also pursued atomic force microscopy (AFM), Transmission electron cryomicroscopy (cryo-TEM), and NMR studies to follow the morphology of particles at different pH (ongoing studies).

Our study confirmed the following observations:

- The dynamic of switchable lipid-containing membranes is significantly higher at acidic pH rather than at neutral pH (qualitatively and quantitative observations). GUV containing CSL at 20 and 50 % molar ratio induced positive membrane curvature (outward protruding

nanotubes) and a high degree of membrane fluidity upon acidification, as observed quantitatively (Table 7) and qualitatively (Figure 45 and 46). Remarkably, molar amount of CSL as low as 20 % added responsive properties to the stiff PDMS<sub>36</sub>-*b*-PEO<sub>23</sub> membrane, quantitatively (GHUV-CSL, Table 7) and qualitatively (Figure 47 and 48). Again, this is a major asset to broaden the portfolio of novel formulations containing CSL.

- CSL lipids are homogeneously distributed within the membrane, ruling out the “pore transient destabilization” hypothesis (iii).
- Finally the mechanism is due to the pH-switching unit, as we confirmed that osmotic shock (NaCl treatment) did not trigger structural changes nor did it confer fluidity in CSL-containing GUV/GHUV membranes. Moreover, such observations required the presence of CSL within membranes, as controlled vesicles (GUV and GHUV formulated with neutral lipid POPC and blended PDMS<sub>36</sub>-*b*-PEO<sub>23</sub>/POPC, respectively) did not behave similarly upon HCl treatment. To further confirm the role of the switchable unit, we observed that giant unilamellar vesicles formulated with 50% of C12diMe (GUV-C12diMe, non-cationic switchable lipid, (130)) also presented structural changes (positive membrane curvature) when exposed to an acidic environment (Table 10 and Figure 55, left). Finally, the pH-switching unit is responsible for modulating membrane fluidity as calcein-loaded GUV-C12diMe rapidly (less than 2 minutes) released encapsulated cargo when exposed to HCl. The quick-release of encapsulated cargo was reported previously in C12diMe containing liposomes (130).

	<b>Number of vesicles analysed</b>	<b>Vesicles with inward structures</b>	<b>Internalized Vesicles</b>	<b>Vesicles with outward structures</b>	<b>Membrane fluctuation</b>
GUV-C12diMe 50%	142	7 %	15 %	6 %	4 %

GUV-C12diMe

50%

167

13 %

10 %

43 %

3 %

+ HCl

Table 10. – Morphological changes in GUV-Di12diMe 50% treated with HCl.

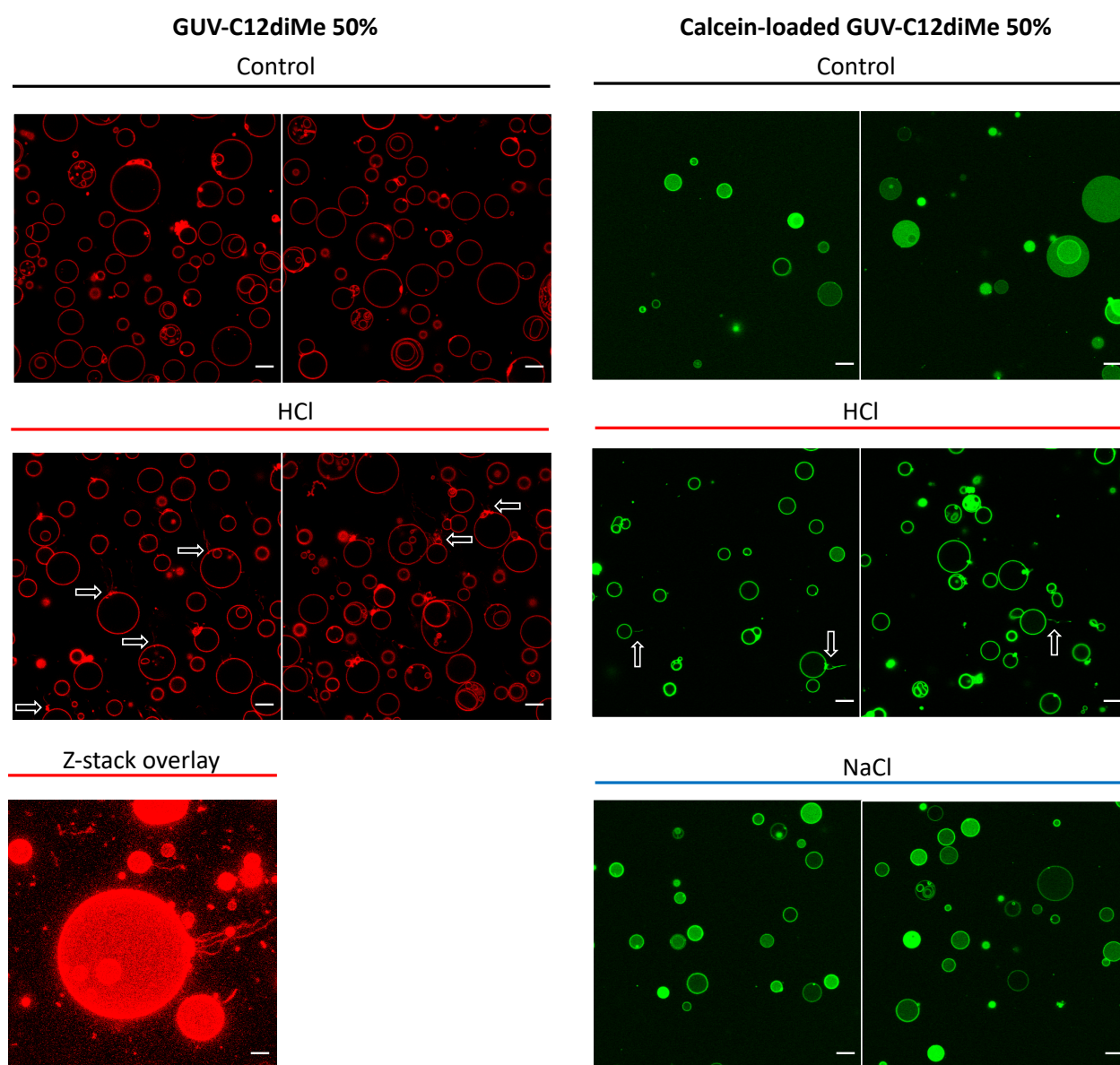


Figure 55. – GUV-C12diMe 50% and calcein-loaded GUV-C12diMe 50% submitted to HCl treatment. Left: GUV-C12diMe 50% exposed to HCl treatment. Bottom left: 3D visualization of GUV-C12diMe 50% exposed to HCl. Right: calcein-loaded GUV-C12diMe 50% exposed to HCl and NaCl. Calcein filter. Open arrows indicate positive membrane curvature. Scale bar: 10  $\mu\text{m}$ .

Therefore, this study is a crucial step in the understanding of the membrane behavior of switchable lipids. It is also very important to note that this membrane fluidity is selective at acidic pH. The vesicles are stable at pH 7, which prevents from fusion with cellular membranes, and potential non-specific toxicity (eg.; red blood cells and hemolysis). Indeed, all the toxicity tests that have been pursued to date did not reveal any toxicity of the switchable lipids when incorporated into liposomes with or without siRNA complexation (hemolysis tests, resazurin-based cell viability assay, LDH and zebrafish model (121, 122, 130, 216) this investigation and ongoing studies). We strongly believe that this difference of membrane fluidity between neutral and acidic pH guarantee switchable LNP biocompatibility.

## 4.4. Perspectives

### 4.4.1. Optimizing survivin targeting strategy in RB

Retinoblastoma is a particular tumor with considerable genomic stability (227). The whole-genome sequence of RB samples identified *RB1* as the sole tumor-driver gene to be mutated (228). Further analysis of epigenetic changes identified the tyrosine kinase SYK as a novel *proto-oncogene* essential for tumor cell survival in RB (228). RB cells are sensitive to SYK inhibition, as demonstrated by Qiu *et al.* (229). In that study, it was demonstrated that lymphocyte-derived microparticles downregulated SYK inducing RB cells (Y79) apoptosis through activation of p53 and p21-dependent pathway (Figure 56).

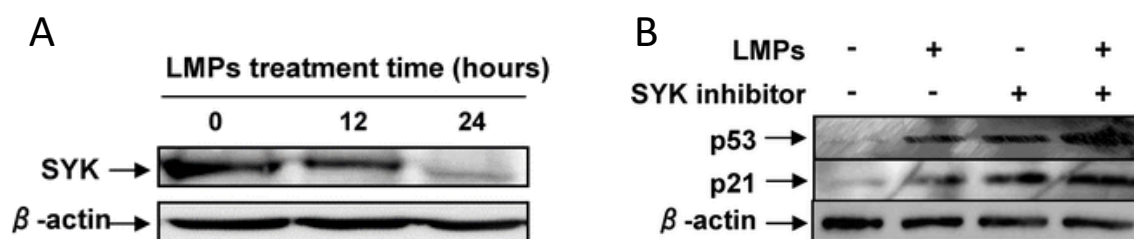


Figure 56. – Lymphocyte-derived microparticles (LMPs) mediate SYK silencing (A) and induce p53 and p21 expression (B) (229).

Survivin plays a key role in preventing apoptosis in tumor cells. In this study, we demonstrated that survivin silencing synergistically improved the cytotoxicity of carboplatin, which induced a p53-p21 response in Y79 cells. Therefore, concomitant targeting of survivin and SYK might be an interesting strategy to potentialize the therapeutic benefit of drugs that induce apoptosis through the p53-p21 axis. Co-encapsulation of the SYK inhibitor, the hydrophobic molecule BAY 61-3606, and survivin-targeted siRNA in switchable LNP might emerge as a potential anti-RB strategy.

#### **4.4.2. Optimizing pH-responsive hybrid polymer/lipid vesicles**

Hybrid vesicles combine the advantages of both liposomes and polymersomes in a single membrane. Studies are focused on tuning membrane properties to maximize hybrid vesicles applicability in cell mimicry studies and as novel drug delivery agents. We demonstrated that it is possible to formulate large and giant hybrid vesicles combining PDMS<sub>36</sub>-*b*-PEO<sub>23</sub> and CSL in an 80:20 molar ratio. Such proportion is in agreement with previous studies, confirming that molar amount up to 60% of lipids in the fluid phase (gel-to-liquid transition phase for CSL is ~ 5 °C) form homogeneous hybrid vesicles with PDMS-PEO (Figure 19). Zong *et al.* (165) demonstrated that the introduction of 17.5% of cholesterol in a hybrid vesicle composed of blended pCMA-block-poly(2-(dimethylamino) Ethyl Methacrylate (polymer, P3) and fluid phase phospholipid POPC produced stable hybrid vesicle with nanodomain's formation (Figure 57). Therefore, adding cholesterol in the blend PDMS-PEO and CSL might yield hybrid vesicle with the presence of pH-responsive gate domains.

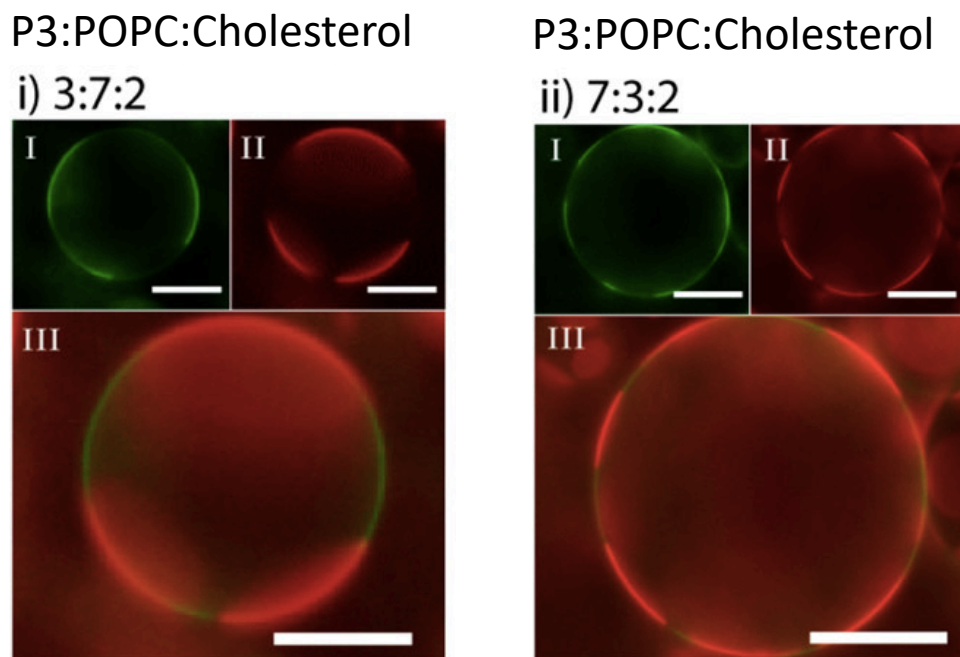


Figure 57. – Giant hybrid polymer/lipid vesicle formulated with P3, POPC and cholesterol. Polymers are labelled in green (filter I), lipids are labelled in red (filter II). Filter III, merged filters. Scale is 20  $\mu\text{m}$  (165).

#### 4.4.3. Further investigation on the mechanism whereby switchable lipid mediates membrane destabilization

The presence of CSL induced structural changes in giant vesicles irrespective of the membrane composition. Characterizing the structure adopted by CSL in acidic conditions by  $^{31}\text{P}$  NMR techniques might unveil if the switchable lipid adopts a non-lamellar phase behavior ( $H_{II}$ ) at lower pH-values. Such behavior is the key structure supporting the ion-pair theory (Figure 9) (119). We hypothesize that the switchable lipid is capable of adopting an  $H_{II}$  phase without the need for mixing with negatively charged lipids. The proposed technique might as well discriminate if the  $H_{II}$  and lamellar phases coexist in acidified CSL-containing GUV/LUV, as we observed that switchable LUV and GUV maintained their vesicular structure at acidic environment.



## Chapter 5 – Conclusion

The unarguable benefits of lipid nanoparticles (LNP) for pharmaceutical applications have led to more than 15 liposomal-based drugs in the clinics. Recently, Patisiran (Onpattro) shed the first light on the promising roadway of RNAi technology. The long term outcomes of the first FDA-approved RNAi-based drug needs to be closely monitored as it will dictate the future of technologies developed now. In this investigation, we added more evidence into the applicability of switchable LNP as a siRNA carrier. We have met all the specific objectives proposed for the 1<sup>st</sup> publication. (I) We demonstrated that switchable LNP successfully silenced survivin in different cancer models *in vitro*; (II) we confirmed survivin protein downregulation in Y79 cells by Western blot; (III) we rationale selected carboplatin and melphalan as the two drugs which cytotoxicity in Y79 cells were benefited from survivin silencing and; (IV) we observed that survivin silencing using siRNA against survivin was not harmful to non-transformed ARPE.19 cells in terms of viability, whereas the survivin chemical inhibitor YM155 was. Therefore, we confirmed our hypothesis that switchable LNP is capable of delivering survivin-targeted siRNA *in vitro*, promoting improved cytotoxicity of chemotherapeutics in survivin-expressing cells only. Subsequently, we demonstrated that cationic switchable lipids preserve their pH-triggered conformation change at the microscale. We have also met the specific objectives for our 2<sup>nd</sup> publication. (I) We successfully formulated CSL-containing GUV and GHUV, confirming CSL incorporation by DLS measurement and H<sup>1</sup> NMR spectroscopy; (II) we categorized structural changes arising from pH-triggered conformation change of CSL in switchable GUV and GHUV; (III) finally, we observed that such structural changes were accompanied by an increased permeability. Taken together, we gathered visual and physicochemical information about the biophysical behavior of switchable membranes in the acidified environment, satisfying, thus, our 2<sup>nd</sup> hypothesis. Therefore, this work provides a solid basis to develop further switchable lipids in pharmaceutical applications, especially for gene delivery in cancer cells. The membrane dynamics observation also strengthens the knowledge of its mechanism and supports the low toxicity observed to date.



## References

1. Breasted JH. The Edwin Smith Surgical Papyrus: published in facsimile and hieroglyphic transliteration with translation and commentary in two volumes: University of Chicago Press Chicago; 1930.
2. Hajdu SI. A note from history: landmarks in history of cancer, part 1. *Cancer-Am Cancer Soc.* 2011;117(5):1097-102.
3. Ferlay J EM, Lam F, Colombet M, Mery L, Piñeros M, Znaor A, Soerjomataram I, Bray F. Global Cancer Observatory: Cancer Today. Lyon, France: International Agency for Research on Cancer 2018 [Available from: <https://gco.iarc.fr/today>].
4. Ferlay J, Colombet M, Soerjomataram I, Mathers C, Parkin DM, Pineros M, et al. Estimating the global cancer incidence and mortality in 2018: GLOBOCAN sources and methods. *Int J Cancer.* 2019;144(8):1941-53.
5. Bray F, Ferlay J, Soerjomataram I, Siegel RL, Torre LA, Jemal A. Global cancer statistics 2018: GLOBOCAN estimates of incidence and mortality worldwide for 36 cancers in 185 countries. *CA Cancer J Clin.* 2018;68(6):394-424.
6. Steliarova-Foucher E, Colombet M, Ries LAG, Moreno F, Dolya A, Bray F, et al. International incidence of childhood cancer, 2001–10: a population-based registry study. *The Lancet Oncology.* 2017;18(6):719-31.
7. Gupta S, Howard SC, Hunger SP, Antillon FG, Metzger ML, Israels T, et al. Treating Childhood Cancer in Low- and Middle-Income Countries. In: Gelband H, Jha P, Sankaranarayanan R, Horton S, editors. *Cancer: Disease Control Priorities, Third Edition (Volume 3)*. Washington (DC)2015.
8. Hanahan D, Weinberg RA. Hallmarks of cancer: the next generation. *Cell.* 2011;144(5):646-74.
9. Gilman A, Philips FS. The Biological Actions and Therapeutic Applications of the B-Chloroethyl Amines and Sulfides. *Science.* 1946;103(2675):409-36.
10. Norin T. Melphalan (L-phenylalanine nitrogen mustard) treatment in myelomatosis. Report of 46 cases. *Acta Radiol Ther Phys Biol.* 1966;4(1):33-40.

11. Blokhin N, Larionov L, Perevodchikova N, Chebotareva L, Merkulova N. [Clinical experiences with sarcolysin in neoplastic diseases]. *Ann N Y Acad Sci.* 1958;68(3):1128-32.
12. Farber S, Diamond LK. Temporary remissions in acute leukemia in children produced by folic acid antagonist, 4-aminopteroyl-glutamic acid. *N Engl J Med.* 1948;238(23):787-93.
13. Kaye SB. New antimetabolites in cancer chemotherapy and their clinical impact. *Br J Cancer.* 1998;78 Suppl 3:1-7.
14. Strebhardt K, Ullrich A. Paul Ehrlich's magic bullet concept: 100 years of progress. *Nat Rev Cancer.* 2008;8(6):473-80.
15. Bernards R. Exploring the uses of RNAi--gene knockdown and the Nobel Prize. *N Engl J Med.* 2006;355(23):2391-3.
16. Monteiro AN, Waizbort R. The accidental cancer geneticist: hilario de gouvea and hereditary retinoblastoma. *Cancer Biol Ther.* 2007;6(5):811-3.
17. Knudson AG, Jr. Mutation and cancer: statistical study of retinoblastoma. *Proc Natl Acad Sci U S A.* 1971;68(4):820-3.
18. Friend SH, Bernards R, Rogelj S, Weinberg RA, Rapaport JM, Albert DM, et al. A human DNA segment with properties of the gene that predisposes to retinoblastoma and osteosarcoma. *Nature.* 1986;323(6089):643-6.
19. Little MP. Are two mutations sufficient to cause cancer? Some generalizations of the two-mutation model of carcinogenesis of Moolgavkar, Venzon, and Knudson, and of the multistage model of Armitage and Doll. *Biometrics.* 1995;51(4):1278-91.
20. Dimaras H, Corson TW, Cobrinik D, White A, Zhao J, Munier FL, et al. Retinoblastoma. *Nat Rev Dis Primers.* 2015;1:15021.
21. Moreno F, Sinaki B, Fandino A, Dussel V, Orellana L, Chantada G. A population-based study of retinoblastoma incidence and survival in Argentine children. *Pediatr Blood Cancer.* 2014;61(9):1610-5.
22. MacCarthy A, Draper GJ, Steliarova-Foucher E, Kingston JE. Retinoblastoma incidence and survival in European children (1978-1997). Report from the Automated Childhood Cancer Information System project. *Eur J Cancer.* 2006;42(13):2092-102.

23. Nyawira G, Kahaki K, Kariuki-Wanyoike M. Survival among retinoblastoma patients at the Kenyatta National Hospital, Kenya. *JOECSA*. 2013;17(1).
24. Canturk S, Qaddoumi I, Khetan V, Ma Z, Furmanchuk A, Antoneli CB, et al. Survival of retinoblastoma in less-developed countries impact of socioeconomic and health-related indicators. *Br J Ophthalmol*. 2010;94(11):1432-6.
25. Qaddoumi I, Nawaiseh I, Mehayar M, Razzouk B, Haik BG, Kharma S, et al. Team management, twinning, and telemedicine in retinoblastoma: a 3-tier approach implemented in the first eye salvage program in Jordan. *Pediatr Blood Cancer*. 2008;51(2):241-4.
26. Wilimas JA, Wilson MW, Haik BG, Barnoya M, Fu L, Castellanos M, et al. Development of retinoblastoma programs in Central America. *Pediatr Blood Cancer*. 2009;53(1):42-6.
27. Mendoza PR, Grossniklaus HE. Therapeutic Options for Retinoblastoma. *Cancer Control*. 2016;23(2):99-109.
28. Yuan S, Friedman DL, Daniels AB. Alternative Chemotherapeutic Agents for the Treatment of Retinoblastoma Using the Intra-Arterial and Intravitreal Routes: A Path Forward Toward Drug Discovery. *Int Ophthalmol Clin*. 2017;57(1):129-41.
29. Chintagumpala M, Chevez-Barríos P, Paysse EA, Plon SE, Hurwitz R. Retinoblastoma: review of current management. *Oncologist*. 2007;12(10):1237-46.
30. Altieri DC. Survivin, versatile modulation of cell division and apoptosis in cancer. *Oncogene*. 2003;22(53):8581-9.
31. Tran J, Master Z, Yu JL, Rak J, Dumont DJ, Kerbel RS. A role for survivin in chemoresistance of endothelial cells mediated by VEGF. *Proc Natl Acad Sci U S A*. 2002;99(7):4349-54.
32. Vequaud E, Desplanques G, Jezequel P, Juin P, Barille-Nion S. Survivin contributes to DNA repair by homologous recombination in breast cancer cells. *Breast Cancer Res Tr*. 2016;155(1):53-63.
33. Mull AN, Klar A, Navara CS. Differential localization and high expression of SURVIVIN splice variants in human embryonic stem cells but not in differentiated cells implicate a role for SURVIVIN in pluripotency. *Stem Cell Res*. 2014;12(2):539-49.
34. Tamm I, Sausville E, Scudiero DA, Reed JC. IAP-family protein survivin inhibits caspase activity and apoptosis induced by Fas, Bax, and anticancer drugs. *Blood*. 1998;92(10):198a-a.

35. Altieri DC. Opinion - Survivin, cancer networks and pathway-directed drug discovery. *Nat Rev Cancer*. 2008;8(1):61-70.
36. Velculescu VE, Madden SL, Zhang L, Lash AE, Yu J, Rago C, et al. Analysis of human transcriptomes. *Nat Genet*. 1999;23(4):387-8.
37. Ambrosini G, Adida C, Altieri DC. A novel anti-apoptosis gene, survivin, expressed in cancer and lymphoma. *Nat Med*. 1997;3(8):917-21.
38. Kawasaki H, Altieri DC, Lu CD, Toyoda M, Tenjo T, Tanigawa N. Inhibition of apoptosis by survivin predicts shorter survival rates in colorectal cancer. *Cancer Res*. 1998;58(22):5071-4.
39. Ryan BM, Konecny GE, Kahlert S, Wang HJ, Untch M, Meng G, et al. Survivin expression in breast cancer predicts clinical outcome and is associated with HER2, VEGF, urokinase plasminogen activator and PAI-1. *Ann Oncol*. 2006;17(4):597-604.
40. Swana HS, Grossman D, Anthony JN, Weiss RM, Altieri DC. Tumor content of the antiapoptosis molecule survivin and recurrence of bladder cancer. *N Engl J Med*. 1999;341(6):452-3.
41. Chakravarti A, Noll E, Black PM, Finkelstein DF, Finkelstein DM, Dyson NJ, et al. Quantitatively determined survivin expression levels are of prognostic value in human gliomas. *J Clin Oncol*. 2002;20(4):1063-8.
42. Grossman D, McNiff JM, Li F, Altieri DC. Expression and targeting of the apoptosis inhibitor, survivin, in human melanoma. *J Invest Dermatol*. 1999;113(6):1076-81.
43. Shehata HH, Abou Ghalia AH, Elsayed EK, Ahmed Said AM, Mahmoud SS. Clinical significance of high levels of survivin and transforming growth factor beta-1 proteins in aqueous humor and serum of retinoblastoma patients. *J AAPOS*. 2016;20(5):444 e1- e9.
44. Tamm I, Wang Y, Sausville E, Scudiero DA, Vigna N, Oltersdorf T, et al. IAP-family protein survivin inhibits caspase activity and apoptosis induced by Fas (CD95), Bax, caspases, and anticancer drugs. *Cancer Res*. 1998;58(23):5315-20.
45. Lens SM, Vader G, Medema RH. The case for Survivin as mitotic regulator. *Curr Opin Cell Biol*. 2006;18(6):616-22.
46. Garg H, Suri P, Gupta JC, Talwar GP, Dubey S. Survivin: a unique target for tumor therapy. *Cancer Cell Int*. 2016;16:49.

47. Altieri DC. Survivin - The inconvenient IAP. *Semin Cell Dev Biol.* 2015;39:91-6.
48. Ye Q, Cai W, Zheng Y, Evers BM, She QB. ERK and AKT signaling cooperate to translationally regulate survivin expression for metastatic progression of colorectal cancer. *Oncogene.* 2014;33(14):1828-39.
49. Mehrotra S, Languino LR, Raskett CM, Mercurio AM, Dohi T, Altieri DC. IAP regulation of metastasis. *Cancer Cell.* 2010;17(1):53-64.
50. Li QX, Zhao J, Liu JY, Jia LT, Huang HY, Xu YM, et al. Survivin stable knockdown by siRNA inhibits tumor cell growth and angiogenesis in breast and cervical cancers. *Cancer Biol Ther.* 2006;5(7):860-6.
51. Wheatley SP, Altieri DC. Survivin at a glance. *J Cell Sci.* 2019;132(7).
52. Altieri DC. Targeting survivin in cancer. *Cancer Lett.* 2013;332(2):225-8.
53. Gordan JD, Vonderheide RH. Universal tumor antigens as targets for immunotherapy. *Cytotherapy.* 2002;4(4):317-27.
54. Al-Khadairi G, Decock J. Cancer Testis Antigens and Immunotherapy: Where Do We Stand in the Targeting of PRAME? *Cancers (Basel).* 2019;11(7).
55. Berinstein NL, Karkada M, Oza AM, Odunsi K, Villella JA, Nemunaitis JJ, et al. Survivin-targeted immunotherapy drives robust polyfunctional T cell generation and differentiation in advanced ovarian cancer patients. *Oncoimmunology.* 2015;4(8):e1026529.
56. Fenstermaker RA, Ciesielski MJ, Qiu J, Yang N, Frank CL, Lee KP, et al. Clinical study of a survivin long peptide vaccine (SurVaxM) in patients with recurrent malignant glioma. *Cancer Immunol Immunother.* 2016;65(11):1339-52.
57. Morrow T. Novartis's Kymriah: Harnessing Immune System Comes With Worry About Reining in Costs. *Manag Care.* 2017;26(10):28-30.
58. Laumont CM, Vincent K, Hesnard L, Audemard E, Bonneil E, Laverdure JP, et al. Noncoding regions are the main source of targetable tumor-specific antigens. *Sci Transl Med.* 2018;10(470).
59. Wobser M, Keikavoussi P, Kunzmann V, Weininger M, Andersen MH, Becker JC. Complete remission of liver metastasis of pancreatic cancer under vaccination with a HLA-A2 restricted peptide derived from the universal tumor antigen survivin. *Cancer Immunol Immunother.* 2006;55(10):1294-8.

60. Nakahara T, Kita A, Yamanaka K, Mori M, Amino N, Takeuchi M, et al. YM155, a novel small-molecule survivin suppressant, induces regression of established human hormone-refractory prostate tumor xenografts. *Cancer Res.* 2007;67(17):8014-21.
61. Rauch A, Hennig D, Schafer C, Wirth M, Marx C, Heinzl T, et al. Survivin and YM155: how faithful is the liaison? *Biochim Biophys Acta.* 2014;1845(2):202-20.
62. Wani TH, Surendran S, Jana A, Chakrabarty A, Chowdhury G. Quinone-Based Antitumor Agent Sepantronium Bromide (YM155) Causes Oxygen-Independent Redox-Activated Oxidative DNA Damage. *Chem Res Toxicol.* 2018;31(7):612-8.
63. Dizdar L, Junemann LM, Werner TA, Verde PE, Baldus SE, Stoecklein NH, et al. Clinicopathological and functional implications of the inhibitor of apoptosis proteins survivin and XIAP in esophageal cancer. *Oncol Lett.* 2018;15(3):3779-89.
64. Cheng SM, Chang YC, Liu CY, Lee JYC, Chan HH, Kuo CW, et al. YM155 down-regulates survivin and XIAP, modulates autophagy and induces autophagy-dependent DNA damage in breast cancer cells. *Brit J Pharmacol.* 2015;172(1):214-34.
65. Kogo R, How C, Chaudary N, Bruce J, Shi W, Hill RP, et al. The microRNA-218~Survivin axis regulates migration, invasion, and lymph node metastasis in cervical cancer. *Oncotarget.* 2015;6(2):1090-100.
66. Yamanaka K, Nakata M, Kaneko N, Fushiki H, Kita A, Nakahara T, et al. YM155, a selective survivin suppressant, inhibits tumor spread and prolongs survival in a spontaneous metastatic model of human triple negative breast cancer. *Int J Oncol.* 2011;39(3):569-75.
67. Yamanaka K, Nakahara T, Yamauchi T, Kita A, Takeuchi M, Kiyonaga F, et al. Antitumor Activity of YM155, a Selective Small-Molecule Survivin Suppressant, Alone and in Combination with Docetaxel in Human Malignant Melanoma Models. *Clin Cancer Res.* 2011;17(16):5423-31.
68. Ferrario A, Luna M, Rucker N, Wong S, Lederman A, Kim J, et al. Targeting Survivin Enhances Chemosensitivity in Retinoblastoma Cells and Orthotopic Tumors. *Plos One.* 2016;11(4).
69. Papadopoulos KP, Lopez-Jimenez J, Smith SE, Steinberg J, Keating A, Sasse C, et al. A multicenter phase II study of sepantronium bromide (YM155) plus rituximab in patients with relapsed aggressive B-cell Non-Hodgkin lymphoma. *Leuk Lymphoma.* 2016;57(8):1848-55.



70. Clemens MR, Gladkov OA, Gartner E, Vladimirov V, Crown J, Steinberg J, et al. Phase II, multicenter, open-label, randomized study of YM155 plus docetaxel as first-line treatment in patients with HER2-negative metastatic breast cancer. *Breast Cancer Res Tr.* 2015;149(1):171-9.
71. Tolcher AW, Quinn DI, Ferrari A, Ahmann F, Giaccone G, Drake T, et al. A phase II study of YM155, a novel small-molecule suppressor of survivin, in castration-resistant taxane-pretreated prostate cancer. *Ann Oncol.* 2012;23(4):968-U9.
72. Giaccone G, Zatloukal P, Roubec J, Floor K, Musil J, Kuta M, et al. Multicenter Phase II Trial of YM155, a Small-Molecule Suppressor of Survivin, in Patients With Advanced, Refractory, Non-Small-Cell Lung Cancer. *J Clin Oncol.* 2009;27(27):4481-6.
73. Kudchadkar R, Ernst S, Chmielowski B, Redman BG, Steinberg J, Keating A, et al. A phase 2, multicenter, open-label study of sepantronium bromide (YM155) plus docetaxel in patients with stage III (unresectable) or stage IV melanoma. *Cancer Med.* 2015;4(5):643-50.
74. Sullivan SM. Development of ribozymes for gene therapy. *J Invest Dermatol.* 1994;103(5 Suppl):85S-9S.
75. Hayashi N, Asano K, Suzuki H, Yamamoto T, Tanigawa N, Egawa S, et al. Adenoviral infection of survivin antisense sensitizes prostate cancer cells to etoposide in vivo. *Prostate.* 2005;65(1):10-9.
76. Olie RA, Simoes-Wust AP, Baumann B, Leech SH, Fabbro D, Stahel RA, et al. A novel antisense oligonucleotide targeting survivin expression induces apoptosis and sensitizes lung cancer cells to chemotherapy. *Cancer Res.* 2000;60(11):2805-9.
77. Choi KS, Lee TH, Jung MH. Ribozyme-mediated cleavage of the human survivin mRNA and inhibition of antiapoptotic function of survivin in MCF-7 cells. *Cancer Gene Ther.* 2003;10(2):87-95.
78. Sharma H, Sen S, Lo Muzio L, Mariggio A, Singh N. Antisense-mediated downregulation of anti-apoptotic proteins induces apoptosis and sensitizes head and neck squamous cell carcinoma cells to chemotherapy. *Cancer Biol Ther.* 2005;4(7):720-7.
79. Watts JK, Corey DR. Silencing disease genes in the laboratory and the clinic. *J Pathol.* 2012;226(2):365-79.

80. Tanioka M, Nokihara H, Yamamoto N, Yamada Y, Yamada K, Goto Y, et al. Phase I study of LY2181308, an antisense oligonucleotide against survivin, in patients with advanced solid tumors. *Cancer Chemother Pharmacol.* 2011;68(2):505-11.
81. Talbot DC, Ranson M, Davies J, Lahn M, Callies S, Andre V, et al. Tumor survivin is downregulated by the antisense oligonucleotide LY2181308: a proof-of-concept, first-in-human dose study. *Clin Cancer Res.* 2010;16(24):6150-8.
82. Wiechno P, Somer BG, Mellado B, Chlostka PL, Grau JMC, Castellano D, et al. A Randomised Phase 2 Study Combining LY2181308 Sodium (Survivin Antisense Oligonucleotide) with First-line Docetaxel/Prednisone in Patients with Castration-resistant Prostate Cancer. *Eur Urol.* 2014;65(3):516-20.
83. Natale R, Blackhall F, Kowalski D, Ramlau R, Bepler G, Grossi F, et al. Evaluation of Antitumor Activity Using Change in Tumor Size of the Survivin Antisense Oligonucleotide LY2181308 in Combination with Docetaxel for Second-Line Treatment of Patients with Non-Small-Cell Lung Cancer A Randomized Open-Label Phase II Study. *J Thorac Oncol.* 2014;9(11):1704-8.
84. Elbashir SM, Harborth J, Lendeckel W, Yalcin A, Weber K, Tuschl T. Duplexes of 21-nucleotide RNAs mediate RNA interference in cultured mammalian cells. *Nature.* 2001;411(6836):494-8.
85. Bartlett DW, Davis ME. Insights into the kinetics of siRNA-mediated gene silencing from live-cell and live-animal bioluminescent imaging. *Nucleic Acids Res.* 2006;34(1):322-33.
86. Whitehead KA, Langer R, Anderson DG. Knocking down barriers: advances in siRNA delivery. *Nature Reviews Drug Discovery.* 2009;8(2):129-38.
87. Pi F, Binzel DW, Lee TJ, Li Z, Sun M, Rychahou P, et al. Nanoparticle orientation to control RNA loading and ligand display on extracellular vesicles for cancer regression. *Nat Nanotechnol.* 2018;13(1):82-9.
88. Kozielski KL, Ruiz-Valls A, Tzeng SY, Guerrero-Cazares H, Rui Y, Li Y, et al. Cancer-selective nanoparticles for combinatorial siRNA delivery to primary human GBM in vitro and in vivo. *Biomaterials.* 2019;209:79-87.
89. Liu K, Liu Y, Zhao G. Targeting survivin suppresses proliferation and invasion of retinoblastoma cells in vitro and in vivo. *Int J Clin Exp Pathol.* 2017;10(9):9352-61.

90. Samuel J, Kanwar RK, Kanwar JR, Khetan V, Krishnakumar S. A Study of Gene Expression of Survivin, its Antiapoptotic Variants, and Targeting Survivin In Vitro for Therapy in Retinoblastoma. *J Pediat Hematol Onc.* 2016;38(7):E230-E42.
91. He C, Liu D, Lin W. Self-assembled nanoscale coordination polymers carrying siRNAs and cisplatin for effective treatment of resistant ovarian cancer. *Biomaterials.* 2015;36:124-33.
92. Chen X, Zhang Y, Tang C, Tian C, Sun Q, Su Z, et al. Co-delivery of paclitaxel and anti-survivin siRNA via redox-sensitive oligopeptide liposomes for the synergistic treatment of breast cancer and metastasis. *Int J Pharm.* 2017;529(1-2):102-15.
93. Chawla-Sarkar M, Bae SI, Reu FJ, Jacobs BS, Lindner DJ, Borden EC. Downregulation of Bcl-2, FLIP or IAPs (XIAP and survivin) by siRNAs sensitizes resistant melanoma cells to Apo2L/TRAIL-induced apoptosis. *Cell Death Differ.* 2004;11(8):915-23.
94. Wang T, Upponi JR, Torchilin VP. Design of multifunctional non-viral gene vectors to overcome physiological barriers: dilemmas and strategies. *Int J Pharm.* 2012;427(1):3-20.
95. Blanco E, Shen H, Ferrari M. Principles of nanoparticle design for overcoming biological barriers to drug delivery. *Nat Biotechnol.* 2015;33(9):941-51.
96. Milani P, Mussinelli R, Perlini S, Palladini G, Obici L. An evaluation of patisiran: a viable treatment option for transthyretin-related hereditary amyloidosis. *Expert Opin Pharmacother.* 2019:1-6.
97. Hu B, Weng Y, Xia XH, Liang XJ, Huang Y. Clinical advances of siRNA therapeutics. *J Gene Med.* 2019;21(7):e3097.
98. Choung S, Kim YJ, Kim S, Park HO, Choi YC. Chemical modification of siRNAs to improve serum stability without loss of efficacy. *Biochem Biophys Res Commun.* 2006;342(3):919-27.
99. van de Water FM, Boerman OC, Wouterse AC, Peters JG, Russel FG, Masereeuw R. Intravenously administered short interfering RNA accumulates in the kidney and selectively suppresses gene function in renal proximal tubules. *Drug Metab Dispos.* 2006;34(8):1393-7.
100. Dominska M, Dykxhoorn DM. Breaking down the barriers: siRNA delivery and endosome escape. *J Cell Sci.* 2010;123(Pt 8):1183-9.

101. Zhang Y, Li H, Sun J, Gao J, Liu W, Li B, et al. DC-Chol/DOPE cationic liposomes: a comparative study of the influence factors on plasmid pDNA and siRNA gene delivery. *Int J Pharm.* 2010;390(2):198-207.
102. Crook K, Stevenson BJ, Dubouchet M, Porteous DJ. Inclusion of cholesterol in DOTAP transfection complexes increases the delivery of DNA to cells in vitro in the presence of serum. *Gene Ther.* 1998;5(1):137-43.
103. Malone RW, Felgner PL, Verma IM. Cationic liposome-mediated RNA transfection. *Proc Natl Acad Sci U S A.* 1989;86(16):6077-81.
104. Grayson AC, Doody AM, Putnam D. Biophysical and structural characterization of polyethylenimine-mediated siRNA delivery in vitro. *Pharm Res.* 2006;23(8):1868-76.
105. Litzinger DC, Brown JM, Wala I, Kaufman SA, Van GY, Farrell CL, et al. Fate of cationic liposomes and their complex with oligonucleotide in vivo. *Biochim Biophys Acta.* 1996;1281(2):139-49.
106. Harris JM, Chess RB. Effect of pegylation on pharmaceuticals. *Nat Rev Drug Discov.* 2003;2(3):214-21.
107. Hatakeyama H, Akita H, Harashima H. A multifunctional envelope type nano device (MEND) for gene delivery to tumours based on the EPR effect: a strategy for overcoming the PEG dilemma. *Adv Drug Deliv Rev.* 2011;63(3):152-60.
108. Semple SC, Klimuk SK, Harasym TO, Dos Santos N, Ansell SM, Wong KF, et al. Efficient encapsulation of antisense oligonucleotides in lipid vesicles using ionizable aminolipids: formation of novel small multilamellar vesicle structures. *Biochim Biophys Acta.* 2001;1510(1-2):152-66.
109. Jayaraman M, Ansell SM, Mui BL, Tam YK, Chen J, Du X, et al. Maximizing the potency of siRNA lipid nanoparticles for hepatic gene silencing in vivo. *Angew Chem Int Ed Engl.* 2012;51(34):8529-33.
110. Love KT, Mahon KP, Levins CG, Whitehead KA, Querbes W, Dorkin JR, et al. Lipid-like materials for low-dose, in vivo gene silencing. *Proc Natl Acad Sci U S A.* 2010;107(5):1864-9.

111. Akinc A, Zumbuehl A, Goldberg M, Leshchiner ES, Busini V, Hossain N, et al. A combinatorial library of lipid-like materials for delivery of RNAi therapeutics. *Nat Biotechnol.* 2008;26(5):561-9.
112. Boussif O, Lezoualc'h F, Zanta MA, Mergny MD, Scherman D, Demeneix B, et al. A versatile vector for gene and oligonucleotide transfer into cells in culture and in vivo: polyethylenimine. *Proc Natl Acad Sci U S A.* 1995;92(16):7297-301.
113. Pires P, Simoes S, Nir S, Gaspar R, Duzgunes N, Pedroso de Lima MC. Interaction of cationic liposomes and their DNA complexes with monocytic leukemia cells. *Biochim Biophys Acta.* 1999;1418(1):71-84.
114. Rejman J, Bragonzi A, Conese M. Role of clathrin- and caveolae-mediated endocytosis in gene transfer mediated by lipo- and polyplexes. *Mol Ther.* 2005;12(3):468-74.
115. Sahay G, Querbes W, Alabi C, Eltoukhy A, Sarkar S, Zurenko C, et al. Efficiency of siRNA delivery by lipid nanoparticles is limited by endocytic recycling. *Nat Biotechnol.* 2013;31(7):653-8.
116. Gilleron J, Querbes W, Zeigerer A, Borodovsky A, Marsico G, Schubert U, et al. Image-based analysis of lipid nanoparticle-mediated siRNA delivery, intracellular trafficking and endosomal escape. *Nat Biotechnol.* 2013;31(7):638-46.
117. Chou LY, Ming K, Chan WC. Strategies for the intracellular delivery of nanoparticles. *Chem Soc Rev.* 2011;40(1):233-45.
118. Stewart MP, Lorenz A, Dahlman J, Sahay G. Challenges in carrier-mediated intracellular delivery: moving beyond endosomal barriers. *Wiley Interdiscip Rev Nanomed Nanobiotechnol.* 2016;8(3):465-78.
119. Hafez IM, Maurer N, Cullis PR. On the mechanism whereby cationic lipids promote intracellular delivery of polynucleic acids. *Gene Ther.* 2001;8(15):1188-96.
120. Cullis PR, Hope MJ. Lipid Nanoparticle Systems for Enabling Gene Therapies. *Mol Ther.* 2017;25(7):1467-75.
121. Viricel W, Poirier S, Mbarek A, Derbali RM, Mayer G, Leblond J. Cationic switchable lipids: pH-triggered molecular switch for siRNA delivery. *Nanoscale.* 2017;9(1):31-6.

122. Tabatabaei SN, Derbali RM, Yang C, Superstein R, Hamel P, Chain JL, et al. Co-delivery of miR-181a and melphalan by lipid nanoparticles for treatment of seeded retinoblastoma. *J Control Release*. 2019;298:177-85.
123. Bangham AD, Standish MM, Watkins JC. Diffusion of univalent ions across the lamellae of swollen phospholipids. *J Mol Biol*. 1965;13(1):238-52.
124. Bangham AD, Horne RW. Negative Staining of Phospholipids and Their Structural Modification by Surface-Active Agents as Observed in the Electron Microscope. *J Mol Biol*. 1964;8:660-8.
125. Torchilin VP. Recent advances with liposomes as pharmaceutical carriers. *Nat Rev Drug Discov*. 2005;4(2):145-60.
126. Ewert KK, Zidovska A, Ahmad A, Bouxsein NF, Evans HM, McAllister CS, et al. Cationic Liposome–Nucleic Acid Complexes for Gene Delivery and Silencing: Pathways and Mechanisms for Plasmid DNA and siRNA. In: Bielke W, Erbacher C, editors. *Nucleic Acid Transfection*. Berlin, Heidelberg: Springer Berlin Heidelberg; 2010. p. 191-226.
127. Desigaux L, Sainlos M, Lambert O, Chevre R, Letrou-Bonneval E, Vigneron JP, et al. Self-assembled lamellar complexes of siRNA with lipidic aminoglycoside derivatives promote efficient siRNA delivery and interference. *Proc Natl Acad Sci U S A*. 2007;104(42):16534-9.
128. Leung AK, Hafez IM, Baoukina S, Belliveau NM, Zhigaltsev IV, Afshinmanesh E, et al. Lipid Nanoparticles Containing siRNA Synthesized by Microfluidic Mixing Exhibit an Electron-Dense Nanostructured Core. *J Phys Chem C Nanomater Interfaces*. 2012;116(34):18440-50.
129. Mbarek A, Moussa G, Chain JL. Pharmaceutical Applications of Molecular Tweezers, Clefts and Clips. *Molecules*. 2019;24(9).
130. Viricel W, Mbarek A, Leblond J. Switchable Lipids: Conformational Change for Fast pH-Triggered Cytoplasmic Delivery. *Angew Chem Int Ed Engl*. 2015;54(43):12743-7.
131. Viricel W. Nanoparticules lipidiques pH-sensibles basées sur une bascule moléculaire pour la délivrance intracytoplasmique de siRNA. Montreal: University of Montreal; 2017.
132. Shin KH, Bae SD, Hong HS, Kim RH, Kang MK, Park NH. miR-181a shows tumor suppressive effect against oral squamous cell carcinoma cells by downregulating K-ras. *Biochem Biophys Res Commun*. 2011;404(4):896-902.

133. Rideau E, Dimova R, Schwille P, Wurm FR, Landfester K. Liposomes and polymersomes: a comparative review towards cell mimicking. *Chem Soc Rev*. 2018;47(23):8572-610.
134. Le Meins JF, Schatz C, Lecommandoux S, Sandre O. Hybrid polymer/lipid vesicles: state of the art and future perspectives. *Materials Today*. 2013;16(10):397-402.
135. Le Meins JF, Sandre O, Lecommandoux S. Recent trends in the tuning of polymersomes' membrane properties. *Eur Phys J E Soft Matter*. 2011;34(2):14.
136. Otrin L, Marusic N, Bednarz C, Vidakovic-Koch T, Lieberwirth I, Landfester K, et al. Toward Artificial Mitochondrion: Mimicking Oxidative Phosphorylation in Polymer and Hybrid Membranes. *Nano Lett*. 2017;17(11):6816-21.
137. De Oliveira H, Thevenot J, Lecommandoux S. Smart polymersomes for therapy and diagnosis: fast progress toward multifunctional biomimetic nanomedicines. *Wiley Interdiscip Rev Nanomed Nanobiotechnol*. 2012;4(5):525-46.
138. Kim KT, Cornelissen JJ, Nolte RJ, van Hest JC. A Polymersome Nanoreactor with Controllable Permeability Induced by Stimuli-Responsive Block Copolymers. *Advanced materials*. 2009;21(27):2787-91.
139. Goni-de-Cerio F, Thevenot J, Oliveira H, Perez-Andres E, Berra E, Masa M, et al. Cellular Uptake and Cytotoxic Effect of Epidermal Growth Factor Receptor Targeted and Plitidepsin Loaded Co-Polymeric Polymersomes on Colorectal Cancer Cell Lines. *J Biomed Nanotechnol*. 2015;11(11):2034-49.
140. Rosselgong J, Chemin M, Almada CC, Hemery G, Guigner JM, Chollet G, et al. Synthesis and Self-Assembly of Xylan-Based Amphiphiles: From Bio-Based Vesicles to Antifungal Properties. *Biomacromolecules*. 2019;20(1):118-29.
141. Dao TPT, Fernandes F, Fauquignon M, Ibarboure E, Prieto M, Le Meins JF. The combination of block copolymers and phospholipids to form giant hybrid unilamellar vesicles (GHUVs) does not systematically lead to "intermediate" membrane properties. *Soft Matter*. 2018;14(31):6476-84.
142. Lim S, de Hoog H-P, Parikh A, Nallani M, Liedberg B. Hybrid, nanoscale phospholipid/block copolymer vesicles. *Polymers*. 2013;5(3):1102-14.

143. Dao TP, Fernandes F, Ibarboure E, Ferji K, Prieto M, Sandre O, et al. Modulation of phase separation at the micron scale and nanoscale in giant polymer/lipid hybrid unilamellar vesicles (GHUVs). *Soft Matter*. 2017;13(3):627-37.
144. Chemin M, Brun P-M, Lecommandoux S, Sandre O, Meins J-FL. Hybrid polymer/lipid vesicles: fine control of the lipid and polymer distribution in the binary membrane. *Soft Matter*. 2012;8(10):2867-74.
145. Chazal N, Gerlier D. Virus entry, assembly, budding, and membrane rafts. *Microbiol Mol Biol Rev*. 2003;67(2):226-37, table of contents.
146. Simons K, Toomre D. Lipid rafts and signal transduction. *Nat Rev Mol Cell Biol*. 2000;1(1):31-9.
147. van Meer G, Sprong H. Membrane lipids and vesicular traffic. *Curr Opin Cell Biol*. 2004;16(4):373-8.
148. Munro S. Lipid Rafts: Elusive or Illusive? *Cell*. 2003;115(4):377-88.
149. Cheng Z, Elias DR, Kamat NP, Johnston ED, Poloukhtine A, Popik V, et al. Improved Tumor Targeting of Polymer-Based Nanovesicles Using Polymer–Lipid Blends. 2011.
150. Khan S, McCabe J, Hill K, Beales P. Biodegradable Hybrid Block Copolymer – Lipid Vesicles as Potential Drug Delivery Systems. *ChemRxiv Preprint*. 2019.
151. Bretscher MS. Asymmetrical lipid bilayer structure for biological membranes. *Nat New Biol*. 1972;236(61):11-2.
152. Schlegel RA, Williamson P. Phosphatidylserine, a death knell. *Cell Death Differ*. 2001;8(6):551-63.
153. Peyret A, Ibarboure E, Le Meins JF, Lecommandoux S. Asymmetric Hybrid Polymer-Lipid Giant Vesicles as Cell Membrane Mimics. *Adv Sci (Weinh)*. 2018;5(1):1700453.
154. Walde P, Cosentino K, Engel H, Stano P. Giant vesicles: preparations and applications. *Chembiochem*. 2010;11(7):848-65.
155. Akashi K, Miyata H, Itoh H, Kinoshita K, Jr. Preparation of giant liposomes in physiological conditions and their characterization under an optical microscope. *Biophys J*. 1996;71(6):3242-50.
156. Dimitrov MIA, Dimiter S. Liposome electroformation. 1986.



157. Herold C, Chwastek G, Schwille P, Petrov EP. Efficient electroformation of supergiant unilamellar vesicles containing cationic lipids on ITO-coated electrodes. *Langmuir*. 2012;28(13):5518-21.
158. Shimanouchi T, Umakoshi H, Kuboi R. Kinetic study on giant vesicle formation with electroformation method. *Langmuir*. 2009;25(9):4835-40.
159. Kato Y, Ozawa S, Miyamoto C, Maehata Y, Suzuki A, Maeda T, et al. Acidic extracellular microenvironment and cancer. *Cancer Cell Int*. 2013;13(1):89.
160. Huotari J, Helenius A. Endosome maturation. *Embo J*. 2011;30(17):3481-500.
161. Ganta S, Devalapally H, Shahiwala A, Amiji M. A review of stimuli-responsive nanocarriers for drug and gene delivery. *J Control Release*. 2008;126(3):187-204.
162. Couvreur P, Vauthier C. Nanotechnology: intelligent design to treat complex disease. *Pharm Res*. 2006;23(7):1417-50.
163. Chen W, Meng F, Cheng R, Zhong Z. pH-Sensitive degradable polymersomes for triggered release of anticancer drugs: a comparative study with micelles. *J Control Release*. 2010;142(1):40-6.
164. Liu G-Y, Lv L-P, Chen C-J, Liu X-S, Hu X-F, Ji J. Biocompatible and biodegradable polymersomes for pH-triggered drug release. *Soft Matter*. 2011(14):6629-36.
165. Zong W, Thingholm B, Itel F, Schattling PS, Brodzskij E, Mayer D, et al. Phospholipid-Block Copolymer Hybrid Vesicles with Lysosomal Escape Ability. *Langmuir*. 2018;34(23):6874-86.
166. Altieri DC. Survivin, cancer networks and pathway-directed drug discovery. *Nat Rev Cancer*. 2008;8(1):61-70.
167. Zhang Y, Yan H, Li R, Guo Y, Zheng R. High expression of survivin predicts poor prognosis in cervical squamous cell carcinoma treated with paclitaxel and carboplatin. *Medicine (Baltimore)*. 2019;98(20):e15607.
168. Shehata HH, Abou Ghalia AH, Elsayed EK, Ziko OO, Mohamed SS. Detection of survivin protein in aqueous humor and serum of retinoblastoma patients and its clinical significance. *Clin Biochem*. 2010;43(4-5):362-6.
169. Huang JC, Lyu H, Wang JX, Liu BL. Influence of survivin-targeted therapy on chemosensitivity in the treatment of acute myeloid leukemia. *Cancer Lett*. 2015;366(2):160-72.

170. Lu CD, Altieri DC, Tanigawa N. Expression of a novel antiapoptosis gene, survivin, correlated with tumor cell apoptosis and p53 accumulation in gastric carcinomas. *Cancer Res.* 1998;58(9):1808-12.
171. Ryan BM, O'Donovan N, Duffy MJ. Survivin: a new target for anti-cancer therapy. *Cancer Treat Rev.* 2009;35(7):553-62.
172. Rauch A, Hennig D, Schafer C, Wirth M, Marx C, Heinzl T, et al. Survivin and YM155: How faithful is the liaison? *Bba-Rev Cancer.* 2014;1845(2):202-20.
173. Altieri DC. Validating survivin as a cancer therapeutic target. *Nat Rev Cancer.* 2003;3(1):46-54.
174. Morgillo F, Woo JK, Kim ES, Hong WK, Lee HY. Heterodimerization of insulin-like growth factor receptor/epidermal growth factor receptor and induction of survivin expression counteract the antitumor action of erlotinib. *Cancer Res.* 2006;66(20):10100-11.
175. Ghosh SK, Yigit MV, Uchida M, Ross AW, Barteneva N, Moore A, et al. Sequence-dependent combination therapy with doxorubicin and a survivin-specific small interfering RNA nanodrug demonstrates efficacy in models of adenocarcinoma. *Int J Cancer.* 2014;134(7):1758-66.
176. Yin Q, Shen J, Chen L, Zhang Z, Gu W, Li Y. Overcoming multidrug resistance by co-delivery of Mdr-1 and survivin-targeting RNA with reduction-responsive cationic poly(beta-amino esters). *Biomaterials.* 2012;33(27):6495-506.
177. Daglioglu C, Kaci FN. Cascade therapy with doxorubicin and survivin-targeted tailored nanoparticles: An effective alternative for sensitization of cancer cells to chemotherapy. *Int J Pharm.* 2019;561:74-81.
178. Sato A, Ito K, Asano T, Sumitomo M, Asano T, Hayakawa M. Synergistic effect of survivin-specific small interfering RNA and topotecan in renal cancer cells: topotecan enhances liposome-mediated transfection by increasing cellular uptake. *Int J Oncol.* 2007;30(3):695-700.
179. Yamamoto M, Suzuki S, Togashi K, Sanomachi T, Seino S, Kitanaka C, et al. AS602801 Sensitizes Ovarian Cancer Stem Cells to Paclitaxel by Down-regulating MDR1. *Anticancer Res.* 2019;39(2):609-17.

180. Wang S, Xu Y, Chan HF, Kim HW, Wang Y, Leong KW, et al. Nanoparticle-mediated inhibition of survivin to overcome drug resistance in cancer therapy. *J Control Release*. 2016;240:454-64.
181. Weinstein S, Toker IA, Emmanuel R, Ramishetti S, Hazan-Halevy I, Rosenblum D, et al. Harnessing RNAi-based nanomedicines for therapeutic gene silencing in B-cell malignancies. *Proc Natl Acad Sci U S A*. 2016;113(1):E16-22.
182. He W, Bennett MJ, Luistro L, Carvajal D, Nevins T, Smith M, et al. Discovery of siRNA lipid nanoparticles to transfect suspension leukemia cells and provide in vivo delivery capability. *Mol Ther*. 2014;22(2):359-70.
183. Cohen ZR, Ramishetti S, Peshes-Yaloz N, Goldsmith M, Wohl A, Zibly Z, et al. Localized RNAi therapeutics of chemoresistant grade IV glioma using hyaluronan-grafted lipid-based nanoparticles. *Acs Nano*. 2015;9(2):1581-91.
184. Lee JB, Zhang K, Tam YY, Tam YK, Belliveau NM, Sung VY, et al. Lipid nanoparticle siRNA systems for silencing the androgen receptor in human prostate cancer in vivo. *Int J Cancer*. 2012;131(5):E781-90.
185. Dimaras H, Kimani K, Dimba EA, Gronsdahl P, White A, Chan HS, et al. Retinoblastoma. *Lancet*. 2012;379(9824):1436-46.
186. Abramson DH, Shields CL, Munier FL, Chantada GL. Treatment of Retinoblastoma in 2015: Agreement and Disagreement. *JAMA Ophthalmol*. 2015;133(11):1341-7.
187. Qiu Q, Yang C, Xiong W, Tahiri H, Payeur M, Superstein R, et al. SYK is a target of lymphocyte-derived microparticles in the induction of apoptosis of human retinoblastoma cells. *Apoptosis*. 2015;20(12):1613-22.
188. Chou TC, Talalay P. Quantitative analysis of dose-effect relationships: the combined effects of multiple drugs or enzyme inhibitors. *Adv Enzyme Regul*. 1984;22:27-55.
189. Wan C, Allen TM, Cullis PR. Lipid nanoparticle delivery systems for siRNA-based therapeutics. *Drug Deliv Transl Res*. 2014;4(1):74-83.
190. Leung AK, Tam YY, Chen S, Hafez IM, Cullis PR. Microfluidic Mixing: A General Method for Encapsulating Macromolecules in Lipid Nanoparticle Systems. *J Phys Chem B*. 2015;119(28):8698-706.

191. Winter U, Mena HA, Negrotto S, Arana E, Pascual-Pasto G, Laurent V, et al. Schedule-Dependent Antiangiogenic and Cytotoxic Effects of Chemotherapy on Vascular Endothelial and Retinoblastoma Cells. *Plos One*. 2016;11(7):e0160094.
192. Shukla S, Srivastava A, Kumar S, Singh U, Goswami S, Chawla B, et al. Expression of multidrug resistance proteins in retinoblastoma. *Int J Ophthalmol*. 2017;10(11):1655-61.
193. Huang J, Lyu H, Wang J, Liu B. Influence of survivin-targeted therapy on chemosensitivity in the treatment of acute myeloid leukemia. *Cancer Lett*. 2015;366(2):160-72.
194. Zhang R, Ma L, Zheng M, Ren J, Wang T, Meng Y, et al. Survivin knockdown by short hairpin RNA abrogates the growth of human hepatocellular carcinoma xenografts in nude mice. *Cancer Gene Ther*. 2010;17(4):275-88.
195. Sato A, Ito K, Asano T, Sumitomo M, Asano T, Hayakawa M. Synergistic effect of survivin-specific small interfering RNA and topotecan in renal cancer cells: Topotecan enhances liposome-mediated transfection by increasing cellular uptake. *Int J Oncol*. 2007;30(3):695-700.
196. Pritchard EM, Dyer MA, Guy RK. Progress in Small Molecule Therapeutics for the Treatment of Retinoblastoma. *Mini-Rev Med Chem*. 2016;16(6):430-54.
197. Chen M, Beck WT. Teniposide-resistant CEM cells, which express mutant DNA topoisomerase II alpha, when treated with non-complex-stabilizing inhibitors of the enzyme, display no cross-resistance and reveal aberrant functions of the mutant enzyme. *Cancer Res*. 1993;53(24):5946-53.
198. Tsubaki M, Takeda T, Tomonari Y, Koumoto YI, Imano M, Satou T, et al. Overexpression of HIF-1alpha contributes to melphalan resistance in multiple myeloma cells by activation of ERK1/2, Akt, and NF-kappaB. *Lab Invest*. 2019;99(1):72-84.
199. Allen TM, Cullis PR. Liposomal drug delivery systems: From concept to clinical applications. *Advanced Drug Delivery Reviews*. 2013;65(1):36-48.
200. Bulbake U, Doppalapudi S, Kommineni N, Khan W. Liposomal Formulations in Clinical Use: An Updated Review. *Pharmaceutics*. 2017;9(2):12.
201. Dong Y, Siegwart DJ, Anderson DG. Strategies, design, and chemistry in siRNA delivery systems. *Adv Drug Deliv Rev*. 2019.

202. Mura S, Nicolas J, Couvreur P. Stimuli-responsive nanocarriers for drug delivery. *Nature Materials*. 2013;12(11):991-1003.
203. Riemann A, Wussling H, Loppnow H, Fu H, Reime S, Thews O. Acidosis differently modulates the inflammatory program in monocytes and macrophages. *Biochim Biophys Acta*. 2016;1862(1):72-81.
204. Cobbe SM, Poole-Wilson PA. The time of onset and severity of acidosis in myocardial ischaemia. *Journal of Molecular and Cellular Cardiology*. 1980;12(8):745-60.
205. Gao GH, Park MJ, Li Y, Im GH, Kim JH, Kim HN, et al. The use of pH-sensitive positively charged polymeric micelles for protein delivery. *Biomaterials*. 2012;33(35):9157-64.
206. Dao TP, Brulet A, Fernandes F, Er-Rafik M, Ferji K, Schweins R, et al. Mixing Block Copolymers with Phospholipids at the Nanoscale: From Hybrid Polymer/Lipid Wormlike Micelles to Vesicles Presenting Lipid Nanodomains. *Langmuir*. 2017;33(7):1705-15.
207. Angelova MI, Dimitrov DS. Liposome electroformation. *Faraday Discuss Chem Soc*. 1986;81:303-11.
208. Steinkuhler J, De Tillieux P, Knorr RL, Lipowsky R, Dimova R. Charged giant unilamellar vesicles prepared by electroformation exhibit nanotubes and transbilayer lipid asymmetry. *Sci Rep*. 2018;8(1):11838.
209. Fauquignon M, Ibarboure E, Carlotti S, Brûlet A, Schmutz M, Le Meins J-F. Large and Giant Unilamellar vesicle(s) obtained by self-assembly of poly(dimethylsiloxane)-b-poly(ethylene oxide) diblock copolymers, membrane properties and preliminary investigation of their ability to form Hybrid Polymer/Lipid vesicles. *Polymers*. 2019;11(12):2013.
210. Leblond J, Petitjean A. Molecular tweezers: concepts and applications. *Chemphyschem*. 2011;12(6):1043-51.
211. Khan S, Li M, Muench SP, Jeuken LJ, Beales PA. Durable proteo-hybrid vesicles for the extended functional lifetime of membrane proteins in bionanotechnology. *Chem Commun (Camb)*. 2016;52(73):11020-3.
212. Pippa N, Stellas D, Skandalis A, Pispas S, Demetzos C, Libera M, et al. Chimeric lipid/block copolymer nanovesicles: Physico-chemical and bio-compatibility evaluation. *Eur J Pharm Biopharm*. 2016;107:295-309.

213. Kirkin AF, Dzhandzhugazyan KN, Guldberg P, Fang JJ, Andersen RS, Dahl C, et al. Adoptive cancer immunotherapy using DNA-demethylated T helper cells as antigen-presenting cells. *Nat Commun.* 2018;9(1):785.
214. Carlsen A, Glaser N, Le Meins JF, Lecommandoux S. Block copolymer vesicle permeability measured by osmotic swelling and shrinking. *Langmuir.* 2011;27(8):4884-90.
215. Leblond J, Gao H, Petitjean A, Leroux JC. pH-Responsive molecular tweezers. *J Am Chem Soc.* 2010;132(25):8544-5.
216. Dauletbaev N, Dintakurti A, Choi Y, Cammisano M, Viricel W, Leblond J, et al. Cytotoxicity of liposome-encapsulated polyinosinic-polycytidylic acid in primary human macrophages is only partially related to interferon- $\beta$ . *Eur Respir J.* 2018;52.
217. Dauletbaev N, Dintakurti A, Viricel W, Leblond-Chain J, Lands L. Cytoplasmic signaling of polyinosinic-polycytidylic acid stimulates a quick and potent interferon response in primary macrophages. *Eur Respir J.* 2017;50.
218. Dauletbaev N, Cammisano M, Viricel W, Laurin S-A, Leblond-Chain J, Lands L. Stimulation with polyinosinic-polycytidylic acid (poly(I:C)) encapsulated within novel pH-sensitive switchable liposomes leads to a faster and more potent interferon response. *Eur Respir J.* 2016;48.
219. Valero L, Alhareth K, Espinoza Romero J, Viricel W, Leblond J, Chissey A, et al. Liposomes as Gene Delivery Vectors for Human Placental Cells. *Molecules.* 2018;23(5).
220. Fenton OS, Kauffman KJ, McClellan RL, Kaczmarek JC, Zeng MD, Andresen JL, et al. Customizable Lipid Nanoparticle Materials for the Delivery of siRNAs and mRNAs. *Angew Chem Int Ed Engl.* 2018;57(41):13582-6.
221. Akinc A, Maier MA, Manoharan M, Fitzgerald K, Jayaraman M, Barros S, et al. The Onpatro story and the clinical translation of nanomedicines containing nucleic acid-based drugs. *Nat Nanotechnol.* 2019;14(12):1084-7.
222. Li FZ, Ambrosini G, Chu EY, Plescia J, Tognin S, Marchisio PC, et al. Control of apoptosis and mitotic spindle checkpoint by survivin. *Nature.* 1998;396(6711):580-4.
223. Li F, Aljahdali I, Ling X. Cancer therapeutics using survivin BIRC5 as a target: what can we do after over two decades of study? *J Exp Clin Cancer Res.* 2019;38(1):368.

224. Lin A, Giuliano CJ, Palladino A, John KM, Abramowicz C, Yuan ML, et al. Off-target toxicity is a common mechanism of action of cancer drugs undergoing clinical trials. *Sci Transl Med*. 2019;11(509).
225. Liu X, Huang G. Formation strategies, mechanism of intracellular delivery and potential clinical applications of pH-sensitive liposomes. *asian journal of pharmaceutical sciences*. 2013;8(6):319-28.
226. Paliwal SR, Paliwal R, Vyas SP. A review of mechanistic insight and application of pH-sensitive liposomes in drug delivery. *Drug Deliv*. 2015;22(3):231-42.
227. Benavente CA, Dyer MA. Genetics and epigenetics of human retinoblastoma. *Annu Rev Pathol*. 2015;10:547-62.
228. Zhang J, Benavente CA, McEvoy J, Flores-Otero J, Ding L, Chen X, et al. A novel retinoblastoma therapy from genomic and epigenetic analyses. *Nature*. 2012;481(7381):329-34.
229. Qiu Q, Yang C, Xiong W, Tahiri H, Payeur M, Superstein R, et al. SYK is a target of lymphocyte-derived microparticles in the induction of apoptosis of human retinoblastoma cells. *Apoptosis*. 2015;20(12):1613-22.